The BIR3 interactome revealed the NLR CSA1 as a component necessary for BIR- and BAK1-mediated cell death

Dissertation

der Mathematisch-Naturwissenschaftlichen Fakultät

der Eberhard Karls Universität Tübingen

zur Erlangung des Grades eines

Doktors der Naturwissenschaften

(Dr. rer. nat.)

vorgelegt von

Dipl. biol. Sarina Schulze

aus Bamberg

Tübingen

2020

Gedruckt mit Genehmigung der Mathematisch-Naturwissenschaftlichen Fakultät der Eberhard Karls Universität Tübingen.

Tag der mündlichen Qualifikation:	25.09.2020
Stellvertretender Dekan:	Prof. Dr. József Fortágh
1. Berichterstatter:	PD Dr. Birgit Kemmerling
2. Berichterstatter:	Prof. Dr. Thorsten Nürnberger

Table of contents

1 Introduction

Having a brief look into nature, one can observe that some plants appear healthy while neighboring ones look infected by a pathogen (Fig. 1.1). Becoming ill or diseased is a phenomenon that appears in all existing organisms over all kingdoms. But why can some plants resist to a certain threat and others cannot? Investigations over the last decades increased our knowledge how plants protect themselves. Firstly, plants defend themselves by the establishment of constitutive barriers, as, for example, the physico-chemical composition of the cell wall, the formation of a cuticle and of preformed toxic components (Bigeard et al., 2015). Secondly, plants evolved a powerful innate immune system as a tool to ward off pathogens. Historically, the innate immune system of plants was described as a two-layered system wherein a first, extracellular perception led to Pattern-Triggered Immunity (PTI). Because pathogens learned to undermine PTI by delivering effectors aiming to shut down the immune response, thus leading to a susceptible plant, an intracellular perception system, the Effector-Triggered Immunity (ETI) was invented to fight back (Jones and Dangl, 2006a; Boller and Felix, 2009a). However, this so-called `zig-zag-model` gets more and more replaced by the danger-model, which unifies host defense via cell-surface- and intracellularly located receptors (Nürnberger et al., 2004; Jones and Dangl, 2006b; Gust et al., 2017; Wan et al., 2019b; Ngou et al., 2020).

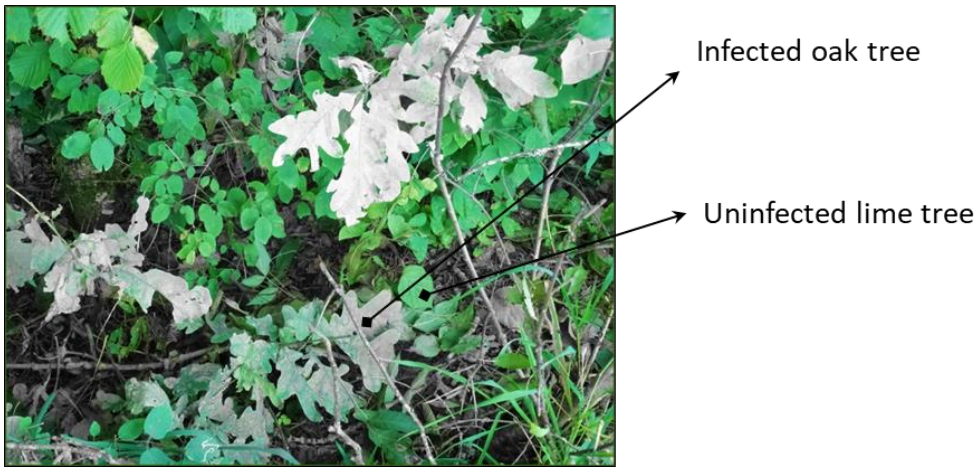

Figure 1.1: Immunity in nature

The lime tree can resist powdery mildew infection while the neighboring oak tree gets infected. The question is why? (picture © B.Kemmerling).

1.1 The plant innate immune system

1.1.1 Perception of danger on the cell surface (PTI)

Immune responses leading to PTI pass through several stages before executing the immune response. These stages are characterized by (i) the perception of a signal, (ii) the formation of a receptor-co-receptor complex, and (iii) the relay of the signal by different transduction pathways / cascades, leading finally (iv) to resistance, referred as to PTI (Fig. 1.2) (Ma et al., 2016).

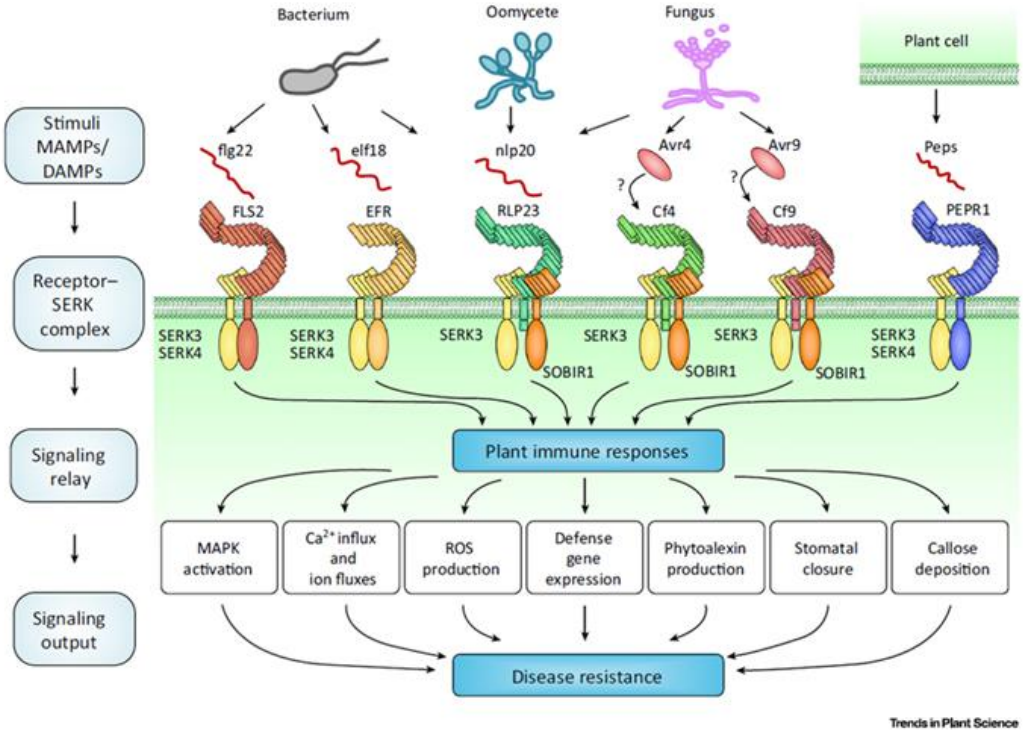

Figure 1.2: Different stages of signal transmission defines PTI

Pattern recognition receptors (PRRs) transmit the perceived signal to the inner part of the cell. This leads to the recruitment of membrane-localized co-receptors of the SERK family. This receptor complex activates a signaling relay, followed by the signaling output like e.g. the induction of defense related genes (Ma et al., 2016).

1.1.1.1 Perceiving signals

The conversion or transfer of an external signal towards the inner part of the cell represents the main work of Pattern-Recognition Receptors (PRRs). A major group of PRRs are Leucine-Rich Repeat Receptor-Like Kinases (LRR-RLKs) and Leucine-Rich Repeat Receptor-Like Proteins (LRR-RLPs), the latter lacking the kinase domain (Böhm et al., 2014; Wan et al., 2019b). LRR-RLKs comprise ~220 members and RLPs count ~60 members in *A. thaliana*,

which are involved in all important processes of the plant, starting from development to plant immunity (Fritz-Laylin et al., 2005; He et al., 2018; Smakowska-Luzan et al., 2018).

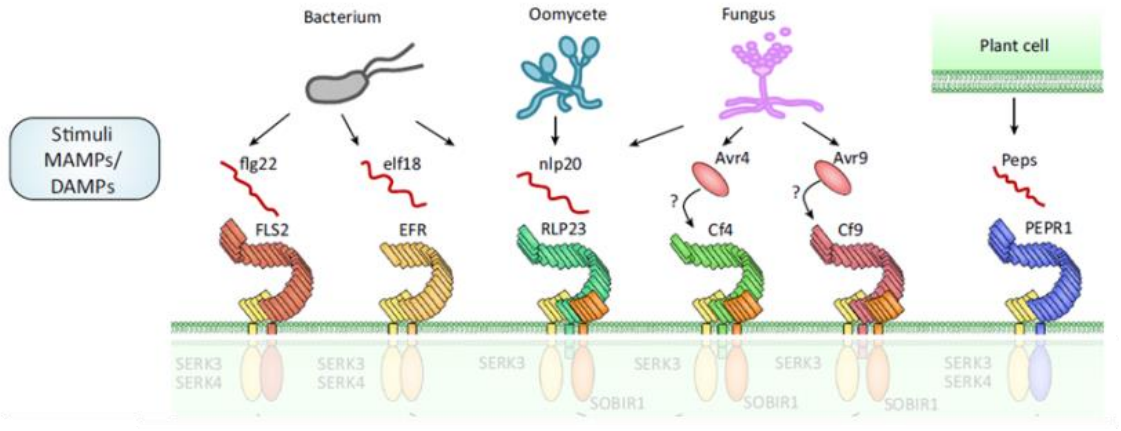

Figure 1.3: PRRs perceive non-host signals from different pathogens

Depending on the extracellular domain of the PRR, plants perceive ligands with different biochemical characteristics in order to transmit the signal to the inner part of the cell (Ma et al., 2016) modified.

PRRs, involved in PTI, include different types of transmembrane receptors responsible for the detection of non-specialized pathogens (Boller and Felix, 2009b; Spoel and Dong, 2012; Böhm et al., 2014; Yu et al., 2017). The type of the extracellular domain is decisive for the specificity of binding ligands with different biochemical characteristics (Böhm et al., 2014; Gust et al., 2017; Yu et al., 2017; Wan et al., 2019b). The spectrum of extracellular domains includes Leucine-Rich Repeats (LRRs), Lysin Motifs (LysMs), lectin motifs and Epidermal Growth Factor (EGF)-like domains (Yu et al., 2017). In order to activate defense, plants recognize conserved structures derived from essential features of a certain pathogen. These conserved structures, so-called Microbe- or Pathogen-Associated Molecular Patterns (M/PAMPs) originate from organisms of all kingdoms: microbes ranging from prokaryota to fungi, as well as animals and even parasitic plants (Pieterse et al., 2009; Bigeard et al., 2015; Couto and Zipfel, 2016; Hegenauer et al., 2016; Yu et al., 2017). One prime example is flg22, a 22-amino acid peptide, originating from the most conserved part of the bacterial flagellum from *Pseudomonas* species (Felix et al., 1999; Gómez-Gómez and Boller, 2000). Flg22 is sensed by its corresponding receptor FLAGELLIN-SENSITIVE 2 (FLS2) in a number of higher plants (Gómez-Gómez and Boller, 2000, 2002; Albert et al., 2010). Additionally, plants sense endogenous Danger- or Damage-Associated Molecular Patterns (DAMPs), which can be released passively after disruption of the cell e.g. after wounding of the plant via insects, or actively after processing of precursor molecules upon infection (Boller and Felix, 2009a; Yu et al., 2017). A prominent example for a processed DAMP is the recognition of Atpep1 and

Atpep2, both deriving from the respective precursor PROPEP1 or 2 and recognized by the cell surface located receptors PEP1 RECEPTOR 1 and 2 (PEPR1 and PEPR2) (Huffaker et al., 2006; Yamaguchi et al., 2006; Yamaguchi et al., 2010). These secondary signals were recently renamed as phytocytokines due to the conceptual similarity to metazoan cytokines of being processed peptides, released upon infection (Gust et al., 2017).

1.1.1.2 Receptor – SERK complex

A successful downstream-signaling is strongly dependent on a complex formation between PRRs and their cognate co-receptor which are mainly represented by the members of the SOMATIC EMBRYOGENESIS RECEPTOR-LIKE KINASE (SERK)-family (Chinchilla et al., 2009; Schwessinger et al., 2011; Ma et al., 2016).

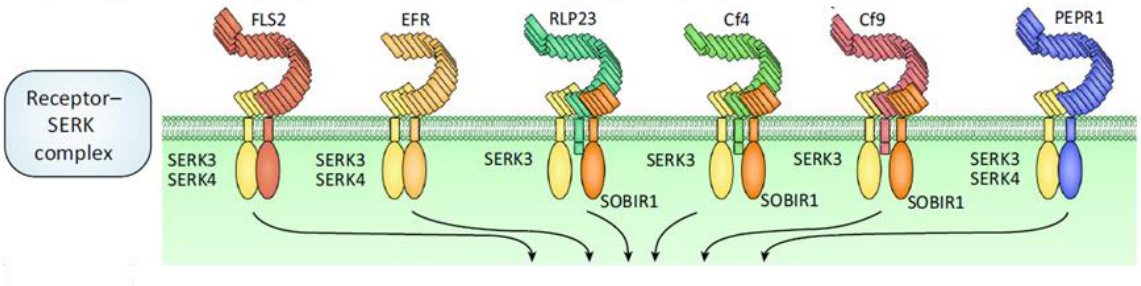

Figure 1.4: PRRs form complexes with SERK proteins for signaling

SERK proteins are recruited to the respective PRR after ligand binding. The receptor-SERK complex leads to phosphorylation events of the kinase domains, leading to downstream signaling (Ma et al., 2016) modified.

The recruitment to the corresponding receptor happens in most cases ligand-dependent (Brandt and Hothorn, 2016). SERKs count five members in the genome of *A. thaliana*, with BRI1-ASSOCIATED RECEPTOR KINASE (BAK1) as its most characterized relative (Brandt and Hothorn, 2016; He et al., 2018). BAK1 was first described as the co-receptor of the BRASSINOSTEROID INSENSITIVE 1-receptor (BRI1), hence involved in plant development (Li et al., 2002; Nam and Li, 2002). Meanwhile, it was shown that BAK1 represents a multifunctional co-receptor, involved also in many immunity-related pathways, as it is the partner for PTI-receptors such as FLS2 and EF-TU RECEPTOR (EFR) (Chinchilla et al., 2009) as well as for the DAMP-receptors PEPR1 and 2 (Postel et al., 2010). Complex-formation of FLS2 and BAK1 takes place within seconds after elicitation with flg22, leading to subsequent downstream signaling (Boller and Felix, 2009b; Schulze et al., 2010). The signaling is mainly, but not fully dependent on BAK1, as *bak1* null mutants are strongly impaired in responses to flg22, but not fully insensitive. This is explained by the redundancy of the members of the

SERK family, where the closest homolog of BAK1, BKK1/SERK4 can replace BAK1 to some extend (Chinchilla et al., 2007; He et al., 2007; Roux et al., 2011). Furthermore, BAK1-binding is crucial for RLP-signaling, as it was shown amongst others that the complex of RECEPTOR-LIKE PROTEIN 23 (RLP23), constitutively bound to SUPPRESSOR OF BIR1 1 (SOBIR1), forms a ligand-dependent binding with BAK1 in NLP-triggered immunity (Albert et al., 2015). It is proposed that spatial separation through nanodomains, forming receptor/-co-receptor-specific islands in the plasma membrane, together with posttranslational modifications such as specific phosphorylation sites of the SERK proteins are decisive for successful and more over specific signaling in PTI (Schwessinger et al., 2011; Bücherl et al., 2017; Perraki et al., 2018). By contrast, RLKs, containing a LysM- or lectin domain, such as LYSM-CONTAINING RECEPTOR PROTEIN 1/3 (LYM1/LYM3) and LYSM-CONTAINING RECEPTOR-LIKE KINASE 5 (LYK5), recognizing bacterial-derived peptidoglycane (PGN) and fungal-derived chitin, respectively, seem to signal independent of BAK1 (Yu et al., 2017).

Moreover, BAK1 plays a role in cell death control, as the single knock-out alone or in combination with its closest homolog *BKK1*, as well as its overexpression leads to a loss of cell death containment (He et al., 2007; Kemmerling et al., 2007b; Belkhadir et al., 2012; Dominguez-Ferreras et al., 2015). The loss of cell death control is linked to plant immunity and further described in chapter 1.1.3.1.

1.1.1.3 Regulating BAK1 – The BAK1-Interacting Receptor-Like Kinase (BIR) family

BAK1 represents a multifunctional co-receptor and its protein level is decisive for proper signaling as well as for destructive consequences for the plant, as null mutants and overexpressors lead to cell death (He et al., 2007; Kemmerling et al., 2007b; Belkhadir et al., 2012; Dominguez-Ferreras et al., 2015). Therefore balanced receptor levels have to be controlled. To gain insight into the regulation of this multifunctional co-receptor the interactome of BAK1 was analyzed by LC/ESI-MS/MS-analysis. This approach revealed two novel negative regulators of BAK1: BAK1-INTERACTING RECEPTOR-LIKE KINASE 2 and 3 (BIR2 and BIR3) (Halter et al., 2014; Imkampe et al., 2017). BIR-proteins belong to the subfamily Xa of leucine-rich kinases and share a similar structure with BAK1; they contain five leucine-rich repeats, a single-pass transmembrane domain and an intracellular kinase-domain (Chinchilla et al., 2009). BIR1 is the most ancient member within the family, containing a functional kinase domain (Gao et al., 2009b). However, BIR2 and BIR3 are pseudokinases, unable to phosphorylate substrates due to an occluded ATP-binding pocket within the kinase domain

(Blaum et al., 2014; Halter et al., 2014; Imkampe et al., 2017). In contrast to BIR2, no phosphorylation by BAK1 of the BIR3-protein could be observed (Imkampe et al., 2017). All three members (BIR1 to BIR3) bind directly to BAK1, thereby preventing the interaction to ligand-binding receptors (Gao et al., 2009b; Halter et al., 2014; Imkampe et al., 2017). Additionally, BIR3, but neither BIR1 nor BIR2 binds to ligand-binding receptors (Halter et al., 2014; Imkampe et al., 2017; Ma et al., 2017). Hence, all three proteins are negative regulators of BAK1-dependent pathways, showing common features in regulation, but display at the same time distinct differences. BIR2 is a negative regulator in the MAMP-pathway by preventing binding of BAK1 to FLS2 in the absence of a ligand. After ligand binding, BIR2 is released, allowing further downstream signaling (Fig. 1.5) (Halter et al., 2014; Schmidt, 2017). BIR2 is not involved in BRI1-dependent signaling pathways, but is impaired in cell death control when knocked out (Halter et al., 2014).

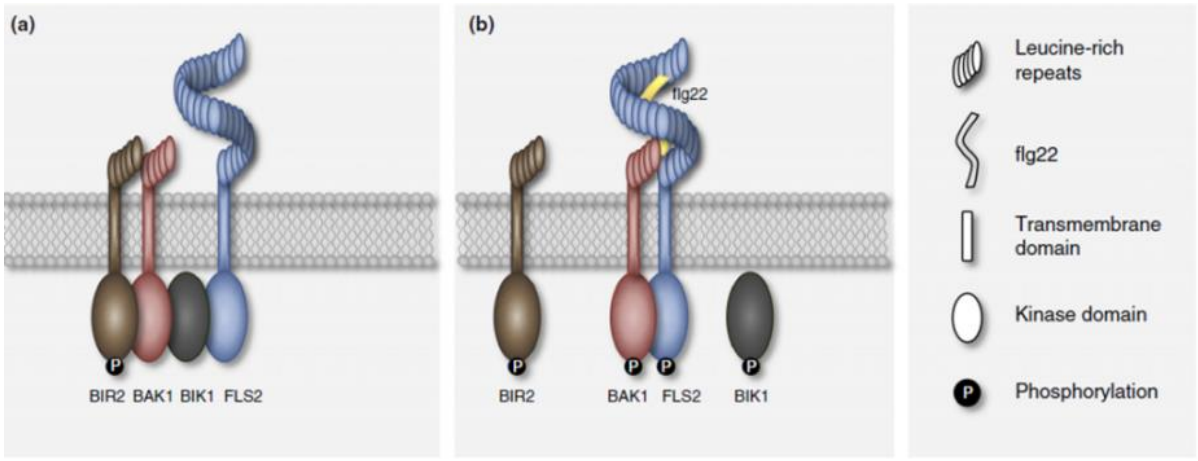

Figure 1.5: BIR2 binds directly to BAK1 to prevent complex formation of BAK1 and FLS2

(a) BIR2 binds constitutively to BAK1 in order to prevent the complex formation of BAK1 and FLS2 in the absence of a pathogen or ligand. (b) After binding of flg22, BIR2 gets released from BAK1, allowing FLS2 and BAK1 to interact. The complex formation ensures subsequent PTI signaling (Böhm et al., 2014).

The negative regulation exerted by BIR3 differs remarkably. It has a strong impact on BRI1-signaling by binding to both, the ligand-binding receptor BRI1 itself and its co-receptor BAK1 (Imkampe et al., 2017). The direct interaction between BIR3 and BRI1 could additionally be confirmed by Großeholz et al. (2020), using Förster resonance energy transfer by fluorescence lifetime imaging (FRET FLIM). In this work in silico-methods were used to get an understanding whether BIR3, BAK1 and BRI1 form a ternary complex or whether BAK1-BIR3 and BRI1-BIR3 interact as independent heterodimers. The results obtained with comparative modeling and molecular docking analysis based on the kinase domains of BIR3, BAK1 and BRI1 indicated that the interaction site of the BIR3-BAK1-complex includes the catalytic site

and the P-loop of BAK1, thus, blocking uncontrolled signaling between BRI1 and BAK1 in the absence of brassinosteroids (Großeholz et al., 2020). Additionally to that, BAK1 has been shown to provide an additional binding site for BRI1, apart from its catalytic site. The second binding site of BAK1 allows a ternary complex without activating the BL-pathway (Großeholz et al., 2020). Only BL-bound BRI1 was able to compete with BIR3 for binding BAK1 (Großeholz et al., 2020), which could also be confirmed by Hohmann et al. (2018), investigating the LRR ectodomains of BIR3, BAK1 and BRI1. In the work of Hohmann et al. (2018), the authors revealed that the surface area of LRRs of SERKs normally used for association with ligand-bound RLKs is also shielded by the LRR-domain of BIR3, thereby preventing interaction, likewise shown *in silico* for the kinase domain of BIR3 by Großeholz et al. (2020). Furthermore, the mode of action of BIR3 is shown to be dose-dependent, as BIR3-overexpression leads to a dwarf phenotype in wild type background, reminiscent of the *bri1* null mutant (Imkampe et al., 2017). This phenotype could be reversed by overexpressing the corresponding receptor BRI1, indicating that the negative regulatory function of BIR3 could be overcome by compensating levels of BRI1, allowing further downstream signaling, resulting in wt-like growth (Fig. 1.6) (Imkampe et al., 2017).

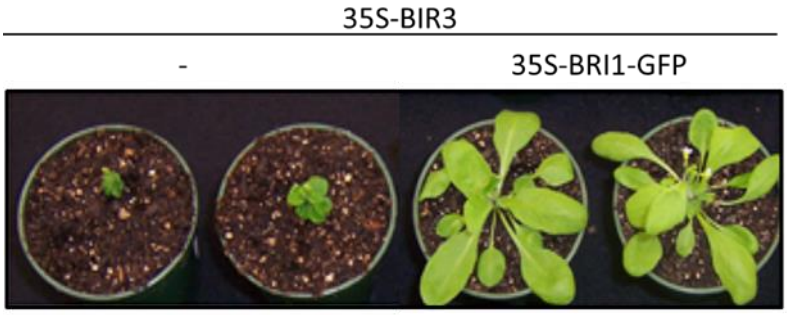

Figure 1.6: The overexpression of BRI1 in the BIR3-overexpressing background compensates the growth phenotype caused by excessive BIR3

The overexpression of BIR3 in the background of Col-0 leads to a dwarf phenotype. This phenotype could be connected to the negative regulation of BIR3 on BRI1, by binding to BRI1 as well as to BAK1. The direct binding could be reversed by overexpression of BRI1, demonstrating a dose-dependent effect of BIR3-signaling (Imkampe et al., 2017).

However, BRI1 is not the only target, BIR3 binds additionally directly to FLS2 to prevent complex formation with BAK1 (Imkampe et al., 2017). Seedling growth-inhibition assays and the measurement of reactive oxygen species (ROS, see chapter 1.1.1.4), confirmed the function of BIR3 of being a negative regulator in MAMP-pathways, likewise dose-dependent. On the basis that BIR3 binds BAK1 in a ligand-independent manner, swapping-domain-experiments of using the LRR- and transmembrane (TM)-domain of BIR3 and the kinase

domain of BAK1-dependent LRR-RLKs, such as FLS2, BRI1, ERECTA (ER) and HAESA (HAE) were conducted. Those chimeras formed tight complexes with endogenous SERK proteins in absence of a ligand and represented gain-of-function mutants for PTI, BL-signaling, stomatal pattering and floral abscission within the respective mutant-line (Hohmann et al., 2020). Benefitting of BIR3 that binds in a ligand-independent manner to BAK1, enabled the authors to show that (i) the ligand-binding specificity is encoded by the ectodomains (LRR domain) and (ii) that the triggered response relies on the kinase domain of the respective RLK and not on the co-receptor (Hohmann et al., 2020). An additional characteristic of BIR3, which differs to BIR2, is its effect on stabilizing BAK1 and its closest homolog BKK1 (Imkampe et al., 2017). *Bir3* null mutants contain less BAK1 protein compared to wild type, while transcript levels are not altered (Imkampe et al., 2017). This feature revealed BIR3 to be a bifunctional protein: it does not only negatively regulate BAK1 and BAK1-involved pathways by preventing their interaction, it also supports the stability of SERK-proteins, positively affecting downstream signaling.

In summary, BIR1, BIR2 and BIR3 have partially overlapping functions in regulating BAK1-dependent pathways and competing for SERKs with ligand-bound receptors (Hohmann et al., 2018; Großeholz et al., 2020; Hohmann et al., 2020). But they also differ in specific characteristics, regarding their contribution to certain pathways, as well as their binding properties to ligand-binding receptors or their ability to phosphorylate (BIR1) or to be phosphorylated (BIR2 but not BIR3) by BAK1. However, BIR3 could be shown to exert a dual role by (i) preventing complex formation by binding to ligand-binding receptors and BAK1 and (ii) the stabilization effect on BAK1/BKK1 which differs from BIR2 and BIR1 so far (Imkampe et al., 2017).

Mis-regulation by members of the BIR-family leading to cell death is an additional feature, which is described in chapter 1.1.3.2 in detail.

1.1.1.4 The signaling relay and output

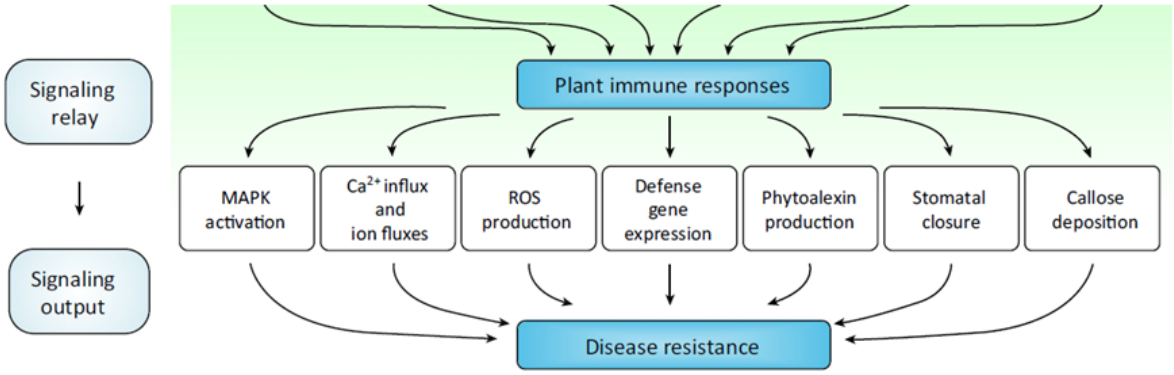

Figure 1.7: Cross talk of cytosolic components leads to PTI and hence the restriction of microbes

The cross talk of intracellular signaling relays leads to the execution of PTI, leading to resistance of the host (Ma et al., 2016) modified.

The signaling relay leading to PTI is characterized by an enormous cross talk of membrane-localized and cytoplasmic proteins / components in order to restrict the growth of pathogenic microbes. This cross talk can be divided in time specific responses which in turn influence each other by positive and negative feedback loops (Boller and Felix, 2009a; Yu et al., 2017). The very early signaling is characterized by a response within five minutes, the early signaling between five and 30 minutes and the late signaling from hours to days (Boller and Felix, 2009a; Yu et al., 2017). The heterodimerization of kinases of an activated receptor-SERK complex leads to subsequent transphosphorylation events in the cytosol. These activated receptor kinase complexes initiate downstream signaling responses via recruitment of cytosolic proteins such as Receptor Like Cytoplasmic Kinases (RLCKs) (Hohmann et al., 2017). Early signaling of PTI after elicitation of PRRs is associated with the activation of Mitogen-Activated Protein Kinases (MAPKs). The so-called MAPK-cascade comprises so far three sequentially phosphorylated kinases, a MAPK Kinase Kinase (MAPKKK), a MAPK Kinase (MAPKK) and a MAP Kinase (MAPK/MPK) (Yu et al., 2017). Stimulation with flg22 is characterized as early response and leads to an increase in AtMAPK6 activity with a lag phase of ~1-2 minutes and culminates after 5-10 minutes (Nühse et al., 2000; Boller and Felix, 2009a; Bigeard et al., 2015). It was shown that the MAPK cascade, activated after flg22 elicitation, regulates the induction of ~1000 and the downregulation of ~200 genes leading to a massive reprogramming of the plant transcriptome (Boller and Felix, 2009a; Bigeard et al., 2015; Yu et al., 2017). This reprogramming includes a switch from growth to defense program, as e.g. auxin responsive genes get downregulated upon flg22 and elf26 treatment (Boller and Felix, 2009a).

Interestingly, the induction of different PRRs, such as FLS2, EFR or CHITIN ELICITOR RECEPTOR KINASE 1 (CERK1) causes the stimulation of an almost similar set of genes, demonstrating a stereotypical gene activation upon D/MAMP treatment, including the upregulation of PRRs, such as FLS2 and EFR, following a positive feedback loop (Boller and Felix, 2009a). The overlapping reprogramming of the transcriptome after elicitation of different PRRs explains why in some ecotypes, such as Ws-0, lacking FLS2, the total fitness of the plant does not suffer from any disadvantage. After flg22-elicitation further RLCKs get activated through phosphorylation by BAK1: e.g. BOTRYTIS-INDUCED KINASE1 (BIK1), leading to an activation of the plasma membrane localized NADPH oxidase RESPIRATORY BURST OXIDASE HOMOLOGUE D (RbohD) (Yu et al., 2017). RbohD conducts, together with cell wall-associated peroxidases, the electron transfer of cytosolic Nicotinamide Adenine Dinucleotide Phosphate (NADPH) or Nicotinamide Adenine Dinucleotide (NADH) to apoplastic oxygen which increases apoplastic Reactive Oxygen Species (ROS). This includes superoxide (O_2^-) which is converted by SUPEROXIDE DISMUTASE (SOD) to hydrogen peroxide (H_2O_2) and hydroxyl radicals (·OH) (Yu et al., 2017). ROS has different measures to restrict the growth of a pathogen as it might act directly as a toxin for invading pathogens, indirectly by strengthening of the cell wall by oxidative cross-linking of polymers and as a signal molecule for further cellular cross-talk (Boller and Felix, 2009a; Yu et al., 2017). As apoplastic ROS increases after a lag phase of about one to two minutes, it belongs to the early signaling events of PTI, temporally similar to membrane depolarization and the change of intracellular and extracellular ion concentrations. The two latter include an efflux of ions such as Cl^-, NO_3^- and K^+ and the influx of H^+ and Ca^{2+}, leading to an alkalization of the extracellular and acidification of the intracellular space (Boller and Felix, 2009a; Jeworutzki et al., 2010; Yu et al., 2017). The regulation of calcium fluxes across the plasma membrane and endomembranes of organelles happens passively *via* Ca^{2+}-channels and actively *via* transporters, such as Ca^{2+}-ATPases and Ca^{2+}-antiporters (Jeworutzki et al., 2010; Yu et al., 2017). The increase of cytosolic Ca^{2+} content differs due to the D/MAMP and its dosage. Flg22 e.g. triggers a biphasic increase, the first initiated by the influx from the apoplast and the second by the mobilization from organelles, whereas chitin displays a single peak (Yu et al., 2017). Phosphorylation events through cytoplasma-located kinases, such as BIK1 or MAP kinases are in close relationship with the cytosolic increase of Ca^{2+}. This crosstalk is exerted by CALCIUM-DEPENDENT PROTEIN KINASEs (CDPKs), as e.g. CPK5 supports flg22-induced ROS bursts by phosphorylation of RbohD on a different phosphorylation site than BIK1 (Yu et

al., 2017). A very important role of PTI is the accumulation of plant hormones due to the regulation of the biosynthesis of Salicylic Acid (SA), Ethylene (ET) and Jasmonic Acid (JA) (Bartels et al., 2013; Bigeard et al., 2015; Genot et al., 2017; Yu et al., 2017). One of the genes induced by flg22, is ISOCHORISMATE SYNTHASE 1 (ICS), which leads to the accumulation of salicylic acid. SA is mainly involved in the defense against biotrophs or hemibiotrophs (Bigeard et al., 2015), likewise ethylene which accumulates about one hour after flg22 treatment by an increased activity of ACC SYNTHASE (ACS) (Boller and Felix, 2009a). Jasmonic acid is a hormone typically produced after an attack of necrotrophic pathogens (Bigeard et al., 2015; Yu et al., 2017). The induction of the different hormones has an impact on the regulation of PTI responses on multiple levels, as e.g. SA regulates the transcription of hundreds of defense-related genes such as PATHOGENESIS-RELATED GENE 1 (PR1), by binding to NONEXPRESSER OF PR GENES 1 (NPR1) (Tsuda et al., 2013). Whereas ethylene contributes together with ROS, to the deposition of callose and the closure of stomata after one hour of D/MAMP treatment (Yu et al., 2017). The first contributes to the strengthening of the cell wall, the latter to close the major entry routes for pathogens. This interplay of temporal and spatial fine-tuning after D/MAMP treatment contributes in its entireness to the containment of disease progression caused by a broad spectrum of pathogens (Boller and Felix, 2009a; Böhm et al., 2014; Bigeard et al., 2015; Gust et al., 2017; Yu et al., 2017; Wan et al., 2019b).

1.1.2 Perception of danger inside the cell (ETI)

Pathogens are also sensed intracellularly, due to the delivery of effectors, which are injected into plant cells by pathogens to increase virulence. The perception of injected effectors via intracellular receptors is referred to as Effector-Triggered Immunity (ETI). ETI is activated by host-adapted pathogens and serves to avoid the spread of pathogens which rely on a biotrophic lifestyle and therefore depend on living host cells (Monteiro and Nishimura, 2018). It is mediated by nucleotide-binding leucine-rich repeat resistance genes (NLRs) in a race-cultivar specific manner (Bent and Mackey, 2007; Yu et al., 2017). In general, NLRs are activated by the presence or the mode of action of translocated effector-proteins injected by the pathogen via a type-III secretion system (Fig. 1.8). These effectors aim to interfere with the PTI-system and their perception is often associated with local cell death also described as hypersensitive response (HR) (Belkhadir et al., 2004; Coll et al., 2011; Bentham et al., 2017). The initiation of local cell death in plant immunity is a powerful tool to ward off

pathogens with a biotrophic lifestyle. Because those organisms rely on a living tissue, local cell death leads also to the restriction of the pathogen.

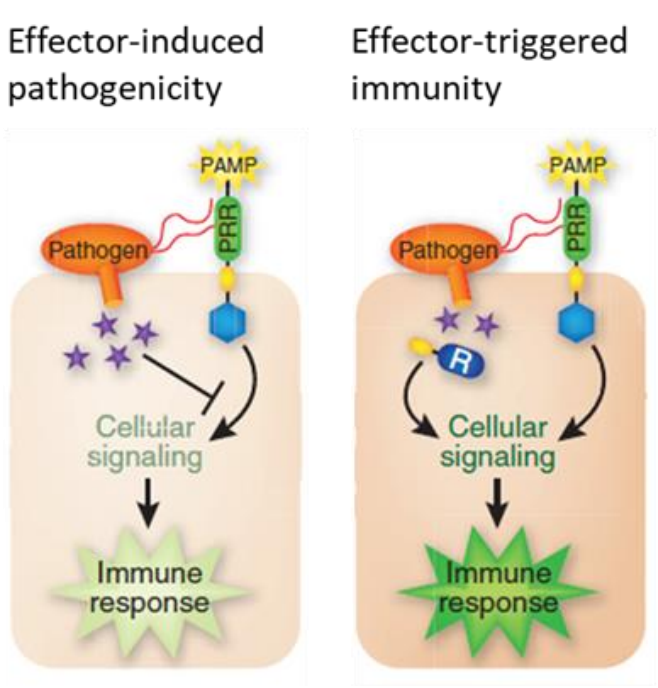

Figure 1.8: NLRs can detect pathogen derived effector molecules

Secreted effectors via the type-III secretion system of a pathogen aim to shut down PTI and to get access to nutrients. This is recognized by intracellular receptors (R) which counteract the pathogen´s attack with a strong immune response called ETI (Pieterse et al., 2009) modified.

NLRs belong to the superfamily of signal transduction ATPases containing numerous domains (STANDs) (Elmore et al., 2011; Bonardi et al., 2012), and can be found from mosses to flowering plants (Sarris et al., 2016). They form the largest group within the group of resistance genes (R-genes) (Yu et al., 2014). R-genes include five major types based on their domain organization: 1) TIR-NB-LRRs (TNLs), 2) Coiled coil-NB-LRRs (CNLs), 3) RLKs, 4) RLPs and 5) serine threonine kinases (Yu et al., 2014). Canonical plant NLR proteins (TNLs, CNLs) are of modular design: they feature typically a variable amino-terminus (N-terminus), a central nucleotide-binding site (NBS) and a carboxyl-terminal (C-terminal) LRR-domain (Monteiro and Nishimura, 2018). The N-terminus is described to be involved in pathogen detection and activation of downstream signaling (Elmore et al., 2011). Furthermore, it is decisive for the classification in three groups: NLRs sharing a homology with the Drosophila toll and human Interleukin-1 receptor are referred to as TNLs, NLRs containing a coiled-coil domain at the N-terminus are abbreviated as CNLs. Both classes show divergence in their sequence, their distribution within the plant kingdom and their signaling pathways (Meyers, 2003; Yu et al., 2014). Recently, a unique subclade of CNLs, referred to as helper NLRs (3rd group) was defined and renamed as RPW8-NB-ARC-LRRs (RNLs), due to the similarity to the coiled-coil N-terminus of RESISTANCE TO POWDERY MILDEW 8 (RPW8) (Jubic et al., 2019). They are supposed to act downstream of TNLs or in parallel with respective CNLs, which are

described in case of paired NLRs as sensor- and executor-NLRs, respectively (Jubic et al., 2019). The sensor-NLR is supposed to detect the effector or the effector´s mode of action, while the executor NLR or the helper NLR is important to translate the recognition into an immune response (Adachi et al., 2019).

The LRR-domain is described to be the interaction platform for effectors, whose recognition either by binding or modification of the horseshoe 3-D-structure of the LRR-domain leads to the activation of the respective NLR (Van Ghelder et al., 2019). However, the intrinsic function of the LRR-region is diverse: some examples describe an endogenous suppressor function, as its deletion causes auto-activity of the respective NLR, such as RESISTANT TO PSEUDOMONAS SYRINGAE 2 (RPS2), RPS5 and RPS6 (Peele et al., 2014). On the other hand, for RESISTANT TO PSEUDOMONAS SYRINGAE 4 (RPS4) it could be shown, that the LRR domain provides a stabilization effect to the TNL and not a suppressor function (Zhang et al., 2004). In conclusion, the intrinsic functions of the N- and C-termini (TIR/CC and LRR) differ in the context of each NLR (Elmore et al., 2011). Effector recognition by NLRs can be direct or indirect by the presence or activity of the respective effector protein (Fig. 1.9A) (DeYoung and Innes, 2006; Coll et al., 2011; Cui et al., 2015; Monteiro and Nishimura, 2018). Direct recognition is characterized by a physical interaction of the effector molecule with the NLR (Elmore et al., 2011). The first direct interaction was reported in rice, describing the NLR *Pi-ta*, recognizing the effector AVR-Pita via its LRR-domain, originating from the fungus *Magnaporthe grisea* (Jia et al., 2000). Indirect recognition, is characterized by monitoring of host proteins (guardees) via the respective NLR / NLR-pair, which act as a guard. One example of an indirect recognition is given by the CNL RESISTANT TO P. SYRINGAE 5 (RPS5), which detects the cleavage of the proteinkinase AVRPPHB SUSCEPTIBLE 1 (PBS1) by the bacterial *Pseudomonas syringae*-effector AvrPphB, a cysteine protease. PBS1 interacts with both RPS5 and the effector AVRPphB, forming a ternary complex (Shao et al., 2002; Shao et al., 2003; DeYoung and Innes, 2006; Sarris et al., 2016). In the guard/decoy model, the guardee can be either a host molecule that is targeted by an effector because of its involvement in plant defense procedures. Or it can be a decoy, mimicking a host target. Either binding or modification of the guardee activates in consequence the NLR (Fig. 1.9B) (Van Der Biezen and Jones, 1998; Sarris et al., 2016). The system of the indirect recognition is extended by the occurrence of specific integrated domains (IDs), shared by 3 – 10% of plant NLRs (Bialas et al., 2018). These IDs represent extraneous domains fused to a NLR and are thought to have evolved from effector targets in order to detect the pathogen´s effector

delivery. Using comparative analysis Sarris et al. (2016) found evidence for NLR-ID fusions already in mosses and across all lineages of flowering plants. IDs can function either as targets of the respective effector or as substrate for its enzymatic activity, leading to NLR activation (Fig. 1.9B / integrated decoy model) (Sarris et al., 2016; Bialas et al., 2018; Grund et al., 2019). They overlap with host targets of effector proteins, including protein kinases, DNA-binding proteins, transcription factors, proteins involved in redox reactions, hormone signaling and proteins involved in the cytoskeleton (Sarris et al., 2016). These cell components, integrated in NLRs, depict hubs, ensuring the integrity of the host and are therefore ideal decoys of effectors, aiming to make nutritive substances available and to dampen the immune system for a successful infection (Boller and Felix, 2009a; Ellis, 2016; Sarris et al., 2016; Grund et al., 2019).

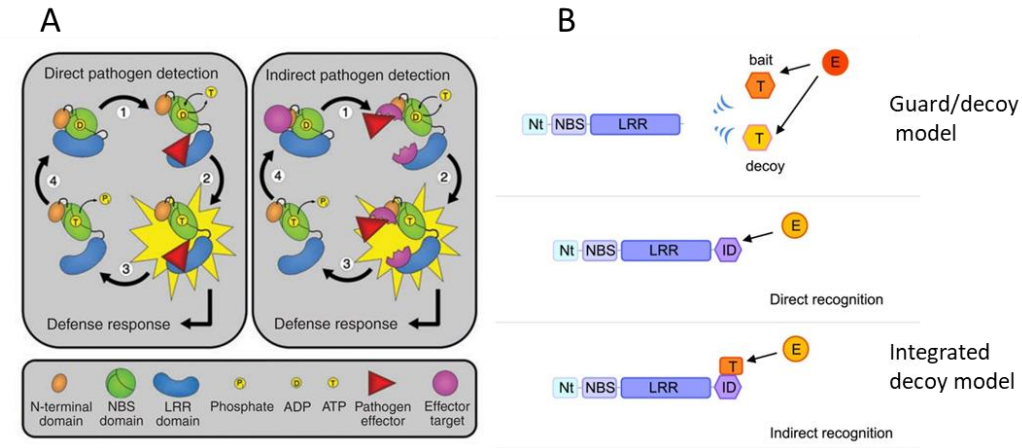

Figure 1.9: Mode of activation of NLRs

A) Direct pathogen detection: (1) the direct binding of the effector to the NLR leads to (2) an exchange of ADP to ATP in the NB-domain which drives (3) the activation of the NLR. Indirect detection: (1) the effector protein binds to a target, which is recognized by the NLR, (2) the modification of the effector target leads to an exchange of ADP to ATP in the NB-domain, leading to (3) the defense response exerted by the NLR. (B) Extended model of indirect detection. The direct interaction is characterized by the interaction of effector and LRR-domain the NLR, leading to the activation of the NLR via the exchange of ADP to ATP. The indirect detection is described by a modification of the effector target (guardee or decoy), which is recognized by the NLR (guard). The indirect model is extended by the recognition of an integrated domain within the NLR, which can be modified by the action of an effector (directly or indirectly), culminating again to the activation of an immune response (DeYoung and Innes, 2006) (Grund et al., 2019) modified.

The fusion of effector targets (ID) into the respective NLR is thought to disrupt its functionality, for which reason it needs to cooperate with a functional partner NLR and form a NLR-pair (Adachi et al., 2019). These NLR-pairs are often genetically linked and oriented in a head-to head manner in the genome (Duxbury et al., 2016; Sarris et al., 2016; Bialas et al., 2018). Thus, the NLR bearing the ID is classified as sensor, responsible for pathogen detection, whereas the signaling-competent, functional partner without ID is named

executor (Bialas et al., 2018; Jubic et al., 2019). The activation of NLRs is connected to an ADP-to ATP exchange, within the NB-domain, leading to a conformational change and activation of the respective NLR (DeYoung and Innes, 2006). Notably, not the hydrolysis of ATP causes the activation, but it is the replacement of ADP ("switch off") to ATP ("switch on") which activates NLRs from a resting state to an active signaling state (Tameling et al., 2006; Gantner et al., 2019). It was shown that the NB-ARC domain was indeed capable to hydrolyze ATP *in vitro* (Tameling et al., 2002), as mutations within conserved motifs that together form the ATP-binding fold of the NB-ARC domain of the tomato NLR I-2 decreased the ability to hydrolyze ATP (thus leading to accumulation of ATP), but did not affect ATP binding. These mutations resulted in auto-activity of the NLR, characterizing the NB-ARC domain as a molecular switch (Tameling et al., 2006). The same molecular mechanism is described for the activation of small G-proteins (DeYoung and Innes, 2006; Tameling et al., 2006). The change due to ATP-binding is supposed to create new binding sites, resulting in e.g. homodimerization of the respective NLR via TIR-domains (Bernoux et al., 2011) and / or binding of downstream partners (Maekawa et al., 2011). In some cases the homodimerization of only the N-terminus is sufficient to activate a HR (TNL Lx / *Linum usitatissimum;* TNL ROQ1 / *N. benthamiana*) (Bernoux et al., 2011; Qi et al., 2018), in others the full length protein is needed for full activation (CNL RPM1 / *Arabidopsis thaliana*) (El Kasmi et al., 2017). Summing this up, canonical NLRs do share on the one hand common architectural structures like the modular design with an N-terminal TIR-/CC-domain, NB- and LRR-domain, but differ considerably with respect to the mode of action, downstream partners and subcellular localization (Chiang and Coaker, 2015).

1.1.2.1 Regulators of NLRs

NLRs are negatively regulated at multiple levels in order to prevent false activation of cell death and metabolically costly immune responses (Deslandes and Rivas, 2012). At the same time, they also have to be stably present to ensure a system which is ready to counteract in case of a pathogenic attack. Therefore, different regulators acting up- and downstream of the NLRs are needed for proper mediation of the immune response.

1.1.2.2 Upstream regulators of NLRs: The HSP90-SGT1-RAR1 complex

In order to ensure downstream signaling after pathogen attack, some NLRs do not only engage in protein interactions contributing to their stabilization (e.g. the LRR-domains of RPS4 and RRS1)(Williams et al., 2014b), they additionally rely on a conserved chaperone complex. This complex is formed by HEAT SHOCK PROTEIN90 (HSP90) and its co-chaperones REQUIRED FOR MLA12 RESISTANCE 1 (RAR1) and SUPPRESSOR OF G2 ALLELE OF S PHASE KINASE-ASSOCIATED PROTEIN 1 (SGT1) (Elmore et al., 2011). Notably, RAR1 acts as a positive regulator of NLR accumulation, whereas SGT1 can influence both directions of NLR-stability (Elmore and Coaker, 2011). In case of the TNL SUPPRESSOR OF NPR1-1, CONSTITUTIVE 1 (SNC1), SGT1b promotes the proteasomal degradation, as it can associate with components of the Skp, Cullin, F-box (SCF)-ubiquitin ligase complex (Elmore and Coaker, 2011). Contrary to SNC1, SGT1b positively regulates the presence of the TNL CHILLING SENSITIVE 3 (CHS3), as it supports together with HSP90 and RAR1 the proper assembly of the CHS3-protein and its genetically linked partner CONSTITUTIVE SHADE AVOIDANCE1 (CSA1) (Xu et al., 2015). Studies indicate that the ternary complex with the stoichiometry of $SGT1_2$-$HSP90_2$-$RAR1_1$ (Fig. 1.10) is not only able to ensure a proper assembly of NLRs by influencing the oligomerization, it can bind to two NLRs simultaneously and thus promotes the activation of the respective NLRs, as the signaling of some NLRs is accompanied by homodimerization, such as e.g. RPS4 (Zhang et al., 2010; Siligardi et al., 2018b; Guo et al., 2019).

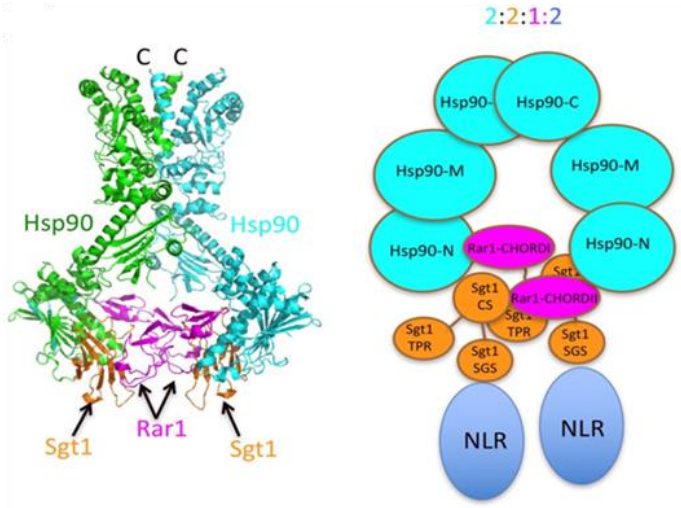

Figure 1.10: Structure and cartoon of the HSP90-SGT1-RAR1 complex

The chaperone complex with the stoichiometry of 2:2:1 ($HSP90_2$-$SGT1_2$-$RAR1_1$) allows a proper assembly of NLRs and is capable of binding two NLRs at the same time, thereby supporting the oligomerization of both (Siligardi et al., 2018a).

Hence, the chaperone complex of HSP90-RAR1-SGT1b is on the one hand important for a proper NLR-turnover and therefore for a balanced NLR-level and on the other hand for some

NLRs important for supporting the activation via promoting the homodimerization in order to ensure ETI-signaling when needed.

1.1.2.3 Downstream regulators of NLRs

1.1.2.3.1 Signaling hubs in NLR signaling: NDR1 and EDS1

NLRs deploy different downstream signaling components depending on the type (TNL or CNL). NLRs bearing the coiled coil domain (CNLs) tend to signal via NON RACE-SPECIFIC DISEASE RESISTANCE 1 (NDR1) (Century et al., 1997), whereas so far, all tested TIR-domain containing NLRs (TNLs) require ENHANCED DISEASE SUSCEPTIBILITY 1 (EDS1) for mediating an immune response (Parker et al., 1996; Aarts et al., 1998; Elmore et al., 2011). Both, NDR1- and EDS1-signaling lead to an accumulation of SA (McDowell et al., 2000). Because of a glycophosphatidyl-inositol (GPI)-anchor, NDR1 is a plasma membrane attached protein which is required for the activation of the three CNLs, RPS2, RPM1 and RPS5 so far (Coppinger et al., 2004). Additionally it could be shown that NDR1 binds directly to RPM1 INTERACTING PROTEIN 4 (RIN4), mediating the activation of RPS2 (Day et al., 2006). These findings suggest NDR1 to exert its role in CNL-mediating resistance, by directing interacting proteins toward the plasma membrane for fulfilling their function in plant immunity. EDS1 instead represents the key hub between TNL activation and the induction of defense responses (Wiermer et al., 2005; Heidrich et al., 2011; Lapin et al., 2019). EDS1 is a member of a protein family which is characterized by a lipase-like domain (α/β-hydrolases) at their N-terminus and an EDS1-PAD4-domain (EP-domain) at their C-terminus (Gantner et al., 2019). EDS1 builds mutually exclusive heterodimers with two proteins, sharing the same domain structure: ARABIDOPSIS PHYTOALEXIN DEFICIENT 4 (PAD4) and SENESCENCE-ASSOCIATED GENE 101 (SAG101) with distinctive implications to plant immunity (Gantner et al., 2019; Lapin et al., 2019). Due to the shared lipase-like and EP-domain, all three proteins (EDS1, SAG101 and PAD4) are defined as the EDS1 family (Wagner et al., 2013; Gantner et al., 2019). Crystal structure analyses of EDS1 revealed recently that the protein forms stable monomers, representing an inactive ground state. The heterodimers, either formed by PAD4/EDS1 or SAG101/EDS1, oligomerize upon NLR-signaling and represent the activation state (Voss et al., 2019) by providing the platform for immune responses (Bhandari et al., 2019; Gantner et al., 2019; Lapin et al., 2019). Interaction assays combined with cell fractionation claimed a differential subcellular distribution of the respective EDS1-complex. While the EDS1/PAD4 dimer was detected in the cytosol as well as in the nucleus, the dimer

of EDS1 and SAG101 could only be detected in the nucleus (Feys et al., 2005). The complex of EDS1 and PAD4 in Arabidopsis is described to support basal immunity by activating transcriptional reprogramming towards a distinct SA-induced defense (by e.g. promoting the expression of ICS1, leading to SA-accumulation) without induction of host cell death (Cui et al., 2017). In contrast, the complex of EDS1 and SAG101 was shown to act as a molecular module leading to cell death, once the TNL-signaling upstream of EDS1 and partners is activated (Lapin et al., 2019). Notably the cell death induction could not be recapitulated when PAD4 was used as signaling partner, underlining the distinctive signaling pathways, depending on the composition of the EDS1 complex in Arabidopsis (Lapin et al., 2019). Moreover, two recent publications showed that the heterodimerization of EDS1 with its family members in TNL signaling differs at least between Brassicaceae and *Nicotiana benthamiana* (Gantner et al., 2019). It was shown that TNL-signaling in *N. benthamiana* mainly relies on the EDS1-SAG101 complex for mediating resistance as PAD4 did not contribute to immunity in tobacco, while, in Brassicaceae, the complex of EDS1 and PAD4 is mainly used for transmitting a basal resistance and for signaling downstream of TNL-mediated immunity, which the authors claimed as an exception in plants (Gantner et al., 2019). These findings showed that EDS1 forms species-specific complexes with the family members PAD4 or SAG101, demonstrating that the specific heterodimer is decisive for the output. To be precise, the EDS1/PAD4 heterodimer and the heterodimer of EDS1/SAG101 form different cavities based on their respective EP-domain after hetero-dimerization and thus have a different impact on signaling (Lapin et al., 2019). How NLRs initiate downstream signaling remains still elusive, but new findings implicate TIR-domains of NLRs as NAD^+-depleting enzymes. This enzymatic activity is dependent on the self-association of the TIR-domains and produces small molecules like cyclic ADP-ribose (cADPR). Those small molecules are supposed to bind to the specifically formed cleft occurring in the EDS1/SAG101 complex, leading to cell death formation (Wan et al., 2019a). How exactly the cascade of downstream signaling culminating in cell death follows after heterodimerization is however still not determined. It was shown that EDS1 is also able to interact directly with the TNL RPS4 and its corresponding effector AvrRPS4, thus representing an effector target (Heidrich et al., 2011). Heidrich et al. (2011) proposed different outputs depending on the subcellular localization: translocated to the nucleus, the EDS1/RPS4 complex triggers a transcriptional reprogramming leading to the amplification of defense responses and thereby resistance to the pathogen, while a localization in the cytoplasm leads to cell death

formation in order to ward off the pathogen. Both compartment-dependent resistance outputs are described to be independent from each other and claimed EDS1 of being a nucleo-cytoplasmic regulator with different signaling capacities due to its subcellular location (Heidrich et al., 2011).

1.1.2.3.2 Helper NLRs

Helper NLRs (hNLRs) are supposed to act downstream or in parallel with canonical NLRs in order to transmit the signal of a host-adapted pathogen. Whereas in Arabidopsis roughly 150 canonical NLRs are described (Meyers, 2003; Yu et al., 2014), only two families with a total number of seven members function as helper NLRs (hNLRs): the ACTIVATED DISEASE RESISTANCE 1 (ADR1) family, containing four paralogs and the N REQUIREMENT GENE 1 (NRG1) family with three paralogs (Bonardi et al., 2011; Castel et al., 2019; Jubic et al., 2019). Strikingly, members of the ADR1 family were found in all flowering plants, whereas members of the NRG1-family are lacking in those clades also lacking TNLs, such as monocots, lamiales and early diverged dicots (Collier et al., 2011; Van Ghelder et al., 2019). In Arabidopsis, both family members share a typical N-terminus, comparable with the CC-domain of RESISTANCE TO POWDERY MILDEW 8 (RPW8) and are thus referred to as RNLs (Collier et al., 2011; Jubic et al., 2019). Furthermore, protein structure prediction identified a domain with similarity to fungal HELL / HeLo-domains responsible for executing cell death when two genetically distinct strains of the filamentous fungus *Podospora anserina* have contact (Seuring et al., 2012). This HELL / HeLo-domain shares sequence homology to the mammalian Mixed Lineage Kinase domain-like protein (MLKL-) domain, which is also involved in cell death formation by forming a four-helical bundle (4HB), predicted to insert into the plasma membrane (Seuring et al., 2012; Robinson, 2015). The insertion comes along with forming pores after oligomerization and either leads to a decline of the membrane integrity or creates a putative cation channel (Jubic et al., 2019). If this is also true for RNLs and if or how they oligomerize are still open questions. Recent studies showed that the type of canonical NLR directs the usage of the respective RNL (Fig. 1.11). So far, all tested TNLs signal via hNLRs (ADR1s, NRG1s), whereas CNLs can function independently or in parallel with the ADRs (Castel et al., 2019; Jubic et al., 2019).

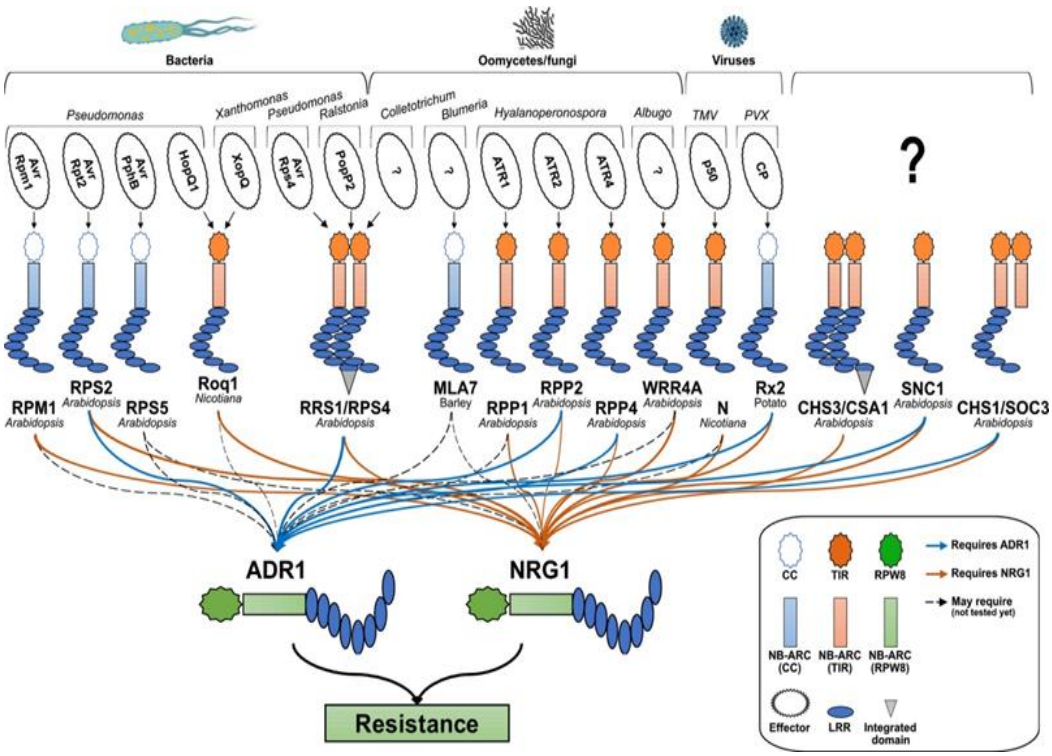

Figure 1.11: Different canonical NLRs use different helper NLRs to mediate downstream signaling

The signaling of some canonical NLRs is dependent exclusively on the helper NLR N REQUIREMENT GENE 1 (NRG1) or ACTIVATED DISEASE RESISTANCE 1 (ADR1). Some NLRs need both for full activation and some do not need any helper NLR for fulfilling their function (Castel et al., 2019).

Not all NLRs conferring resistance to bacteria also trigger an HR, such as AvrRps4, recognized by the NLR-pair RRS1/RPS4 in Arabidopsis (Guo et al., 2019; Lapin et al., 2019). Moreover, the CNL RPS2, activated by AvrRpt2, revealed ADR1 to be required for SA-signaling (Bonardi et al., 2011) which could recently be connected to EDS1, despite the dogma that CNLs are signaling via NDR1 (Bhandari et al., 2019). Lapin et al. (2019) postulated finally that EDS1-SAG101 and NRG1 co-evolved as functional TNL-dependent cell-death-module and that NRG1 acts downstream of EDS1 (Fig. 1.12). However, similar to canonical NLRs, also RNL-mediated responses are poorly defined in ETI-signaling and need further investigations.

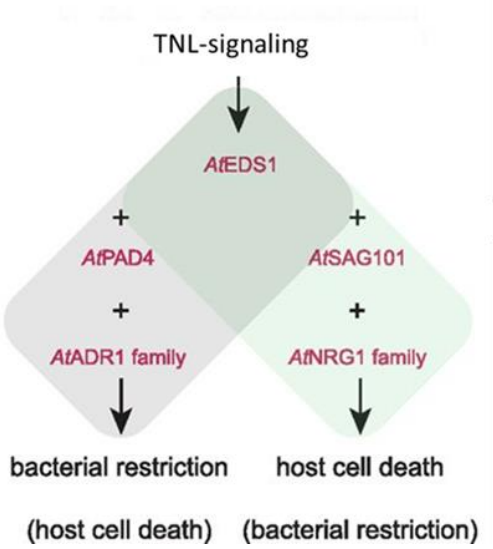

Figure 1.12: Early TNL signaling complexes (EDS1/PAD4 or EDS1/SAG101) define the immune response

The heterodimer of EDS1/PAD4 directs plant immunity toward anti-microbial pathways by e.g. supporting the accumulation of cellular SA, leading to bacterial restriction. The heterodimer of EDS1/SAG101 instead leads to the execution of local cell death in the host in order to prevent bacterial growth (Lapin et al., 2019) modified**.**

1.1.3 Cell death regulation by BAK1 and members of the BIR family

The initiation of cell death has several implications for plant development and responses to biotic and abiotic stresses. The development of cells, like e.g. the forming of male and female parts of a flower, as well as the formation of specific tissue in the plant such as xylem and sclerenchyma cells are controlled by a programmed cell death (PCD) (Buchanan et al., 2015). PCD in response to biotic stresses is often equated with the hypersensitive response and compared with inflammatory cell death types of animals such as the necroptosis or vacuolar cell death of the plant (Coll et al., 2011; Van Doorn et al., 2011). Whereas during vacuolar cell death, cell contents get removed by autophagy-like processes and released hydrolases of the collapsed vacuole, the necroptosis is characterized by a loss of plasma membrane integrity and shrinkage of the protoplast (Van Doorn et al., 2011). Cell death with regards to biotic stresses is often related to SERK-proteins, especially to BAK1 (and its closest homolog BKK1) (He et al., 2007; Kemmerling et al., 2007b; Dominguez-Ferreras et al., 2015; Gao et al., 2018). The BAK1-interacting receptor-like kinases BIR1 to BIR3 are also involved in plant immunity as well as in development, by negatively regulating BAK1 and BAK1-dependent pathways. Also here autoimmune phenotypes to different extends could be observed, when knocked out with or without *BAK1* (Fig. 1.13) (Gao et al., 2009a; Halter et al., 2014; Imkampe, 2015; Imkampe et al., 2017).

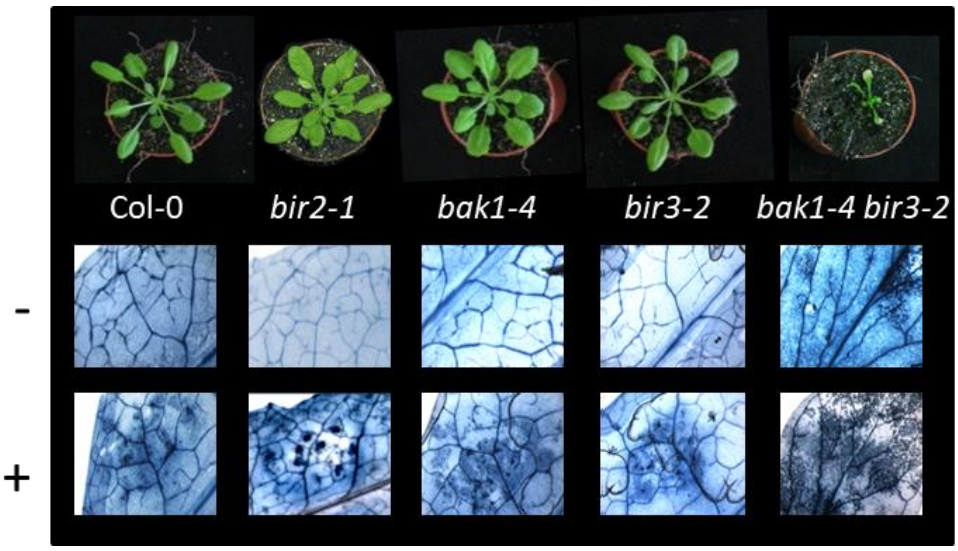

Figure 1.13: Gradual differences of cell death within the BIR-family and BAK1

The double knock-out mutant *bak1-4bir3-2* shows the strongest degree of cell death, followed by *bir2-1* and *bak1-4*, compared to wild type Col-0 in uninfected plants and when inoculated with the necrotrophic fungus *Alternaria brassicicola* visualized by trypan blue staining of dead cells in leaves 4 days after inoculation with *A. brassicicola* (+) or untreated (-). (Imkampe et al., 2017) modified and complemented with *bir2-1.*

1.1.3.1 Cell death regulation by BAK1

Both, the loss as well as the overexpression of BAK1 leads to cell death (He et al., 2007; Kemmerling et al., 2007b; Belkhadir et al., 2012; Dominguez-Ferreras et al., 2015). The overexpression of BAK1 in Arabidopsis causes a stunted growth phenotype, leaf necrosis and premature cell death due to a constitutive activation of defense responses (Dominguez-Ferreras et al., 2015). The phenotype of the *bak1*-single knock-out shows instead a slightly smaller rosette diameter compared to wild type, which is related to the insensitivity to the hormone brassinosteroid (BL) (Nam and Li, 2002; Kemmerling et al., 2007b). This BL-insensitivity was shown to be independent of the loss of cell death control, as exogenous BL complementation restored the growth phenotype but not the cell death phenotype observed in *bak1* mutants (He et al., 2007; Kemmerling et al., 2007b). Furthermore, it could be shown, that the double mutant of *bak1* and its closest homolog *bkk1/serk4* shows seedling lethality after two weeks of cultivation (He et al., 2007; Boller and Felix, 2009a). A recent study on the Ca^{2+}-channels CYCLIC NUCLEOTIDE GATED CHANNEL 19 and 20 (CNGC19/20) revealed, how the cell death in the double mutant of *bak1/bkk1* is partially regulated. Yu et al. (2019) demonstrated that the phosphorylation of CNGC19/20 via BAK1/BKK1 causes the degradation of the channel, thereby preventing a Ca^{2+}-influx and thus supporting the survival of the plant. Conversely, the loss of both SERK proteins causes the loss of phosphorylated CNGC19/20, leading to an intracellular accumulation of Ca^{2+} due to a

higher channel abundance with cell death as consequence (Yu et al., 2019). As mentioned before, BAK1-related cell death is correlated with its protein level, as the overexpression leads to an autoimmune phenotype due to constitutive activation of immune responses (Belkhadir et al., 2012; Dominguez-Ferreras et al., 2015). A suppressor screen revealed that the overexpression of *BAK1* is not only a consequence of overshooting PRR activation as the knock-out of *sobir1* rescued the *BAK1*-overexpressing phenotype (Dominguez-Ferreras et al., 2015). Additionally to that, the mutant line *bak1-5*, only impaired in PTI-responses, does not show cell death when crossed with *bkk1-1*, confirming the observation that BAK1-mediated PTI and BAK1-mediated cell death belong to two distinct pathways (Schwessinger et al., 2011; Gao et al., 2017). Interestingly, Dominguez-Ferreras et al. (2015) could only detect BIR1 and BIR3, but not BIR2 in complex with BAK1, when purifying BAK1-immunoprecipitated complexes from seedlings. Using a truncated protein of BAK1, containing the extracellular and transmembrane domain under a strong promoter, they additionally observed a constitutive activation of immune responses. The authors speculated that the truncated BAK1 protein forms complexes with negative regulators of BAK1, such as members of the BIR-family, which in turn increases the pool of endogenous free BAK1, equally to BAK1-overexpressors. Furthermore, a low-expressed truncated BAK1-protein, containing the LRR and transmembrane domain instead, outcompeted endogenous BAK1, leading to the inhibition of PTI (Dominguez-Ferreras et al., 2015). The idea that well-balanced receptor levels of BAK1 are important for maintaining a proper development of a plant is supported by Zhou et al. (2019), who could show, that BAK1 is proteolytically processed by a Ca^{2+}-dependent protease, cleaving BAK1. This was claimed as a novel mechanism to regulate BAK1-levels and BAK1-dependent pathways, preventing harmful BAK1-accumulations, when reaching a certain threshold value (Zhou et al., 2019). In accordance with Dominguez-Ferreras et al. (2015), who showed that BAK1-overexpressing plants could partially be rescued by the loss of *SOBIR1*, Zhou et al. (2019) could likewise demonstrate that the cell death caused by a cleavage-insensitive BAK1-mutant ($BAK1^{D187A}$) is also SOBIR1-dependent. These studies underline that the well-balanced receptor ratio of BAK1 is pivotal for maintaining cell integrity. As BAK1 is also a target of several effectors (AvrPto, AvrPtoB, HopB1) (Chinchilla et al., 2009; Bigeard et al., 2015; Li et al., 2016) and the effector-triggered cleavage of BAK1 by HopB1 aims to dampen PTI, it was proposed, that BAK1 is probably guarded by an NLR, which might be monitoring the integrity of the kinase domain (Dominguez-Ferreras et al., 2015; Li et al., 2016). This idea could be underpinned by

creating triple knock-out mutants using *eds1* or *pad4* for crossings with the *bak1bkk1*-double-knock-out mutant line. Crossings with *eds1* led to a partial rescue of cell death, whereas the crossing with *pad4* led to a strong reduction of lesion symptoms, indicating that the cell death occurring in *bak1bkk1*-double mutants is likely NLR-mediated (Gao et al., 2017). Furthermore, the authors could show that cell death in the double-mutant *bak1bkk1* is partially SA-dependent as crossings with SALICYLIC ACID INDUCTION DEFICIENT 2/ISOCHORISMATE SYNTHASE 1 (*sid2/ics1*) or ENHANCED DISEASE SUSCEPTIBILITY 5 (*eds5*), two chloroplast-localized SA-mediators, important for the accumulation of the hormone, led to a partial suppression of cell death symptoms as well. Interestingly, additive crossings to *bak1bkk1sid1*-crossings with either *eds1* or *pad4* contributed to an additive suppression of the cell death (Gao et al., 2017). Crossings with *ndr1* did not alter any cell death symptoms of the *bak1bkk1*-autoimmune phenotype, confirming the idea, that rather a TNL-type of resistance gene than a CNL-type NLR is involved in mediating cell death in the double mutant *bak1bkk1* (Gao et al., 2017).

1.1.3.2 Cell death regulation by members of the BIR family

1.1.3.2.1 BIR1

Bir1-mutant-lines show seedling lethality at 22°C, elevated SA-level, constitutive expression of PATHOGENESIS-RELATED GENE 1 and 2 (PR1 and 2) and enhanced resistance to the obligate biotrophic pathogen *Hyaloperonospora parasitica noco 2* (Gao et al., 2009b). This autoimmune phenotype can be partially reverted when grown at 28°C, as the plants show e.g. reduced PR1/2-expression. Furthermore, a complete life cycle including seed production could be restored by cultivation at 28°C (Gao et al., 2009a). It was shown that BIR1 interacts with all SERK-proteins but not with ligand-binding receptors, such as BRI1, FLS2 and CLAVATA 1 (CLV1) (Gao et al., 2009a). Crossings with the null-mutants *sobir1*, *pad4, eds1* or *ndr1* led to a partial rescue in the respective double-mutant with *bir1.* A full restoration back to wild type could be obtained in the triple-mutant *bir1sobir1pad4* (Gao et al., 2009a). So far no interaction of BIR1 with SOBIR1 could be observed. Crossings with loss-of-function mutants of the SA-biosynthesis, such as ENHANCED DISEASE SUSCEPTIBILITY 5 (*eds5*) and SALICYLIC ACID INDUCTION DEFICIENT1 (*sid1*), as well as NONEXPRESSER OF PR GENES 1 (*npr1*), showed partial rescue with reduced H_2O_2 and PR1-levels, demonstrating a SA-dependency in *bir1*-null mutants (Gao et al., 2009a). As the triple-mutant of *bir1sobir1pad4* is bigger than the double-mutant of *bir1sobir1* or *bir1pad4* compared to *bir1*-single mutants,

it seems that SOBIR1 and PAD4 act in parallel as positive regulators of a BIR1-dependent cell death, probably guarded by at least two independent R-genes (Gao et al., 2009b). Later work on BIR1, revealed that BIR1 interacts with the phospholipid-binding protein BONZAI 1 (BON1), additionally to BAK1 and that the cell death phenotype due to the loss of *BIR1* and/or *BON1* is connected to the TNL SUPPRESSOR OF NPR1-1, CONSTITUTIVE 1 (SNC1), which gets activated when both are absent (Wang et al., 2011). The idea of Gao et al. (2009a), proposing at least two different R-mediated pathways, one exerted by a TNL (at least SNC1), signaling via EDS1 and PAD4 and the second by SOBIR1, were supported for the first one, as *bon1*-mutants crossed with *pad4* and *eds1*, showed similar results as *bir1pad4* and *bir1eds1*-double mutants (Wang et al., 2011). The cell death pathway exerted by SOBIR1, could be connected to the negative regulation of BIR1 to BAK1. Interaction analyses revealed that BAK1 only associates with SOBIR1 in the absence of BIR1, leading to cell death exerted by a BAK1/SOBIR1 association (Liu et al., 2016). The autoimmune phenotype of *bir1* was partially suppressed by the lack of *BAK1* (Liu et al., 2016), which could also be confirmed by Wierzba and Tax (2016). Furthermore the triple-mutant line *bir1bak1pad4* were bigger than the double mutant line *bir1bak1*, which is in line with Gao et al., showing that *bir1sobir1pad4* are also bigger than *bir1sobir1* which is why they are proposing at least two independent signaling pathways (Gao et al., 2009a; Liu et al., 2016). Additionally, it could be shown that *BIR1*-overexpressing lines also lead to premature cell death, correlated with constitutive activation of immune responses (Guzmán-Benito et al., 2019). This demonstrates that mis-regulated BIR1-levels result in constitutive defense responses, thereby negatively influencing the fitness of the plant (Guzmán-Benito et al., 2019). The exact mechanism of cell death regulation by BIR1 is still elusive.

1.1.3.2.2 BIR2

BIR2 is a negative regulator of PTI by binding to and negatively regulating BAK1 (Halter et al., 2014). Additionally to that*, bir2*-mutants reveal elevated cell death formation when treated with *A. brassicicola,* observed by subsequent staining with trypan blue. In order to classify the cell death occurring in *bir2*-mutants, double-mutants with mutant-lines of *snc1, pad4* and *nahG*, a salicylate hydroxylase, were generated (Imkampe, 2015). Subsequent infection assays with *A. brassicicola*, revealed no alteration compared to wild type in the *bir2snc1*- and *bir2pad4*-mutant lines. Only the crossing with *nahG* led to a restriction of cell death, demonstrating that the cell death in *bir2*-mutants is SA-dependent (Imkampe, 2015). It could be shown that the loss of *bir2* as well as the overexpression leads to a higher disease index

after treatment with *A. brassicicola*, demonstrating similar to BIR1 and BAK1, that the relative amount of BIR2 is decisive for maintaining or loss of cell death containment (Belkhadir et al., 2012; Halter et al., 2014; Dominguez-Ferreras et al., 2015; Imkampe, 2015).

1.1.3.2.3 BIR3

In contrast to BIR1 and 2, the knock-out of *BIR3* has no impact on cell death when treated with *A. brassicicola* compared to wild type. Surprisingly, the double knock-out of *bak1bir3* leads to a strong loss of cell-death-containment, including elevated levels of the stress hormones SA and JA, the induction of PR1 and PDF1.2, and remarkably also the loss of fertility (Imkampe et al., 2017). Double mutants show seedling lethality at 22°C and cannot be rescued by the cultivation at 28°C. Additionally, overexpressing lines of BIR3 show a higher disease index after *A. brassicicola* infection (Imkampe et al., 2017). So far, the molecular mechanism underlying the cell death in the double mutant line is still elusive.

1.2 Aim of the thesis

BIR3 prevents BAK1 complex formation with ligand-binding receptors in the absence of a ligand. The presence and balanced levels of BIR3 and BAK1 are necessary to prevent cell death. To study how BIR3 adds to the cell death control and how it exerts its receptor regulatory function, we used ESI-LC-MS/MS in order to identify further components of the interactome of BIR3. We focused on (i) additional RLKs which would indicate that BIR3 might be a general regulator of receptor kinases (RLKs) and (ii) candidates which might be involved in cell death. The latter were of strong interest as they could help elucidating the molecular mechanism underlying the cell death containment mediated by BAK1 or the BIR-family.

2 Material and Methods

2.1 Materials

2.1.1 Media and Antibiotics

The composition of used media is listed in the following table. After dissolution of the indicated components with ultrapure water (MQ water), each solution was autoclaved at 121°C.

Table 2.1: Components of different media used for cultivation of bacterial and plant material

Medium	Components
LB	10 g/l Bacto-Trypton, 5 g/l Bacto-Yeast extract, 5 g/l NaCl, to solidify add 15 g/l Agar
SOC	2.0 g/l Trypton, 0.5 g/l Yeast extract, 10 mM NaCl, 2.5 mM KCl, 10 mM $MgCl_2$, 10 mM $MgSO_4$, 20 mM Glucose, set pH 7 with NaOH
½ MS	2.2 g/l MS-salts (Duchefa), 1% sucrose when indicated, set pH 5.7 with KOH, to solidify add 8 g/l Select-Agar

All antibiotics (table 2.2) were added with following concentrations when the media were cooled down to a temperature of ~60°C.

Table 2.2: Antibiotics used for the preparation of different media

Antibiotic	Stock	Final concentration	Solvent
Kanamycin	50 mg/ml	50 µg/ml	Water
Rifampicin	12,5 mg/ml	50 µg/ml	Methanol
Spectinomycin	50 mg/ml	100 µg/ml	Water
Gentamycin	10 mg/ml	25 µg/ml	Water
Carbenicillin	50 mg/ml	50 µg/ml	Water
Hygromycin	50mg/ml	40-50 µg/ml	Water

2.1.2 Bacterial strains

The *Escherichia coli* strain DH5α was used for all cloning experiments and amplification of the respective vectors. The *Agrobacterium tumefaciens* strain GV3101 was used for protein expression in *Nicotiana benthamiana*-plants.

Table 2.3: Bacterial strains

Strain	Genotype
E. coli strain DH5α	(F-(Φ80lacZΔM15) Δ(lacZYA-argF) U169 recA1 endA1 hsdR17 (rK–, mK+) phoA supE44 λ– thi-1 gyrA96 relA1))
A. tumefaciens strain GV3101	T-DNA- vir+ rifr, pMP90 genr

2.1.3 Plasmids

Table 2.4: List of plasmids

Plasmid	Features	Reference
pB7FWG2 BIR3	Expression of 35S-BIR3-eGFP *in planta*	This work
pB7FWG2 BAK1	Expression of 35S-BAK1-eGFP *in planta*	This work
pB7FWG2 BKK1	Expression of 35S-BKK1-eGFP *in planta*	This work
pBINAR eGFP	Expression of 35S-eGFP *in planta*	Obtained by Andreas Wachter
pGWB17 BIR3	Expression of 35S-BIR3-4xmyc *in planta*	This work
pGWB17 EFR	Expression of 35S-EFR-4xmyc *in planta*	Imkampe, 2017
pGWB17 PEPR1	Expression of 35S-PEPR1-4xmyc *in planta*	This work
pUSER-FR	Expression of 35S-CSA1-V5 *in planta*	Obtained by Volkan Cevik
pUSER-FR	Expression of 35S-CHS3-V5 *in planta*	Obtained by Volkan Cevik

2.1.4 Primers

All primers were designed using OligoCalc-Software and ordered by GATC. The lyophilized pellet was diluted to a final concentration of 100 µM. The working solution was diluted to a final concentration of 100 pmol/µl in nuclease-free water

Table 2.5: List of oligonucleotides

Name	Sequence 5'→ 3'	Characteristics
At1g27190 F3	CTCGCCGGTGAGATTCCTGAGTCTCTTA	Genotyping *bir3-2*
At1g27190 R3	ACAGACAAAGGCTTTTGCCCTGTAACCA	Genotyping *bir3-2*
bak1-4_LP_SiSa	CATGACATCATCATCATTCGC	Genotyping *bak1-4*
bak1-4_RP_SiSa	ATTTTGCAGTTTTGCCAACAC	Genotyping *bak1-4*
csa1-LP-WT	CATCGCATCGTTTAAGCGCAC	Genotyping *csa1-2*

csa1-RP-WT	tgttgttcattgccccagGAT	Genotyping *csa1-2*
csa1-KO-LB	CGCTTGCTGCAACTCTCTCAGG	Genotyping *csa1-2*
At3g28450F	ttaaataggaagtcgctaaccatgggag	Genotyping *bir2-1*
At3g28450R	acg acc aca aag acc ttt att ccc act a	Genotyping *bir2-1*
GK_8474_fwd	ATAATAACGCTGCGGACATCTACATTTT	Genotyping *bir2-1*
Lba1	TGGTTCACGTAGTGGGCCATCG	Genotyping
At1g73080_f	TCA GTT GTT ATC TGA GCC GTC G	Cloning PEPR1
At1g73080_r	TTC ACA GCG TAG ACC TTT CCG G	Cloning PEPR1

2.1.5 Antibodies

Antibodies were ordered from the respective companies.

Table 2.6: List of primary antibodies

Primary Antibody	Origin	Use	Provider
α-GFP	goat	1:5000	Acris
α-Myc	rabbit	1:5000	Sigma-Aldrich
α-BAK1	rabbit	1:5000	Agrisera
α-FLS2	rabbit	1:2500	Agrisera
α-BIR3	rabbit	1:500	Custom made /Agrisera
α-V5	mouse	1:3000	Sigma-Aldrich
α-BRI1	rabbit	1:3000	Agrisera

Table 2.7: List of secondary antibodies

Secondary Antibody	Conjugated amplifier	Use	Provider
α-goat IgG	HRP	1:10000	Sigma-Aldrich
α-rabbit IgG	HRP	1:75000	Agrisera
α-mouse IgG	HRP	1:5000	Santa Cruz

2.1.6 Plant genotypes

Single knock-out mutants were ordered from the Nottingham Arabidopsis Stock Centre (NASC). Overexpression lines were stable transformed Arabidopsis lines, generated previously (Halter et al., 2014; Imkampe et al., 2017).

Table 2.8: Plant genotypes

Genotype	Mutation	Reference / Source
Col-0	Wild type	
bak1-4	SALK_116202, T-DNA insertion in *bak1* (At4g33430)	Kemmerling, 2007
bir2-1	GABI N 733599, T-DNA insertion in *bir2* (At3g28450)	Halter, 2014
bir3-2	SALK_116632, T-DNA insertion in *bir3* (At1g27190)	Halter, 2014
35S-BIR3-YFP	pB7YWG2-BIR3 transformed in Col-0	Halter, 2014
bak1-4 bir3-2	Crossing of *bak1-4* with *bir3-2*	Imkampe, 2017
csa1-2	SALK_023219, T-DNA insertion in *csa1* (At5g17880)	Faigon-Soverna, 2006
csa1-2 bak1-4	Crossing of *csa1-2* with *bak1-4*	This work
csa1-2 bir2-1	Crossing of *csa1-2* with *bir2-1*	This work
csa1-2 bak1-4 bir3-2	Crossing of *csa1-2* with *bak1-4 and bir3-2*	This work
At5g14210-1	SALK_N673881; T-DNA insertion in At5g14210	This work

2.1.7 Chemicals

Chemicals, used in this work, were purchased from different companies: Sigma-Aldrich, Carl-Roth, Merck, Duchefa or Applichem. Enzymes used for nucleic acid studies (PCR, cloning etc.) were obtained either from Thermo Scientific or NEB Biolabs.

2.2 Methods

2.2.1 DNA-analysis

2.2.1.1 Transformation of *Escherichia coli* (DH5α)

In this work chemical competent *E. coli* cells were used in order to propagate respective transformed plasmids. Vials containing 200 µl-bacteria solution (stored at -80°C) were slowly defrosted on ice. When thawed*, E. coli* were mixed with 2-4 µl plasmid DNA or cloning reaction and kept for 15 minutes on ice. The further conducted heat shock at 42°C for 90 sec was followed by an incubation step on ice for 3 minutes. In order to regenerate, 800 µl SOC-

medium was added to the suspension, followed by an incubation at 37°C, 200 rpm for 1 hour. The suspension was divided into two portions of 200 µl and 800 µl and plated on selective LB-medium containing the appropriate antibiotics. Bacteria were grown over night at 37°C.

2.2.1.2 Transformation of Agrobacterium tumefaciens

Chemical competent Agrobacteria (GV3101) were taken in order to transform vectors for protein expression in tobacco or for stable transformation in *A. thaliana*. Therefore, vials containing 200 µl-bacteria solution (stored at -80°C) were slowly defrosted on ice and subsequently incubated with 1-5 µg of plasmid DNA on ice for 5 minutes, followed by 5 min in liquid nitrogen and further 5 min in 37°C (water bath). LB medium (500 µl) was added to the cells and after a shaking period of 1.5-2 h at 28°C, 180 rpm, the material was spread on selective LB plates (strain has rifampicin and gentamycin resistance). *A. tumefaciens* GV3101 cells were grown at 28°C in order to obtain colonies.

2.2.1.3 Plasmid extraction from bacteria

2 ml of a 5 ml-overnight-culture of *E. coli* cells, containing the plasmid of interest were centrifuged at 13000 rpm at room temperature. According to the protocol of the GeneJET Plasmid Miniprep Kit (Thermo Scientific - #K0503) purified plasmid DNA was isolated. The concentration of the plasmid DNA was determined using the NanoDrop 2000 Spectrophotometer (Peqlab). Long-term storage was done at -20°C.

2.2.1.4 Genomic DNA extraction from plants

The isolation of genomic DNA was conducted according to the Edwards protocol (Edwards et al., 1991). Therefore a frozen middle-sized leaf (liquid nitrogen) was ground together with glass beads (2.85 mm – 3.45 mm / Roth) in the tissue lyzer (TissueLyzer II / Qiagen) for 1 minute in order to obtain leaf powder. 200 µl Edwards buffer (200 mM Tris/HCl, pH 7.5; 250 mM NaCl; 25 mM EDTA pH 8; 0.5% SDS (w/v)) was added to the vial and mixed. The suspension was centrifuged for 5 minutes at 13000 rpm. The supernatant was transferred into a fresh vial and 200 µl isopropanol was added. The precipitation of the DNA was conducted at room temperature for 30 minutes and subsequently centrifuged at 14000 rpm at 4°C for 10 minutes. The supernatant was removed and 70% ethanol was added to the pellet, followed by an additional centrifugation step at 13000 rpm at room temperature for 5

minutes. After air-drying the pellet, it was dissolved in with 100 µl 10 mM Tris/HCl, pH 8.0. The solution was stored at 4°C.

2.2.1.5 Polymerase-Chain Reaction (PCR)

PCRs used for genotyping were conducted with a Taq polymerase, expressed and purified in hous. For genotyping PCRs a 20 µl-reaction consisting of 1 x reaction buffer (67 mM Tris, 16 mM $(NH_4)_2SO_4$, 2.5 mM $MgCl_2$, 0.01% Tween, pH 8.8), 125 µM dNTPs, 0.5 µM fwd and rev primer, 0.5 µl Taq polymerase and 2 µl DNA from the Edwards protocol was taken. The protocol was as follows: Initial denaturation for 3 min at 95°C, 30 cycles of denaturation (30 s 95°C), annealing (30 s at melting temperature (Tm) minus -3°C) and elongation (1 min/kb at 72°C), 5 min final elongation at 72°C.

For cloning purposes, the proofreading polymerase Pfu (Thermo Scientific) was used according to manufacturer´s instructions, in order to minimize mutation events within the sequence to be proliferated.

2.2.1.6 Colony-PCR

A colony PCR was used in order to screen single colonies for the transformed plasmid in either *E. coli* or *A. tumefaciens.* A 10 µl tip was dipped into a single colony and subsequently put into a PCR tube, containing 10 µl of nuclease-free water. After 10 minutes of incubation the same tip was used to spread the material on a selective LB petri dish and incubated at 37°C or 28°C, respectively. The program for PCR is similar to the above-described protocol, when using the homemade Taq polymerase.

2.2.1.7 Restriction enzyme digestion of DNA

Additional to the colony PCR, a restriction enzyme digestion served to control the correct implementation of the target sequence into the respective plasmid. Commercially available restriction enzymes and appropriate protocols from Thermo Scientific were used. DNA fragments were analyzed by agarose gel electrophoresis.

2.2.1.8 DNA-agarose gel electrophoresis

DNA fragments were separated by molecular weight with the help of a 1% agarose gel. Here 1 % of agarose was mixed with 1 x TAE buffer (40 mM Tris, 50mM acetic acid, 1 mM EDTA pH 8.5). The agarose powder was melted in a microwave and afterwards supplemented with the

DNA stain peqGreen (Peqlab) in a dilution of 1:5. Agarose gels were run at 90-100 V / 400mA in 1 x TAE buffer. A 1kb DNA GeneRuler ladder (Thermo Scientific) was used to compare the size of the respective DNA fragment. The visualization of DNA was achieved by using an UV Transilluminator (Infinity-3026 WL/26 MX, Peqlab).

2.2.1.9 In-gel purification of DNA-fragments

After multiplication of a PCR-fragment via PCR, an in-gel purification was conducted to eliminate unspecific sequences. For that purpose the selected band of a lane was cut out under UV light with a scalpel and transferred into a 1.5 ml Eppendorf tube. Further steps were performed according to the instruction from the GeneJet Gel Extraction Kit (Thermo Scientific).

2.2.1.10 Gateway TOPO-cloning

In order to clone a purified DNA fragment into an entry vector, the pCR™8/GW/TOPO®TA Cloning®Kit (Life Technologies) was chosen. This cloning relies on T-overhangs for which reason adenine nucleotides had to be added to the amplicon. Here, 7.9 µl PCR amplicon was mixed with 1 µl dATP (10 mM), 1 µl 10 x Taq buffer and 0.1 µl homemade Taq polymerase. This mix was incubated for 10 min at 72°C. 4 µl of the reaction were used directly for the TOPO-reaction by mixing with 1 µl salt solution and 1 µl pCR™8/GW/TOPO®TA vector. After 5 minutes of incubation at room temperature, 2µl of the TOPO reaction were transformed into competent *E. coli* cells (see 2.2.1.1).

2.2.1.11 DNA sequencing

Amplicons in Gateway entry vectors were sequenced prior to the transfer into expression vectors, using the light run service of GATC Biotech. The sequencing results were analyzed using the CLC Main Workbench (CLC bio) by aligning genes of interests with those successfully cloned into the entry vector (see 2.2.1.10).

2.2.1.12 L/R-reaction – Gateway

The transfer of a sequence-verified amplicon into the expression-/destination vector was done with the Gateway® LR Clonase® II Enzyme Mix kit (Life Technologies). 50-150 ng entry and destination vector were mixed to a final volume of 4 µl with 1 x TE-buffer (pH 8). 1 µl LR clonase II enzyme mix was subsequently added to start the reaction at 25°C for 1 hour. 0.2 µl Proteinase K was added into the solution and incubated at 37°C for 10 min in order to stop

the reaction. For amplification of the created destination vector the mix was transferred into competent *E. coli* cells. Results of the LR reaction were analyzed by either colony-PCR and/or restriction digestion.

2.2.2 Protein analysis

In order to ectract proteins from plant material, the tissue was ground in liquid nitrogen in a mortar to a fine powder. This was conducted as a first step for all leaf material derived either from Arabidopsis or *Nicotiana benthamiana*.

2.2.2.1 Protein extraction

There were distinct protocols used for protein extraction. One for checking expression levels of the respective protein either in *N. benthamiana* or in Arabidopsis. The other protocol was used when co-immunoprecipitation experiments were performed.

2.2.2.1.1 Protein extraction for checking protein expression level

300 µl extraction buffer (10% glycerol, 150 nM Tris/HCl, pH 7.5, 1 mM EDTA, 150 mM NaCl, 10 mM DTT, 0.2% Nonidet P-40, 2% PVPP, 1 tablet of proteinase inhibitor cocktail (Roche) per 10 ml solution) was mixed with 100 mg leaf material and incubated for 20 min on a rotator at 4°C. A centrifugation step at 4°C, 5000 x g for 20 min followed. The supernatant was then transferred through a one-layer Miracloth (Roche) in a fresh pre-chilled 1.5 ml Eppendorf tube on ice. 100 µl cleared and filtered extract was mixed with 50 µl 3 x SDS loading buffer (12 ml glycerol, 12 ml SDS 10%, 7.5 ml 0.5 M Tris/HCl pH 6.8, 2 ml 1% bromophenol blue, 6.5 ml ddH_2O) supplemented with 10 mM DTT. The samples were boiled at 95°C for 5 minutes, before the gel was loaded with 20 µl protein extract per lane.

2.2.2.1.2 Protein extraction and co-immunoprecipitation

The composition of the protein extraction buffer and 3 x SDS-loading buffer is described in the previous chapter 2.2.2.1.1. Here, 200 mg leaf material were mixed with 800 µl ice-cold extraction buffer and subsequently incubated at 4°C on a rotator for 1 hour. In this time 20 µl per sample of GFP-coupled beads (Chromotek) were transferred into a fresh tube with a cut tip. The beads were washed 3 times with 1 ml GTEN buffer (10% glycerol, 150 mM Tris/HCl, pH 7.5, 1 mM EDTA, 150 mM NaCl, 10 mM DTT, 0.2% Nonidet P-40) in order to remove residuals of the storage buffer. The centrifugation steps were conducted at 2500 x g at 4°C for 2 min. After the last removal of the supernatant the beads were resuspended with 100 µl GTEN buffer per sample and kept on ice. After the solublization protein extracts were

centrifuged at 5000 x g for 20 minutes and filtered through one layer of Miracloth (Roche). Before mixing with the beads, 30 µl protein extract per sample were removed and kept to monitor the input expression level. The washed beads (100 µl) were added to the 1.5 ml Eppendorf tube containing filtered and cleared protein extract. This mixture was incubated for 1 hour at 4°C on a rotator to bind the GFP-tagged proteins to the beads. In order to remove unspecific binding, the beads were washed two times with washing buffer A (50 mM Tris/HCl, pH 7.5, 150 mM NaCl) and two times with washing buffer B (50 mM Tris/HCl, pH 7.5, 50 mM NaCl). Centrifugation was performed at 2500 x g at 4°C for 2 min. After the washing steps, the supernatant was removed and 60 µl 3 x SDS loading buffer was added to the beads.

2.2.2.1.3 Protein extraction used for mass spectrometry analysis

In order to analyze the interactome 2 g of leaf material of stably transformed Arabidopsis lines were taken and mixed with 5 ml ice-cold extraction buffer (50 mM Tris/HCl pH 7.5, 150 mM NaCl, 1% Nonidet P-40, proteinase inhibitor cocktail (Roche)). The samples were incubated for 1 h at 4°C on a rotation machine and centrifuged at 45000 rpm, 4°C for 1 h, using the ultra-centrifuge (SORVALL WX Ultra80). In the meanwhile, 80 µl GFP-agarose beads (Chromotek) per sample were washed 3 times with 1 ml washing buffer A (see 2.2.2.1.2) and kept on ice. The supernatant was mixed with the GFP-beads and again incubated for 1 h at 4°C on a rotation machine after which 4 washing steps followed in order to remove unbound and unspecifically bound proteins: 2 times with washing buffer A and 2 times with washing buffer B (see 2.2.2.1.2). The centrifugation steps were performed at 4°C at 2500 x g for 2 minutes each time. After the washing steps, the supernatant was removed and 80 µl 5 x SDS loading buffer (312.5 mM Tris/HCl pH 6.8, 10% (w/v) SDS, 25% (v/v) β-mercaptoethanol, 50% (v/v) glycerol, 0.05% (w/v) bromophenol blue) was added to the beads with subsequent incubation at 95°C for 5 minutes.

2.2.2.2 SDS-Polyacrylamid gel electrophoresis (SDS-PAGE)

Protein extracts or GFP-beads after pulldown containing 3 x (Co-IP) or 5 x (mass spectrometry analysis) SDS loading buffer were boiled at 95°C for 5 minutes before separation on a polyacrylamide gel. 20 µl of total volume was loaded on an 8% homemade SDS-polyacrylamide gel. This gel was divided into a 5% stacking gel and a 8% resolving gel First, the resolving gel was conducted by mixing 2.3 ml H_2O, 1.3 ml acrylamide-bisacrylamide mix (37.5:1), 1.3 ml 1.5 M Tris pH 8.8, 50 µl 10% SDS, 50 µl 10% Ammonium persulfate (APS)

and 3 µl Tetramethylethylenediamine (Temed / Roth). This mixture was poured between glass plates with 1 mm spacers and covered with propan-2-ol. When the gel was solid, the propan-2-ol was removed and replaced by the 5% stacking gel (2.6 ml H_2O, 0.67 ml acrylamide-bisacrylamide mix (37.5:1), 0.5 ml 1M Tris pH 6.8, 10 µl 40% SDS, 10 µl 40% APS and 4 µl Temed). A comb for 10 slots was inserted into the stacking gel. In this work the system of Biorad Mini-PROTEAN Tetra Cell was used. Therefore, the gel was fixed into a frame of the running tank and covered with 1 x SDS running buffer (25 mM Tris base, 192 mM glycine, 0.1% (w/v) SDS). The first lane of the gel was filled with 5 µl of the PageRuler prestained protein ladder (Thermo Scientific). The gel ran at 20 mA per gel for ~1 hour until the bromophenol blue was running out. After removing the gels out of the glass plates, they were further processed either for immunoblot analysis (see 2.2.2.3) or directly stained for protein visualization or for ESI-LC MS/MS analysis (see 2.2.2.4).

2.2.2.3 Immunoblot analysis

Proteins separated by molecular weight through SDS-PAGE were transferred to a nitrocellulose membrane (GE Healthcare) using the BioRad Tetra Blotting Module. Membrane and gel were pre-incubated in pre-cooled transfer buffer (25 mM Tris base, 192 mM glycine, 20% methanol). The transfer was achieved in transfer buffer at 105 V for 1 h. In order to block unspecific antibody-binding sites the blotted membranes were further incubated in 5% milk powder in PBS-T (137 mM NaCl, 27 mM KCl, 10 mM Na_2HPO_4, 2 mM KH_2PO_4, pH 7.4, 0.1% Tween 20) for 1 hour at room temperature. The incubation with the first antibody diluted in 5% milk powder in PBS-T was performed overnight at 4°C. Prior to the incubation with the secondary antibody for 1 h at room temperature, the membrane was washed 3 times for 5 minutes each time in PBS-T. After the incubation time the previously described washing steps were repeated. As all secondary antibodies were coupled to the horseradish peroxidase (HRP) the detection was performed with luminol (ECL prime reagent, GE Healthcare), incubated for 2 minutes at room temperature in the dark. The detection of the emitted light signal was performed with the Amersham Imager 600 (GE Healthcare). For visualization of equal protein loading, membranes were either stained before the blocking step with Ponceau-S, or Coomassie Blue-staining solution, after the detection of the light signal.

2.2.2.4 Coomassie blue staining

Proteins present in the gel were visualized by incubation in Coomassie staining solution (0.125% (w/v) Coomassie blue R-250, 25% (v/v) 2-propanol and 10% (v/v) acetic acid) for 30 minutes. After incubation the gel was destained using the destaining solution (45% (v/v) 2-propanol, 10% (v/v) acetic acid) until single bands were visible. The gels were kept in water and transported to the Proteome Center / Tübingen in order to perform the electron spray ionization liquid chromatography double mass spectrometry (ESI-LC MS/MS).

2.2.2.5 ESI-LC MS/MS (Mirita Franz-Wachtel)

Coomassie-stained gel pieces were digested in gel with trypsin as described previously (Borchert *et al.*, 2010). After desalting using C18 stage tips (Rappsilber *et al.*, 2007), extracted peptides were separated on an EasyLC nano-HPLC (Thermo Scientific) either coupled to an LTQ Orbitrap XL (Thermo Scientific) or a QExactive HF (Thermo Scientific) mass spectrometer as described elsewhere (Franz-Wachtel *et al*, 2012; Kelstrup *et al*, 2014) with slight modifications: the peptide mixtures were injected onto the column in HPLC solvent A (0.1% formic acid) at a flow rate of 500 nl/min and subsequently eluted with a 57 minute segmented gradient of 5–33-50-90% of HPLC solvent B (80% acetonitrile in 0.1% formic acid) at a flow rate of 200 nl/min. For analysis on the LTQ Orbitrap XL precursor ions were acquired in the mass range from m/z 300 to 2000 in the Orbitrap mass analyzer at a resolution of 60,000. Accumulation target value of 10^6 charges was set and the lock mass option was used for internal calibration (Olsen *et al.*, 2005). The 10 most intense ions were sequentially isolated and fragmented in the linear ion trap using collision-induced dissociation (CID) at the ion accumulation target value of 5000 and default CID settings. Sequenced precursor masses were excluded from further selection for 90 seconds. On the QExactive mass spectrometer full scan was acquired in the mass range from m/z 300 to 1650 at a resolution of 120,000 followed by HCD fragmentation of the 7 most intense precursor ions. High-resolution HCD MS/MS spectra were acquired with a resolution of 60,000. The target values for the MS scan and MS/MS fragmentation were 3x 10^6 and 10^5 charges, respectively. Precursor ions were excluded from sequencing for 30 s after MS/MS.

2.2.3 Plant methods

2.2.3.1 Plant growth conditions

A. thaliana plants, used for functional assays were grown under short day conditions for 6 weeks in a growth chamber (8 hours light, 16 hours dark, 22°C, 110mE$m^{-2}s^{-1}$, 60% relative humidity). Seeds were stratified for 2 days at 4°C before transfer into the growth chamber. The seedlings were separated into individual pots after two weeks. For seed production and genetic transformation, plants were grown under long day conditions in the greenhouse (16 hours light, 8 hours dark). *N. benthamiana* plants were grown in the greenhouse under long day conditions for 3 to 4 weeks prior to Agrobacterium mediated transformation (see 2.2.1.2) for co-immunoprecipitation experiments (see 2.2.2.1.2).

2.2.3.2 Crossing

Plants of different genotypes were crossed in order to analyze epistatic effects of genes of interest. One mutant was chosen as female plant, meaning that this plant was grown under long day conditions until buds were developed. Sepals, petals and stamen were removed with forceps in order to prevent self-fertilization. Only the carpel remained on the flower and was fertilized with the pollen of the plant chosen as male. The artificially fertilized plants were grown under long day conditions (16 hours light, 8 hours dark). Developed seeds in siliques after crossing were considered as F1-generation. The success of a crossing was monitored via PCR for the presence of the male T-DNA insertion of the respective gene. The F2-generation was equally selected by PCR-genotyping for homozygous offspring. Homozygous F3-generations were used for functional analysis.

2.2.3.3 Transient transformation in *Nicotiana benthamiana* by *Agrobacterium tumefaciens*

For transient protein expression in tobacco *A. tumefaciens* GV3101 was cultivated in a 5-10 ml liquid culture (LB-medium with the appropriate antibiotic) at 28°C and 180 rpm overnight. The next morning, cells were harvested by centrifugation at 4000 x g for 5 min. The cell pellets were resuspended twice in 10 mM $MgCl_2$ in order to remove residual antibiotics and media. The cultures were diluted to a OD_{600} = 1 with 10 mM $MgCl_2$, which represented the dilution of all used strains, including the silencing inhibitor p19 (Voinnet, 2015). The strains were mixed in a ratio of 1:1 with p19, and acetosyringone (150 µM final concentration) was added to the mix which was incubated 2 h at room temperature. During this time the

tobacco plants were watered and kept under a lid in order to enhance stomatal opening. Tobacco leaves were infiltrated with a needleless syringe. Leaves were harvested 2 to 3 days after infiltration and immediately frozen in liquid N_2. For storage the leaves were ground to a fine powder and kept at -80°C.

2.2.4 Functional assays

2.2.4.1 Oxidative burst

Based on a luminol assay the production of reactive oxygen species (ROS) was measured in a luminometer in a 96-well scale. Leaves of 5-6 week-old *A. thaliana* plants were cut into equal squares of about $2mm^2$ and floated on MilliQ-water for 18-22 h. The leaf pieces were placed individually in 96-well plates containing 90 µl of the substrate solution (5 µM luminol L-012 (Wako) and 2 µg/ml peroxidase). The background was measured in the luminometer (Centro LB 960, Berthold Technologies) for ~15 min, after which the elicitors (final concentration 100 nM) were added. The ROS burst was monitored for 30 min for 3 plants per line and three leaf pieces per plant for one assay (=9 replicates).

2.2.4.2 Infection with *Alternaria brassicicola* spores

The cultivation and spore production of *A. brassicicola* MUCL 20297 was conducted as described (Thomma et al., 1999). *Alternaria* spores were stored in a dilution of 2×10^7 spores/ml in a glycerol stock at -80°C. For infection assays 5-6 week old *A. thaliana* plants were used. The spores were brought to room temperature and diluted with sterile water to 1×10^6 spores/ml. Two leaves per plant were inoculated with each two droplets each of 5 µl of the diluted spores. Nine plants per line were distributed randomly in three trays and positions. Trays were kept under 100% humidity in a short day chamber. Symptom bonitation of infection sites was conducted at day 7, 10 and 13 according to the following scheme: 1: no symptoms, 2: light brown spots at infection site, 3: dark brown spots at infection site, 4: spreading necrosis, 5: leaf maceration, 6: sporulation. The disease index (DI) was calculated using the following formula: $DI = \Sigma\, i * ni$. ‘‘i’’ is the symptom category, and ‘‘n_i’’ is the percentage of leaves in ‘‘i.

2.2.4.3 Trypan blue staining

Trypan blue staining was used in this work to visualize cell death formation in *Arabidopsis* plants as it only stains dead tissue. The setup of the experiment was conducted according to

Kemmerling et al. (Kemmerling et al., 2007b). *A. thaliana* leaves were put into 6-well plates containing 2 ml trypan blue staining solution (8% (v/v) lactic acid, 8% (v/v) glycerol, 8% (v/v) Aqua-Phenol; 66% (v/v) EtOH; 0.36% (w/v) trypan blue) and incubated in a 100°C water bath for 45 s - 1 min. The staining solution was replaced by chloralhydrate solution (1 g/ml) for destaining and incubated first for 6 h and again overnight, after replacing the destaining solution. Destained leaves were analyzed in 20% glycerol under a binocular.

2.2.4.4 Hormone measurements

The measurement of SA content in *A. thaliana*-lines was performed in collaboration with the ZMBP analytics department at the University of Tübingen. The measurements were performed as described in the publication of Lenz et al. (2011).

2.2.4.5 Recording the phenotypes of plants

Pictures of plants were taken by a Nikon camera (Digital-Sight DS-U1), and were treated in Adobe Photoshop CS5.

2.2.4.6 Statistical analysis

Statistical evaluations were performed using the JMP 14.2.0-software. Error bars show the standard deviation of the mean, student t-test indicates a significant difference ($p<0.05$) for bars labelled with different letters.

2.2.4.7 Annotations of protein domains

In order to check domains of a protein, predicted domains according to Uniprot and Expasy Prosite / ScanProsite results viewer were used.

3 Results

3.1 Identification of the BAK1-INTERACTING KINASE 3 (BIR3)-interactome

The pseudokinase BAK1-INTERACTING KINASE 3 (BIR3) interacts with BRI1-ASSOCIATED RECEPTOR KINASE 1 (BAK1) (Fig. 3.1A), as well as with ligand-binding receptors such as BRASSINOSTEROID INSENSITIVE 1 (BRI1) (Fig. 3.1B) and FLAGELLIN-SENSITIVE 2 (FLS2) in order to prevent association of ligand-binding receptors with BAK1 (Imkampe et al., 2017). To test whether BIR3 might also regulate further immunity-related LRR-RLKs, Co-IP experiments transiently in tobacco were performed, testing PEP1 RECEPTOR 1 (PEPR1) and EF-TU RECEPTOR (EFR) as potential binding partners of BIR3 (Fig. 3.2).

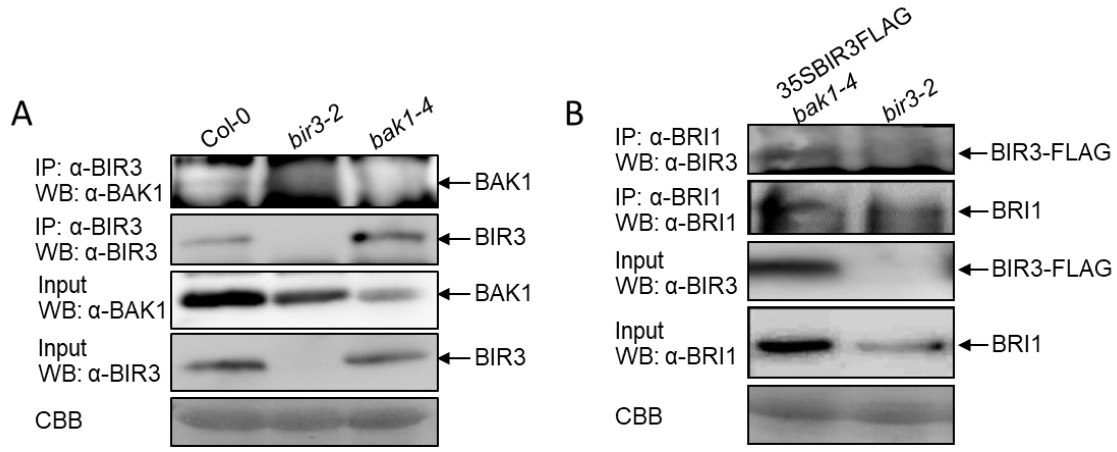

Figure 3.1: BIR3 interacts with BAK1 in *Arabidopsis thaliana*

A) Co-IP was performed with 14-day old Arabidopsis seedlings. IP was performed with α-BIR3 antibodies and co-immunoprecipitated BAK1 was detected with specific α-BAK1 antibodies. Protein input is shown by Western blot analysis of protein extracts before IP with α-BAK1 and α-BIR3 antibodies, respectively. Coomassie brilliant blue (CBB) staining shows equal protein loading. B) Co-IP was performed with 14-days Arabidopsis seedlings expressing BIR3-FLAG in *bak1-4* background and *bir3-2* mutants as controls. IP was performed with α-BRI1 antibodies. Precipitated BRI1 and co-immunoprecipitated BIR3 protein were detected with specific α-BRI1 and α-BIR3 antibodies, respectively. Protein input is shown by Western blot analysis of protein extracts before IP detected with α-BRI1 and α-BIR3 antibodies. Coomassie brilliant blue (CBB) staining shows equal protein loading.

All tested proteins were under the control of the 35S-promoter. For the expression of respective proteins, p19, a RNA silencing suppressor from the Tomato bushy stunt virus (TBSV) was co-infiltrated in order to bypass the RNA silencing machinery from the plant. The individual expression of EFR-Myc and PEPR1-Myc served as negative controls, to ensure no unspecific binding of both receptors to the beads.

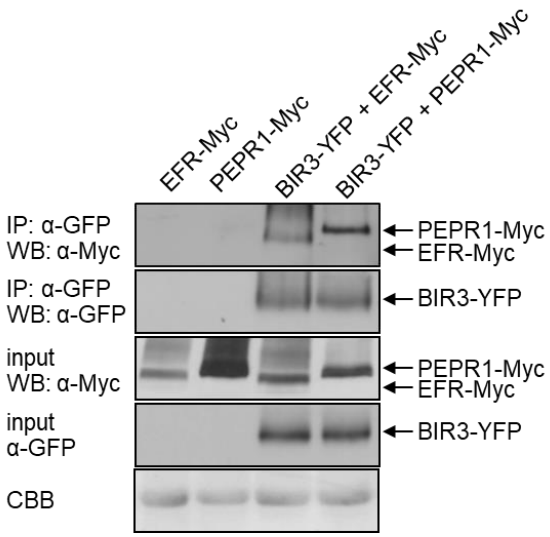

Figure 3.2: BIR3 interacts with ligand-binding receptors, such as BRI1 (*Arabidopsis thaliana*), EFR and PEPR1 (*Nicotiana benthamiana*)

Co-IP experiments with BIR3-YFP and EFR-Myc or PEPR1-Myc. 35S-BIR3-YFP and other indicated constructs were transiently expressed in *N. benthamiana* leaves and IP was performed with GFP-trap beads (Chromotek). Precipitated BIR3 and co-immunoprecipitated proteins were detected with α-GFP and antibodies against the tag of the respective protein. Protein input is shown by Western blot analysis of protein extracts before IP and antibodies against the respective tags. Coomassie brilliant blue (CBB) staining shows equal protein loading.

The Co-IP-experiments revealed that BIR3 can also interact with PEPR1 and EFR (Fig. 3.2), when transiently co-expressed in *N. benthamiana*. In both cases, the respective GFP-tagged BIR3-protein was pulled down with GFP-beads while PEPR1-Myc and EFR-Myc were co-immunoprecipitated using Myc-antibody for its detection. The expression of only PEPR1-Myc and EFR-Myc did not show unspecific binding to the beads. Hence, BIR3 seems to be a general negative regulator of BAK1-dependent pathways ranging from plant development to immunity. In addition, a mutation in *BIR3* strongly enhances cell death in *bak1* mutants. To get further insights into the multiple pathways BIR3 is affecting, we immunoprecipitated BIR3-YFP from stably transformed *A. thaliana* lines and performed an electron spray ionization liquid chromatography double mass spectrometry (ESI LC-MS/MS-spectrometry), aiming at the identification of novel targets and downstream interaction partners.

3.1.1 Co-immunoprecipitation of BIR3-YFP, followed by MS analysis

Co-immunoprecipitations (Co-IP) were performed with adult F2 plants expressing BIR3-YFP under the strong constitutive 35S-promotor and beads coupled with an antibody against GFP, as described in chapter 2.2.2. The immunoprecipitated proteins were eluted from the beads by cooking with SDS sample buffer and separated by Sodium dodecylsulfate–polyacrylamide gel electrophoresis (SDS-PAGE) (see 2.2.2.2) (Fig. 3.3). Two different Co-IP-experiments were analyzed by mass spectrometry (MS) by the Proteome Center Tübingen.

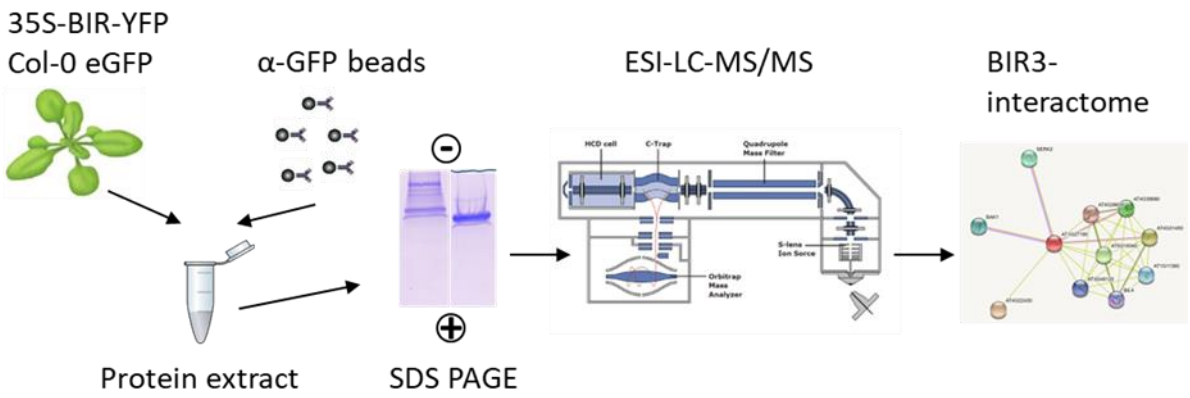

Figure 3.3: Schematic setup for identification of putative BIR3-interactors via ESI-LC-MS/MS (https://www.wur.nl/en/product/Q-ExactivePlus-Orbitrap-LC-MSMS.htm; https://string-db.org)

Proteins were isolated from 6-week old Arabidopsis lines either expressing free eGFP (control) or YFP-tagged BIR3 (sample). After a pulldown of G/YFP-labeled proteins via GFP-beads, a SDS-PAGE followed in order to separate GFP-enriched proteins by mass. ESI-LC-MS/MS was used to identify the peptides of interest via their m/z values. Interacting proteins were evaluated with MaxQuant software package version 1.5.1.0 (Cox and Mann, 2008) and an integrated Andromeda search engine (Cox et al., 2011).

Both gels were fragmented into two fractions (Fig. 3.4). Proteins present in these sections were in-gel digested with trypsin. Plants expressing free eGFP under the control of the 35S promoter in the background of Col-0 were chosen as control to detect proteins unspecifically binding to GFP. MS analyses were performed with either an LTQ Orbitrap XL (Thermo Scientific) or a QExactive HF (Thermo Scientific) mass spectrometer (see 2.2.2.5). MS-spectra were processed by the Proteome Center Tübingen with MaxQuant software package version 1.5.1.0 (Cox and Mann, 2008) and an integrated Andromeda search engine (Cox et al., 2011). The database search was performed against a target-decoy *Arabidopsis thaliana* database obtained from Uniprot, containing 33,351 protein entries, and 245 commonly observed contaminants. Endoprotease trypsin was defined as protease with a maximum of two missed cleavages (provided by Mirita Franz-Wachtel). This raw data list was further ranked in this work in order to narrow down the number of candidate interactors to be analyzed: First, the ratio of intensity values of candidates found in the pull down of precipitated BIR3-YFP and plant material from eGFP-expressing plants (control) were calculated and ranked. At least two-fold enriched proteins were considered significantly enriched in BIR3-specific IPs. Second, the Q-value served as quality control. It describes the level of false positive candidates for a given cut-off value, the smaller the Q-value, the smaller the probability of a false positive candidate. We further compared the rate of twice-enriched putative interactors of BIR3 for both MS experiments to see which and how many candidates could be found in more than one experiment (Fig. 3.4). The candidate lists contained 503 two-fold

enriched proteins in MSI and 2042 proteins in MSII. The about four times higher number of candidates can be explained by a higher yield of pulldown BIR3-protein in the second MS-analysis (Fig. 3.4) and therefore a more efficient pulldown of binding partners. Taking all two-fold enriched candidates of both MS analyses together, we calculated overall 277 common candidates shared in both MS analyses (Fig. 3.4).

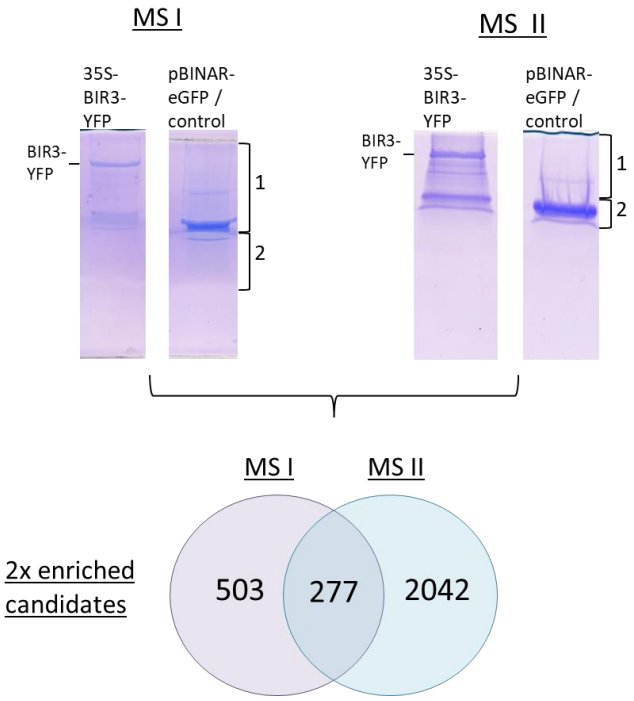

Figure 3.4: BIR3 co-immunoprecipitations for the identification of the BIR3 interactome

BIR3-YFP was precipitated using GFP-labeled beads. Following 8% SDS-PAGE and Coomassie staining the indicated fragments were separately analyzed by ESI LC MS/MS spectrometry. Brackets with Arabian numbers indicate how the gels were fractionated for MS analysis. BIR3-YFP Co-IPs were analyzed by MS in two independent experiments. Intensity rates two-fold higher than in the control samples were considered significant, resulting in the indicated number of candidate BIR3-interacting proteins.

3.1.2 Identification of kinases

We checked for specifically kinases and leucine-rich repeat receptor kinases (LRR-RLKs), as BIR3 was shown to negatively regulate LRR-RLKs involved in a broad spectrum of reactions ranging from BL-signaling to plant immunity (Imkampe et al., 2017). In the analyzed MS-datasets we detected multiple kinases involved in different signaling pathways, indicating that BIR3 is a general interactor of this protein family (complete list of kinases see Appendix: table A1 and A2). About 2/3 of all kinases showing up in MSI showed an overlap in MSII (21 out of 35 candidates of MSI) (Fig. 3.5A).

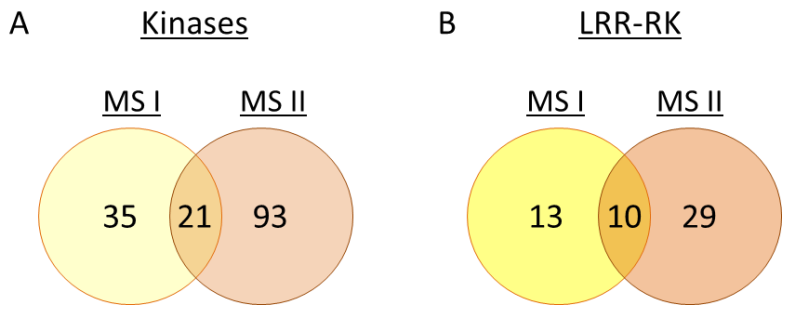

Figure 3.5: Overlap of all kinases versus LRR-RLKs detected in both MS analyses

Venn-Diagram shows the overlap of two-fold enriched candidates for all kinases (A) and for LRR-RLKs (B) as putative BIR3-interactors, when comparing both MS analyses.

All four SERK-proteins (MS-dataset could not differentiate between SERK4 and 5) appeared in both MS analyses with a clear preference for SERK3 / BAK1, as it appeared at position no 1 (MSI) and no 2 (MSII) after ranking the candidates, both sharing a q-value of zero (complete list of LRR-RKs see Appendix: table A3 and A4). This confirms the interaction between all SERK-proteins and BIR3, shown by Imkampe et al. (2017) in a yeast-two hybrid assay and served as a proof of concept, indicating the reproducibility of the Co-IP / MS analyses. Having a closer look at LRR-RLKs, almost all candidates from MSI showed an overlap with candidates of MSII (10 out of 13 LRR-RKs of MSI were found in MSII, Fig. 3.5B). Apart from the SERK-proteins and BIR3, At5G14210, an uncharacterized LRR-RLK turned up in both lists on position three directly after the SERK proteins with a q-value of zero after ranking all two-fold enriched proteins. At5g14210 belongs to the subfamily VI of receptor kinases and contains 10 LRRs in total and could additionally be confirmed in a MS analysis performed by the group of Sacco de Vries (personal communications), using BIR3 as trap, too. Two additional LRR-RLKs, found in both MS datasets were confirmed by literature to be interactors of BAK1 and additionally being active in plant defense: SUPPRESSOR OF BIR1 1 (SOBIR1) (Liebrand et al., 2014; Albert et al., 2015; Wu et al., 2019b) and STRESS INDUCED FACTOR 3 (SIF3) (Yuan et al., 2018). Additionally, HYDROGEN-PEROXIDE-INDUCED CA^{2+} INCREASES1 (HPCA1) and MDIS1-INTERACTING RECEPTOR LIKE KINASE2 (MIK2), two LRR-RLKs appeared in both MS-analyses and are described to signal independently of BAK1 so far (Van der Does et al., 2017a; Wu et al., 2020b). MIK2 is involved in cell wall integrity sensing, playing a role in the defense of the fungal root pathogen *Fusarium oxysporum* and salt stress sensing (Van der Does et al., 2017b), whereas HPCA1 plays a role in stomatal closure (Wu et al., 2020b). These results confirmed the hypothesis of BIR3 being a general interactor of RLKs and thus possibly acting as a negative regulator in the same way as for FLS2 and BRI1. With

MIK2 and HPCA1 being found in both MS analyses, it could be shown, that BIR3 might also interact with receptors which do not rely on BAK1 for signaling. Whether and in what manner BIR3 regulates these pathways will be interesting to find out in the future.

3.1.3 Identification of candidates involved in cell death

In this work, potential cell death candidates were of strong interest as the mechanism of the cell death-phenomena within the BIR- and SERK-family is still elusive. Our MS analyses revealed several candidates involved in cell death (for a complete list see Appendix: table A5 and A6). The list was established again by checking all two-times enriched candidates against the database of tair10 for cell death-involved proteins. Both analyses showed a nearly similar number of cell death candidates (14 in MSI and 18 in MSII), three of which were common (Fig. 3.6; table 3.1).

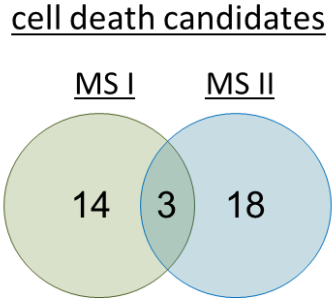

Figure 3.6: Overlap of proteins involved in cell death found in both MS analyses

Venn diagram showing the number of putative cell death-related candidates found in both MS analyses identified by means of tair10-data.

These three candidates shared a q-value of zero, which underpinned their reliability. As shown in table 3.1, they do appear in different positions and intensity values when MSI and II are compared. This is explainable by the method, as a pull-down of interactors is always associated with the risk of losing candidates after several washing steps in the protocol and therefore a risk of losing bound proteins. These washing steps are necessary in order to eliminate proteins which bind non-specifically to the beads.

Table 3.1: List of shared cell death-involved proteins of both MS analyses

Cell death-candidates	AGI-code	ratio of intensities BIR3/eGFP	unique in BIR3YFP-lane?	Q-value
MS-analysis I				
SOBIR1 / SUPPRESSOR OF BIR1	AT2G31880	5,1E+07	yes	0
MC4 / METACASPASE 4	AT1G79340	1,2E+07	yes	0
HXK1 / HEXOKINASE 1	AT4G29130	2	no	0
MS-analysis II				
HXK1 / HEXOKINASE 1	AT4G29130	2,7E+08	yes	0
SOBIR1 / SUPPRESSOR OF BIR1	AT2G31880	1,7E+08	yes	0
MC4 / METACASPASE 4	AT1G79340	1,5E+08	yes	0

Within the list of 14 cell death-candidates of MSI one canonical Toll/interleukin-1 receptor-nucleotide-binding site – leucine-rich repeat protein (TNL), CONSTITUTIVE SHADE-AVOIDANCE1 (CSA1), was identified. In contrast, MSII uncovered three additional nucleotide-binding domain leucine-rich repeat containing (NLR) immune receptors; two TNLs lacking the LRR domain: TOLL/INTERLEUKIN-1 RECEPTOR-LIKE (TN10) and RESISTANCE TO LEPTOSPHAERIA MACULANS 3 (RLM3) and a third NLR belonging to the class of canonical coiled-coil nucleotide-binding domain leucine-rich repeat receptors (CC-NLRs): RECOGNITION OF PERONOSPORA PARASITICA 8 (RPP8). Remarkably, almost all candidates (table 3.2) were uniquely found in the BIR3-pulldown, whereas the control with GFP-trapped beads did not show any binding to one of these candidates. As NLRs are described to induce HR cell death, these candidates are of high interest in order to investigate their potential contribution in sensing the absence of BAK1 or BIRs (table 3.2).

Table 3.2: List of NLRs detected in each MS analysis

NLR	AGI-code	ratio of intensities BIR3/eGFP	unique in BIR3YFP-lane?	Q-value
MS-analysis I				
CSA1 / CONSTITUTIVE SHADE-AVOIDANCE1	AT5G17880	7,1E+08	yes	9,9E-03
MS-analysis II				
RPP8 / RECOGNITION OF PERONOSPORA PARASITICA 8	AT5G43470	3,2E+08	yes	0
TN10 / TOLL/INTERLEUKIN-1 RECEPTOR-LIKE	AT1G72930	1,9E+08	yes	0
RLM3 / RESISTANCE TO LEPTOSPHAERIA MACULANS 3	AT4G16990	3,2E+07	yes	9,9E-04

All NLR candidates bear the possibility to play a role in cell death control. As CSA1 was the first NLR to be identified (from MSI) it was also the first candidate which was chosen for further investigations.

3.1.3.1 Identification of CSA1 as BIR3-interacting protein

An unique peptide sequence of the CSA1 protein (Fig. 3.7) was identified in the BIR3-interactome by MS analysis. The spectrum shows the peptide LPDSLGQLK that was identified in the BIR3-GFP expressing samples.

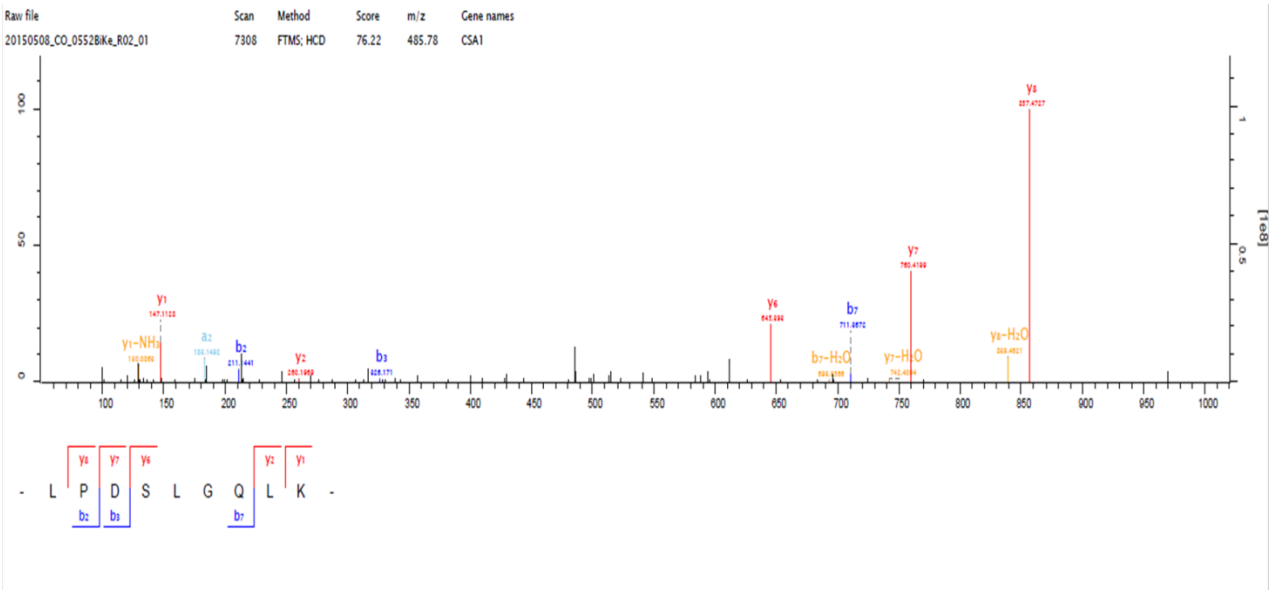

Figure 3.7: The spectrum shows the peptide LPDSLGQLK leading to the identification of CSA1

Product ion spectra (b and y ions) of CSA1 peptides generated from a tryptic digest of a BIR3-GFP IP of 6-week-old whole Arabidopsis plants using ion trap LC/MS MS analysis (MSI), processed by the Proteome Center of Tübingen. All spectra were also verified by manual inspection.

CSA1 was not detected in the control MS analyses using eGFP-expressing plants, showing that its appearance is unique to immune-precipitated BIR3-YFP. After listing the candidates using the above described criteria, CSA1 appeared on position no. 5 of the total list of candidates in MSI (~500 candidates of 2x enriched proteins in total) and was therefore the best candidate for studying the BIR- and/or BAK1-mediated cell death. We hypothesized that CSA1 could act as a potential guard sensing the homeostasis of BIR-proteins and BAK1.

3.1.3.2 CSA1 is a canonical TNL

According to Uniprot (UniProtKB - F4KIF3 (CSA1_ARATH)), the sequence of CSA1 exhibits a TIR-, NB-ARC- and LRR-domain, hence represents a canonical TNL. Starting at the N-terminus, the TIR-domain is annotated from aa15 to aa178 and is described to mediate NAD^+

hydrolase activity after self-association of the TIR-domains (Source: UniProtKB-EC). Neither homo-dimerization of CSA1, nor a catalytic active TIR-domain(s) is shown so far for the protein itself and needs further investigations. The NB-ARC domain starts at aa210 to aa480 (comprising the P-loop according to the conserved motif: G-x(4)-GK-[TS], starting from aa233 to aa240). The LRR-domains comprise 10 LRRs in total and starts from aa614 to aa889 (entire sequence with predicted domains, see Appendix Fig. A1).

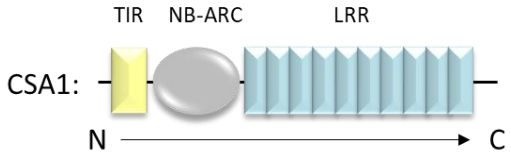

Figure 3.8: Structure of CSA1

Structure of CSA based on Uniprot and Expasy Prosite / ScanProsite Results Viewer. The boxes mark TIR domain (TIR / yellow), NB-ARC-domain (grey) and LRR-domain (LRR / turquoise) starting at the N-terminus (N) to the C-terminus (C).

3.1.4 CSA1 interacts with BIR3 confirmed by Co-IP in *N. benthamiana*

In order to confirm the interaction of CSA1 and BIR3 found *in planta* using MS analysis, Co-IP experiments in *N. benthamiana* were performed. All tested proteins were under the control of the 35S-promoter. For the expression of respective proteins, p19, a RNA silencing suppressor from the Tomato bushy stunt virus (TBSV) was co-infiltrated in order to bypass the RNA silencing machinery from the plant. Leaves, infiltrated with only p19 served as negative controls. The individual expression of CSA1-V5 and BAK1-myc served as additional negative controls, to ensure that no unspecific binding of CSA1-V5, BAK1-myc or any expressed protein within the plant to the beads is detected instead of co-immunoprecipitation with BIR3-eGFP.

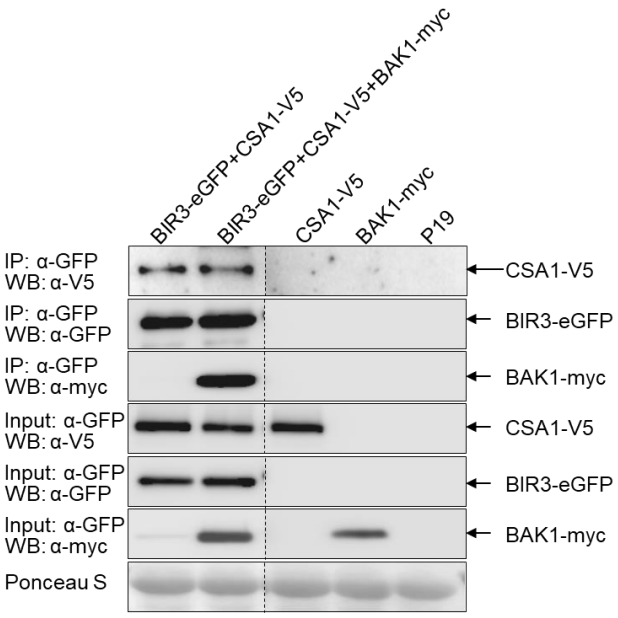

Figure 3.9: BIR3 shows interaction with CSA1 in tobacco

35S-BIR3-eGFP and 35S-CSA1-V5 were transiently expressed in *N. benthamiana* leaves and IP was performed with GFP-trap beads. Precipitated BIR3-eGFP and co-immunoprecipitated CSA1-V5 and BAK1-myc were detected with α-GFP and antibodies against the tag of the respective fusion protein. Protein input for all three proteins was shown by Western blot analysis of protein extracts before IP and antibodies against the respective tags. Additional p19-infiltration served as negative control. Ponceau S-staining shows equal protein loading.

The detection of CSA1-V5 after immuno-precipitating BIR3-eGFP demonstrated an interaction of CSA1 and BIR3, when transiently expressed in *N. benthamiana* (Fig. 3.9). Additionally, co-expressed BAK1 did not alter the intensity of detected CSA1, shown when all three proteins were expressed and the input of all tested proteins appeared equally. As none of the tested controls showed unspecific binding, the detection of CSA1 after pulling down BIR3 hints at a real interaction of both proteins.

3.2 The components of the CSA1-complex

BIR3 belongs to a small protein family with four members. BIR1 and BIR2 are both described to bind to BAK1 and involved in cell death control, but display gradual differences: the knock-out of *bir1* leads to a severe autoimmune phenotype resulting in small plants with strong cell death formation and autoimmunity (Gao et al., 2009a), whereas the loss of the *BIR2*-gene causes yellow lesion sites, elevated SA and JA levels and spreading necrosis after infection with the necrotrophic fungus *Alternaria brassicicola* (Halter et al., 2014). This involvement prompted us to perform Co-IP experiments as well to check if CSA1 might be an interacting NLR of both, BIR1 and BIR2.

3.2.1 BIR1 and BIR2 can interact with CSA1 in Co-IP experiments in *N. benthamiana*

The experiments were simultaneously performed with the CSA1-BIR3-interaction assay. The Co-IP-experiments revealed that CSA1 can also interact with BIR1 and BIR2 (Fig. 3.10A and B), when transiently co-expressed in *N. benthamiana*. In both cases, the respective GFP-tagged BIR-protein was pulled down with GFP-beads while CSA1-V5 was co-immunoprecipitated using V5-antibody for its detection. Negative controls, such as p19 and the expression of only CSA1-V5 did not show unspecific binding to the beads.

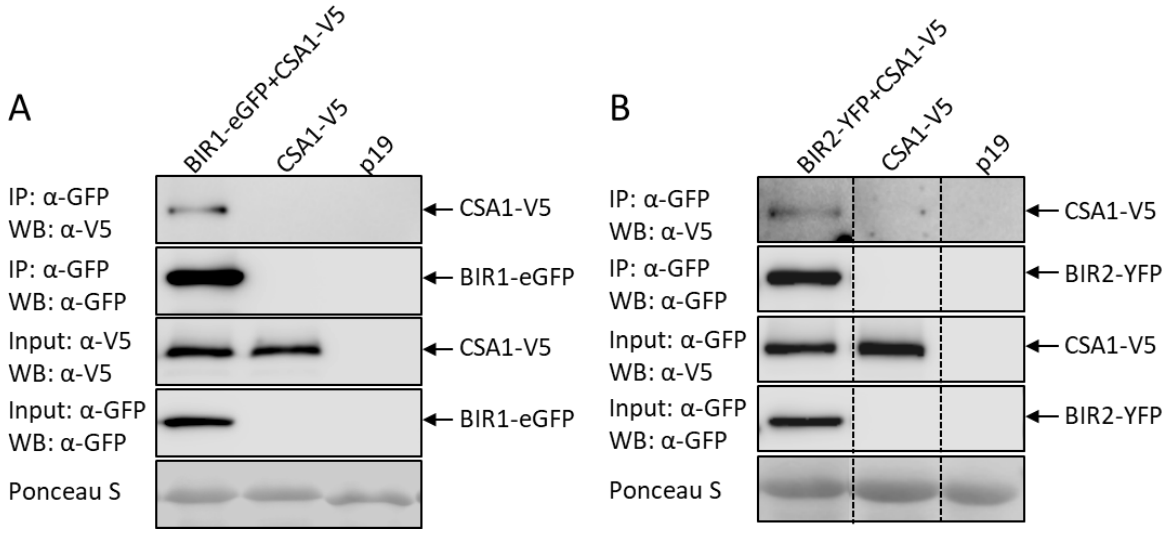

Figure 3.10: Co-immunoprecipitation-experiments of BIR1 and BIR2 with CSA1.

35S-BIR1 and BIR2-eGFP/YFP and 35S-CSA1-V5 were transiently expressed in *N. benthamiana* leaves and IP was performed with GFP-trap beads. Precipitated BIR1 or BIR2 and co-immunoprecipitated CSA1 were detected with α-GFP and α-V5 antibodies. Additional p19-infiltration served as negative control. Protein input is shown by Western blot analysis of protein extracts before IP and antibodies against the respective tags. Ponceau S-staining shows equal protein loading.

Taken together, all tested BIR-proteins (BIR1 to BIR3) can interact with CSA1 when transiently expressed in *N. benthamiana*.

3.2.2 BAK1 can interact with CSA1 in Co-IP experiments in *N. benthamiana*

BAK1 is involved in cell death control, resulting in spreading cell death formation in the single knock-out after inoculation with the necrotrophic fungus *Alternaria brassicicola* (Kemmerling et al., 2007a). Additionally, BAK1 is a constitutive interactor of BIR1 (Gao et al., 2009a), BIR2 and BIR3 (Halter et al., 2014; Imkampe et al., 2017). For these two reasons, it was of strong interest to test if CSA1 interacts also with BAK1. As shown in figure 3.11, BAK1 and CSA1 show an interaction when transiently co-expressed in tobacco. All negative

controls remained without unspecific binding of the respective proteins to the beads, underpinning the specific interaction of both tested proteins.

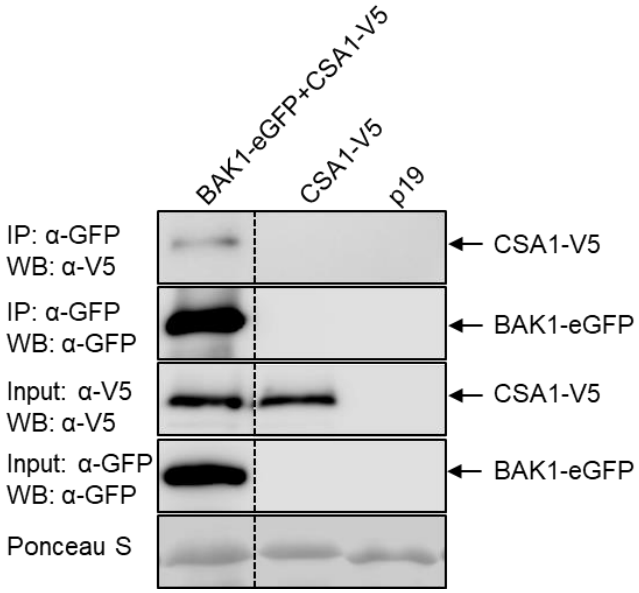

Figure 3.11: CSA1 interacts with BAK1 / SERK3 in *N. benthamiana*

35S-BAK1-eGFP and 35S-CSA1-V5 were transiently expressed in *N. benthamiana* leaves and IP was performed with GFP-trap beads. Precipitated BAK1 and co-immunoprecipitated CSA1 were detected with α-GFP and α-V5 antibodies. Additional p19-infiltration served as negative control. Protein input is shown by Western blot analysis of protein extracts before IP and antibodies against the respective tags. Ponceau S-staining shows equal protein loading.

Summarizing these results, we could show that all tested members of the BIR-family as well as BAK1 do interact with CSA1 when transiently co-expressed in *N. benthamiana*.

3.2.3 The TNL-complex: CSA1 and CHS3

CSA1 and CHILLING SENSITIVE 3 (CHS3) represent a TNL-pair, both required for downstream signaling resulting in HR (Xu et al., 2015). CHS3 is a TIR-NBS-LRR with an additional Protein LIN-11/Lin11, Islet-1/Isl-1 & Mechanosensory protein 3/Mec-3 (LIM)-domain (Freyd et al., 1990) at its C-terminus (Yang et al., 2010). The gain-of-function mutant allele *chs3*-2D exhibits a severe autoimmune phenotype, including a strong dwarfism and constitutively activated defense signaling (Xu et al., 2015). The phenotype is caused by a substitution of C1340Y close to the LIM-domain of CHS3. A suppressor screen revealed that a loss of its genomically adjacent partner CSA1 (*soc5 to 8)* is sufficient to rescue the autoimmune phenotype occurring in the *chs3*-2D-mutant (Fig. 3.12). Both NLRs are presumed to act upstream of EDS1, but their target is not yet known (Xu et al., 2015).

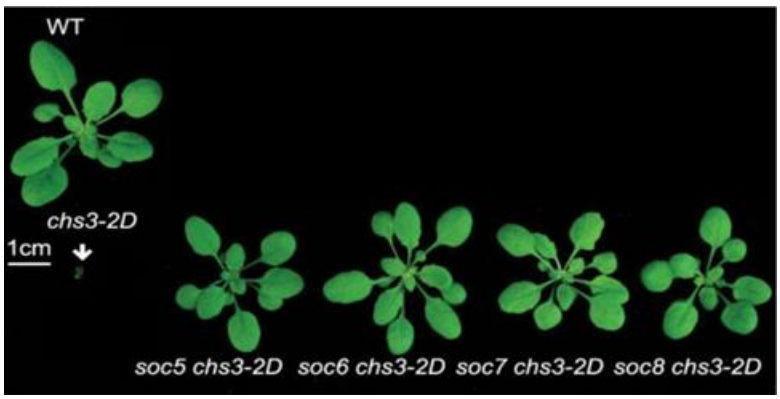

Figure 3.12: CSA1 can suppress the dwarf phenotype of the constitutive autoimmune mutant *chs3-2D*

Morphology of the gain-of-function mutant allele *chs3-2D* and suppressor lines *soc5 to 8* mutated additionally at different positions of CSA1 leading to a complete suppression of the autoimmune dwarf phenotype in *chs3-2D* (Xu et al., 2015) modified.

3.2.3.1 CHS3 contains a predicted zinc protease domain

According to Uniprot, the sequence of CHS3 contains typical structural elements of a TNL, such as TIR-, NB-ARC- and LRR-domain. Starting at the N-terminus, the TIR-domain is annotated from aa15 to aa163 , followed by the NB-ARC domain starting at aa178 to aa427 (comprising the P-loop according to the conserved motif: G-x(4)-GK-[TS], starting from aa196 to aa203). The LRR-domains comprise 14 LRRs in total, starting from aa449 to aa911. Apart of these typical TNL domains, a coiled coil domain (CC) is annotated from aa1109 to aa1234, followed by a LIM-Zinc finger (LIM) domain from aa1238-1297. Additionally to the LIM-domain at the C-terminus, CHS3 contains a Zinc-protease domain (position aa1485 to aa1494), defined by the conserved HExxH-motif at position aa1488 to aa1492 corresponding to UniPRot and Expasy Prosite / ScanProsite results viewer (entire sequence with predicted domains, see Appendix Fig. A2). The HExxH-motif of the zinc-protease domain is necessary for proteolytic function of proteases in general. Whether CHS3 displays a proteolytic active peptidase is not yet described and needs further investigations.

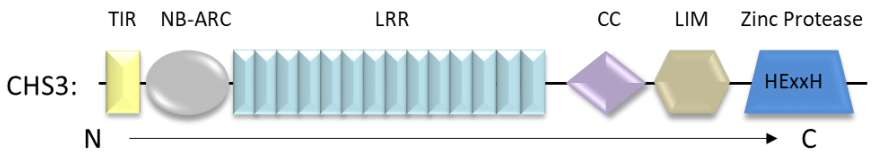

Figure 3.13: Structure of CHS3

Annotated domains of CHS3 based on Uniprot and Expasy Prosite / ScanProsite Results Viewer. The boxes mark TIR domain (TIR / yellow), NB-ARC-domain (grey), LRR-domain (LRR / turquoise), coiled-coil domain (CC / purple), LIM-domain (LIM / brown) and a zinc protease domain including the HExxH motif (blue), required for protease function of peptidases. Sequence starts at the N-terminus (N) and ends at the C-terminus (C).

3.2.3.2 CHS3 can interact with BIR1 /2 /3 in *N. benthamiana*

We did not find CHS3 in our MS-analyses but this does not exclude that CHS3 might be able to interact with BIR3, as it is genetically linked with CSA1 (Xu et al., 2015). We therefore performed Co-IP-experiments with the same setting as we did for the CSA1-interaction. The genomic sequence of CHS3 under the control of the 35S-promoter fused to a V5-tag was co-expressed with the BIR-proteins tagged with either eGFP or YFP, co-immunoprecipitated and detected with V5-specific antibody. The controls using the single expressed CHS3 protein and p19-infiltrated leaf material did not show any unspecific binding to the GFP-beads (Fig. 3.14).

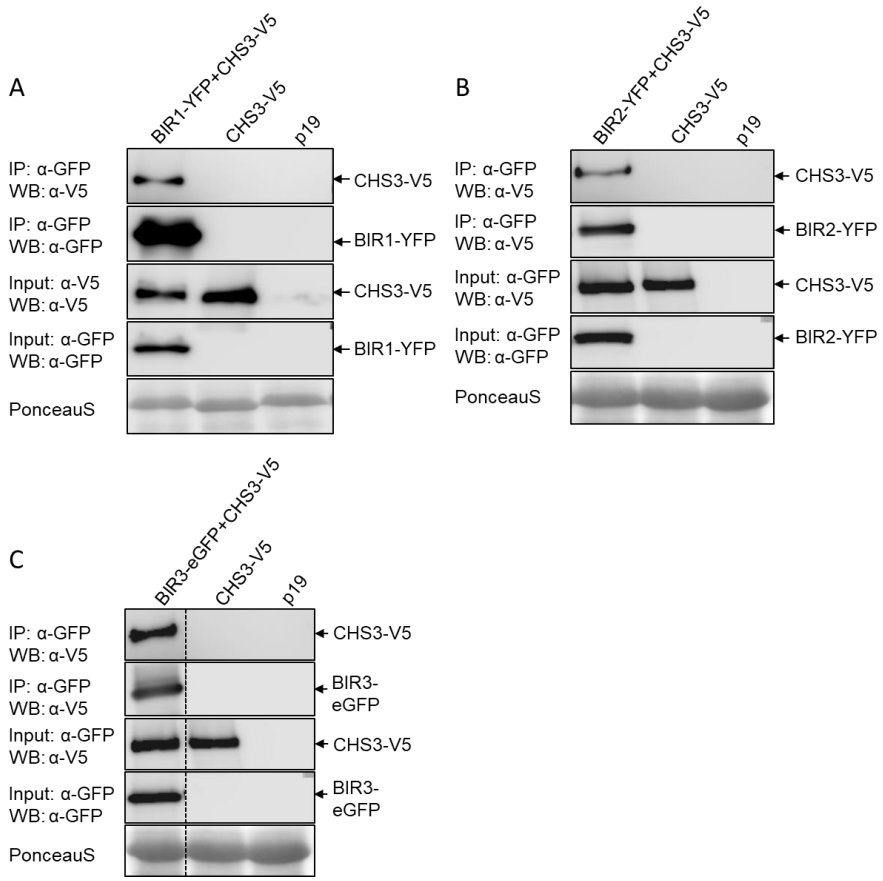

Figure 3.14: CHS3 can interact with the BIR family members 1 to 3 in *N. benthamiana*

35S-BIR1, 2 or 3-YFP/eGFP and 35S-CHS3-V5 were transiently expressed in *N. benthamiana* leaves and IP was performed with GFP-trap beads. Precipitated BIR proteins and co-immunoprecipitated CHS3 were detected with α-GFP and with α-V5 antibodies. Additional p19-infiltration served as negative control. Protein input is shown by Western blot analysis of protein extracts before IP and antibodies against the respective tags. Ponceau S-staining shows protein loading.

All Co-IP experiments showed an interaction between CHS3 and all tested BIR-family members (Fig. 3.14), when transiently expressed in *N. benthamiana.*

3.2.3.3 BAK1 can interact with CHS3 in *N. benthamiana*

We tested whether BAK1 is interacting with CHS3, as it binds constitutively to BIR3. In Figure 3.15, we could show that CHS3-V5 was detectable in the co-immunoprecipitate after pulling down BAK1 via its C-terminal eGFP-tag. Both controls, solely expressing CHS3-V5 and p19, remained undetectable, demonstrating the detected CHS3 was not caused by unspecific binding to the GFP beads, but via an interaction with BAK1.

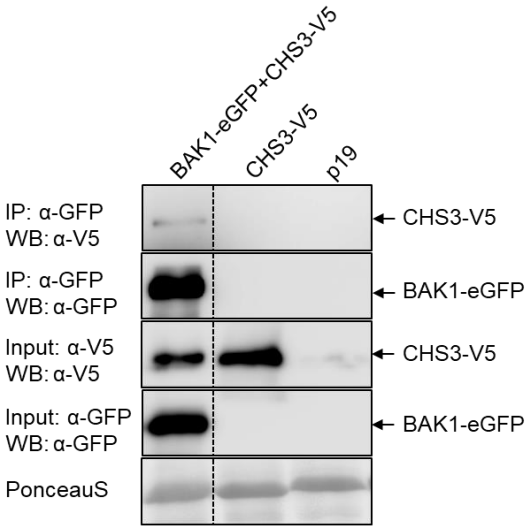

Figure 3.15: BAK1/SERK3 can interact with CHS3 in *N. benthamiana*

35S-BAK1-eGFP and 35S-CHS3-V5 were transiently expressed in *N. benthamiana* leaves and IP was performed with GFP-trap beads. Precipitated BAK1 and co-immunoprecipitated CHS3 were detected with α-GFP and α-V5 antibodies. Additional p19-infiltration served as negative control. Protein input is shown by Western blot analysis of protein extracts before IP and antibodies against the respective tags. Ponceau S-staining shows protein loading.

Taken together, we demonstrated that CHS3 can also bind to all tested BIR proteins and BAK1.

3.3 Functional analysis of the *csa1-2* knock-out line

The T-DNA-insertion line *csa1-2* is reported to be a knock-out mutant with almost no residual mRNA detectable (Faigon-Soverna et al., 2006). Results published by Xu et al. (2015), showed that the autoimmune phenotype of the *chs3-2D*-line could be fully suppressed by mutations within the *CSA1*-gene. These findings prompted us to use the knock-out line *csa1-2* to investigate if the downstream signaling culminating in cell death within the BIR-family and BAK1 could be suppressed by a loss of *CSA1*.

The knock-out of the *CSA1*-gene leads to a larger rosette diameter (Fig. 3.16A), as well as elongated petioles and bigger leaves (Fig. 3.16B), which is in accordance with the described shade avoidance phenotype described for the *csa1-1* line by Faigon-Soverna et al. (Faigon-Soverna et al., 2006).

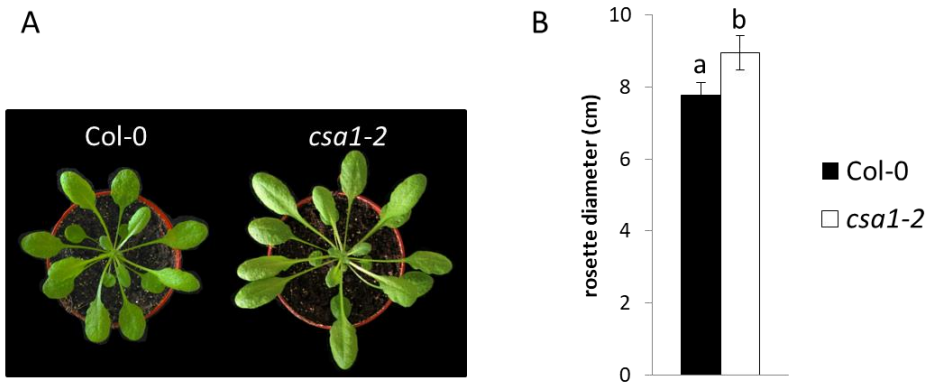

Figure 3.16: CSA1 mutants show an enhanced rosette diameter phenotype

A) Representative pictures of 6week-old Arabidopsis plants grown under short day conditions. B) Rosette diameter of wild type Col-0 and *csa1-2*-mutants of 6 week-old plants, error bars show the standard deviation of the mean, student t-test indicates a significant difference for bars labelled with different letters ($p<0.05$).

3.3.1 CSA1 shows less cell death-formation after infection with the necrotrophic fungus *Alternaria brassicicola*

We tested the impact of the mutant *csa1-2* on cell death formation in an infection experiment using the necrotrophic fungus *Alternaria brassicicola*. In this experiment, reduced symptom development after *Alternaria* infection was observed in *csa1*-2 mutants 13 days after inoculation (Fig. 3.17A and B). Additional staining with trypan blue confirmed that *csa1-2*-mutants showed less cell death formation compared to wild type Col-0 (Fig. 3.17C). These results indicate that the TIR-NLR CSA1 might have a role in cell death containment after *Alternaria* treatment.

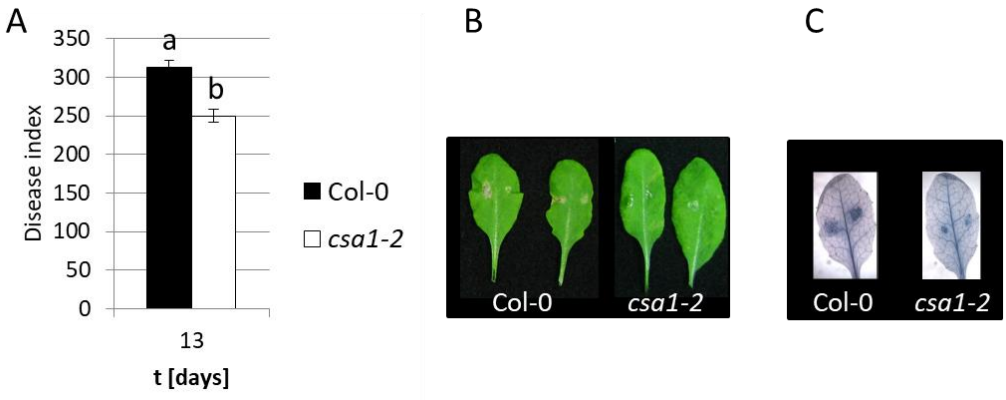

Figure 3.17: Mutation of *CSA1* results in less cell death symptoms after infection with the necrotrophic fungus *Alternaria brassicicola*

Infection experiment with the necrotrophic fungal pathogen *Alternaria brassicicola* on indicated 6-week old Arabidopsis lines: A) disease index after 13 days is shown as mean ± SE (n=4). Different letters indicate significant differences according to Students t-test ($p<0.05$). B) Picture of the symptom development on two representative leaves of each line 13 days after infection. C) Trypan blue staining of infected leafs with *Alternaria brassicicola* after 4 days.

3.3.2 CSA1 has no effect on MAMP induced ROS burst

MAMPs can activate fast responses in plants, including reactive oxygen species (ROS) production also called ROS burst. BAK1 and BIR-proteins positively and negatively regulate MAMP responses, respectively. Using the ROS assay, we analyzed whether CSA1 has also an effect on flg22 and elf18-signaling. We performed the ROS assay using the *bir2*-mutant as positive control, as it is a well described negative regulator of the MAMP-pathway and involved in cell death control (Halter et al., 2014).

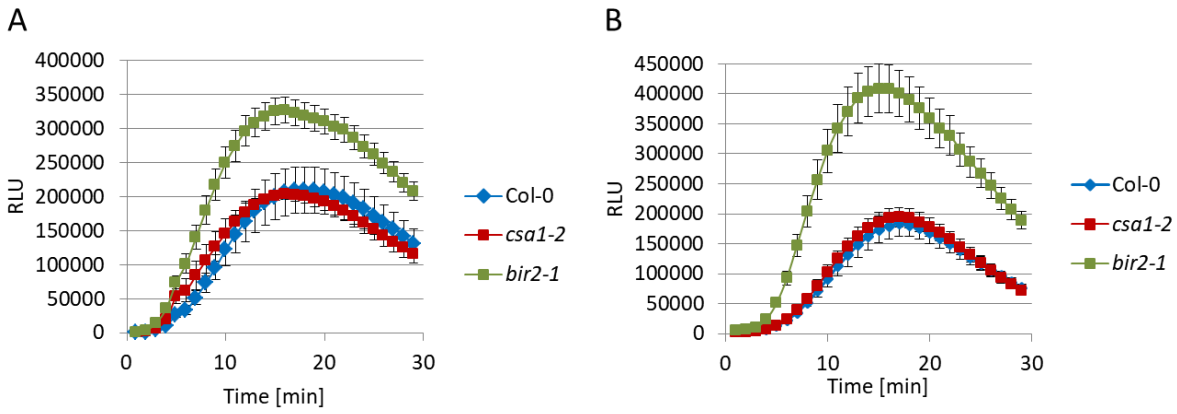

Figure 3.18: CSA1 has no influence on MAMP-induced ROS burst

ROS production was measured with a luminol-based assay on leaf discs of the indicated *Arabidopsis* lines over a period of 30 min after elicitation with 100 nM flg22 (A) and elf18 (B). ROS production is represented as relative light units (RLU) and results are mean ± SE (n=9).

As expected, the knock-out of *bir2-1* led to an elevated production of ROS with both tested elicitors (flg22 and elf18). Independent of the chosen ligand, there was no change of the ROS production in the *csa1-2* mutant line in comparison to the wild type Col-0 (Fig. 3.18) These results indicate that CSA1 plays a role in cell death formation but does not influence FLS2- or EFR-mediated signaling.

3.3.3 CSA1 is necessary for BIR- and BAK1 mediated cell death

The BIR-family exhibits considerable differences in the degree of cell death formation, after knocking out the respective protein. To test whether CSA1 plays a role in BAK1- or BIR-mediated-cell death, we did epistasis experiments with *bak1-4, bir2-1* and the double

mutant *bak1-4bir3-2* lines. These crossings should give us information if and to which extend BAK1 and/or BIR family-mediated cell death is dependent on CSA1.

3.3.3.1 Loss of CSA1 shows partial rescue of the *bak1bir3* cell death phenotype

The strongest cell death occurrence within the BIR-/SERK-family in this study is exhibited by the double mutant *bak1-4bir3-2*. Those plants show a strong spontaneous lesion phenotype with chlorotic small leaves and increased SA- and JA-levels pointing to already ongoing cell death (Imkampe et al., 2017). Additionally, those plants are almost sterile and cannot be rescued when growing at 28°C, which is described for other cell death candidates within the BIR-family, such as *bir1-1* (Gao et al., 2009b). To check whether CSA1 is part of the cell death within the *bak1-4bir3-2* mutant line, we generated the triple mutant *bak1-4bir3-2csa1-2*. Already the morphology of the plant, growing under short day conditions for 6 weeks, showed a strong increase in rosette diameter and leaf biomass, as well as the recuperation of fertility (Fig. 3.19A and B). These triple mutants were more stunted than Col-0, but in contrast to the double mutant *bak1-4bir3-2*, they were flowering and developed seed-producing siliques in a bushy manner with short inflorescences but fertile seeds (Fig. 3.19B). This indicates that indeed the growth and fertility phenotypes present in *bak1-4bir3-2* double mutants are partially dependent on CSA1. It can be assumed that a constitutive cell death program is responsible for the strong cell death phenotype, as the knock-out of *CSA1* restored at least a fertile plant, including a full life cylce.

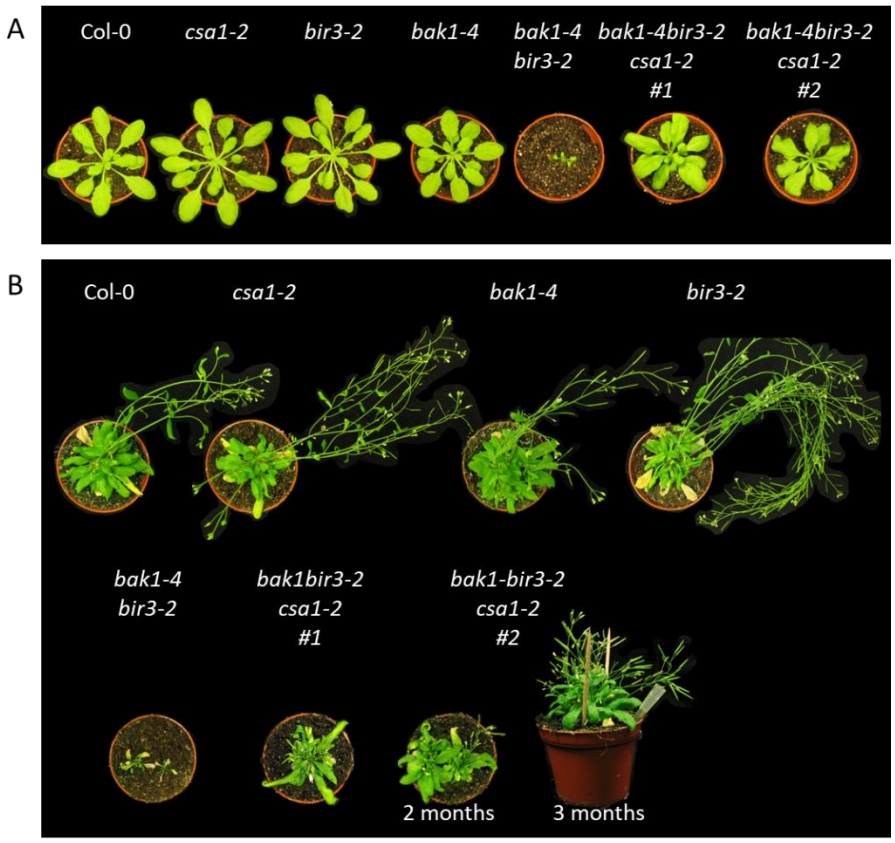

Figure 3.19: The loss of *CSA1* in the background of the double mutant *bak1-4bir3-2* leads to partial rescue of the dwarf phenotype and to the recovery of fertility

A) Phenotype of the line *bak1-4bir3-2csa1-2* in comparison to Col-0 and the respective single-/double mutants. 6 week old plants cultivated under short day conditions are shown. B) Comparison of flowering plants. Cultivation under long day conditions for about 12 weeks.

To investigate to which extend the cell death formation is restricted within the triple-mutant in comparison to the double-mutant, infection experiments with *A. brassicicola* were performed (Fig. 3.20). A significant reduction of symptom development of both tested triple-mutant lines could be observed when compared to the double-mutant *bak1-4bir3-2.* The level of the disease index reached the level of the single-knock-out mutant *bak1-4* or even less (Fig. 3.20C; triple-mutant #2). This result can be considered as a partial rescue in terms of less cell death symptom formation once *CSA1* got lost. Also here, trypan blue staining was used to visualize cell death within the indicated Arabidopsis lines after five days of infection with *A. brassicicola*. The results are in accordance with previous infection assays and reproduced the former results (Fig. 3.20C), since the sites of infection of the triple-mutants were slightly bigger in comparison to wild type, but cell death was clearly restricted. In comparison, the double-mutant *bak1-4bir3-2* lost its ability to restrict the fungus to any extend, exemplified in a leaf in which the fungus overgrew almost two thirds of the whole leaf (Fig. 3.20B).

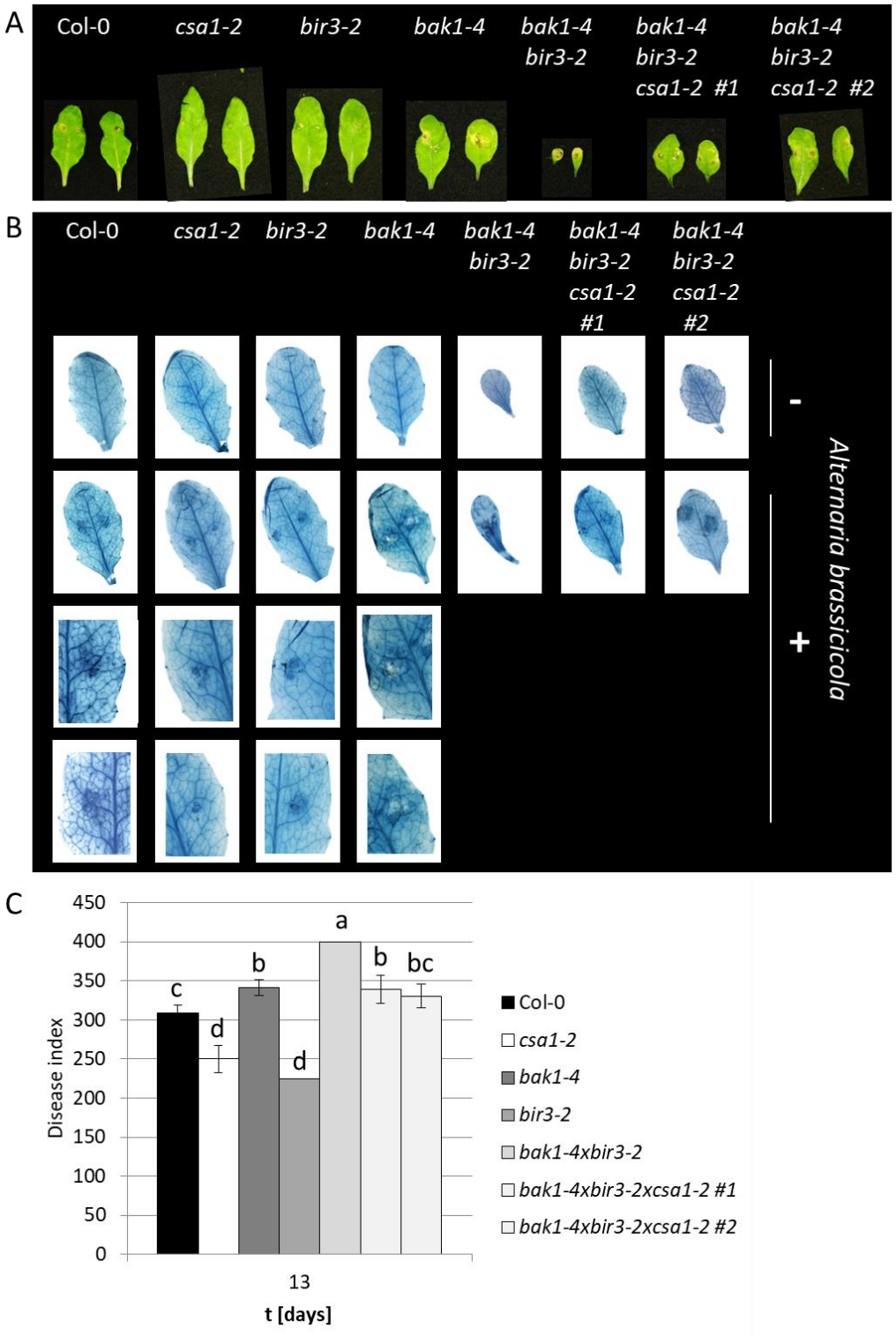

Figure 3.20: Loss of *CSA1* partially recues the *bak1bir3* double-mutant phenotype

Mutant phenotypes of 6 week old plants of the indicated genotypes were monitored after infection with the necrotrophic fungal pathogen *Alternaria brassicicola*. A) representative pictures of the symptom development on two representative leaves of each line 13 days after inoculation. B) Trypan blue staining five days plus or minus infection (+/-) visualizes dead cells C) Disease index after 13 days is shown as mean ± SE (n=6). Error bars show the standard deviation of the mean, student t-test indicates a significant difference for bars labelled with different letters ($p<0.05$).

High salicylic acid (SA) levels were already described for the double-mutant *bak1-4bir3-2* (Imkampe et al., 2017). To test whether the loss of *CSA1* decreases these high levels, we measured the SA content of *csa1-2* in the background of *bak1-4bir3-2* double-mutants and compared those to wild type and corresponding single-mutant lines. The results showed a significant reduction of SA in both triple-mutant lines *bak1-4bir3-2csa1-2*#1 and #2 compared to the double mutant *bak1-4bir3-2* (Fig. 3.21).

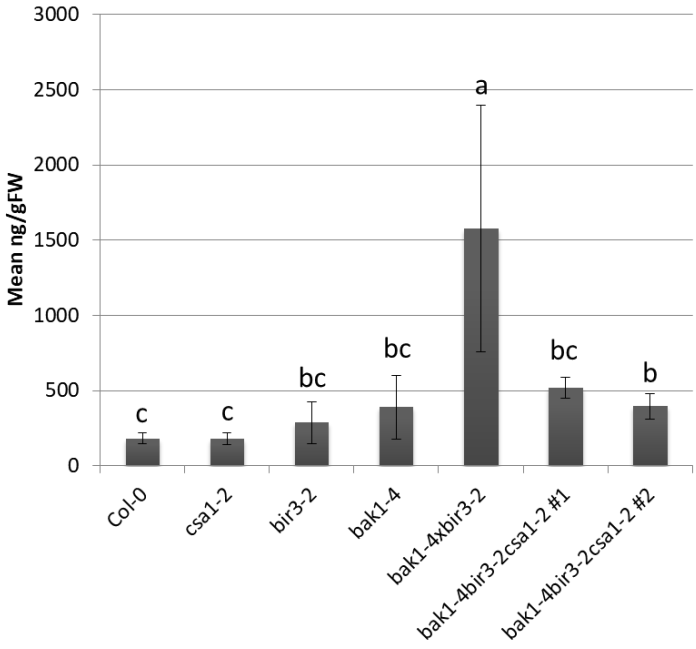

Figure 3.21: Loss of *CSA1* strongly reduces the SA-level in the background of *bak1-4bir3-2*

Total SA levels were detected in untreated 6 week old Arabidopsis plants of the indicated genotypes by method. Results are mean ratios of ng SA to g fresh weight ± SE (n=6). Error bars show the standard deviation of the mean, student t-test indicates a significant difference for bars labelled with different letters ($p<0.05$).

Summarizing the results, the loss of *CSA1* can partially rescue the following phenotypes of the double mutant *bak1-4bir3-2*: (i) plants of the double-mutant die after 6 weeks and are therefore sterile. The knock-out of the *CSA1*-gene in the background of *bak1-4bir3-2* remarkably rescued this phenotype, as those plants developed siliques with viable seeds. (ii) Triple-mutants produced more leaves and exhibited bigger rosettes compared to the double mutant *bak1-4bir3-2*. (iii) Trypan blue staining revealed less cell death in the triple-mutants than in the doubles. (iv) *Alternaria* experiments revealed a restriction in cell death formation for the triple-mutant *bak1-4bir3-2csa1-2* compared to the double-mutant *bak1-4bir3-2* to the level of the single-knock-out *bak1-4*. (v) Monitoring the SA-levels confirmed the dependency of SA signaling for CSA1, as the loss led to a decrease of SA in the triple-mutant. CSA1 can interact with both BIR3 and BAK. Additionally to this, the absence of *CSA1* can partially complement the *bak1-4bir3-2* double-mutant phenotype, showing that CSA1 is an essential component of BAK1- and BIR-mediated cell death.

3.3.3.2 Loss of CSA1 shows partial rescue of the *bir2*-cell death phenotype

To investigate the role of CSA1 in BIR2-dependent pathways, functional experiments on double-mutants were conducted. The knock-out of *BIR2* leads to smaller plants and yellow leaves after 6 weeks of cultivation under short day conditions. This yellowing of leaves correlates with elevated SA levels and enhanced defense responses and therefore is likely an autoimmune phenotype (Halter et al., 2014). Double-mutants of *csa1-2* and *bir2-1* showed phenotypically less yellow leaves and a slightly larger rosette diameter compared to the single-mutant line *bir2-1* (Fig. 3.22A). *Bir2-1* single-mutants displayed additionally shorter stems, when flowering (Fig. 3.22B). The crossing with *csa1-2* did not show any alteration of this phenomenon, indicating that CSA1 does not affect this growth phenotype.

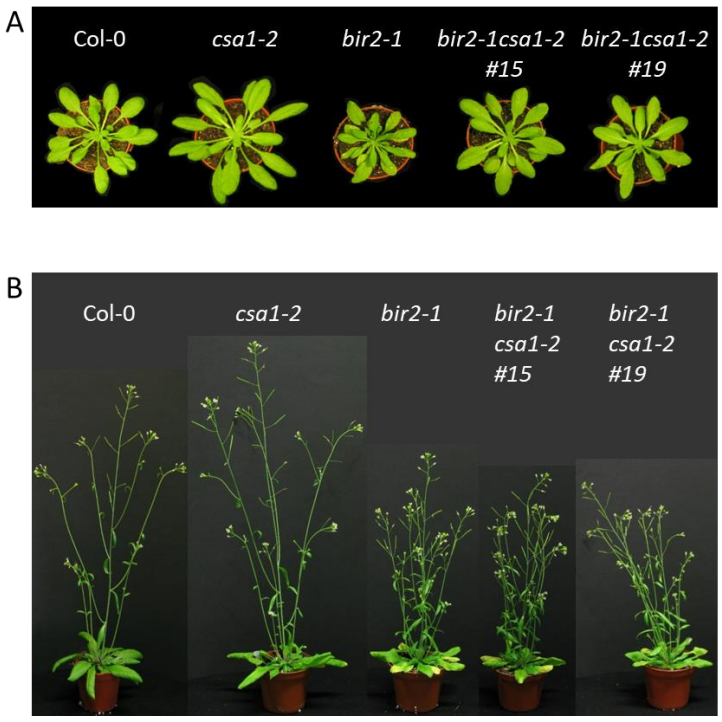

Figure 3.22: The morphology of the double mutant *bir2-1csa1-2* shows less yellow spots but does not differ in the flowering phenotype

A) Phenotype of the crossed line *bir2-1csa1-2* in comparison to Col-0 and respective single mutants. 6 week old plants cultivated under short day conditions. B) Comparison of flowering plants. Cultivation under long day conditions for 8-9 weeks of growth. Double mutants of *bir2-1csa1-2* exhibit the same phenotype as the single knock-out of *bir2-1*, whereas *csa1-2* ko-mutants show a slightly taller flowering stem, compared to wild type Col-0.

One important feature besides the negative regulation of BAK1-dependent pathways is the loss of cell-death-control in the single-mutants of *bir2-1* Arabidopsis plants (Halter et al., 2014). In order to address the influence of CSA1 in the cell death pathway, trypan blue stains for dead cells were conducted with and without *Alternaria* infection.

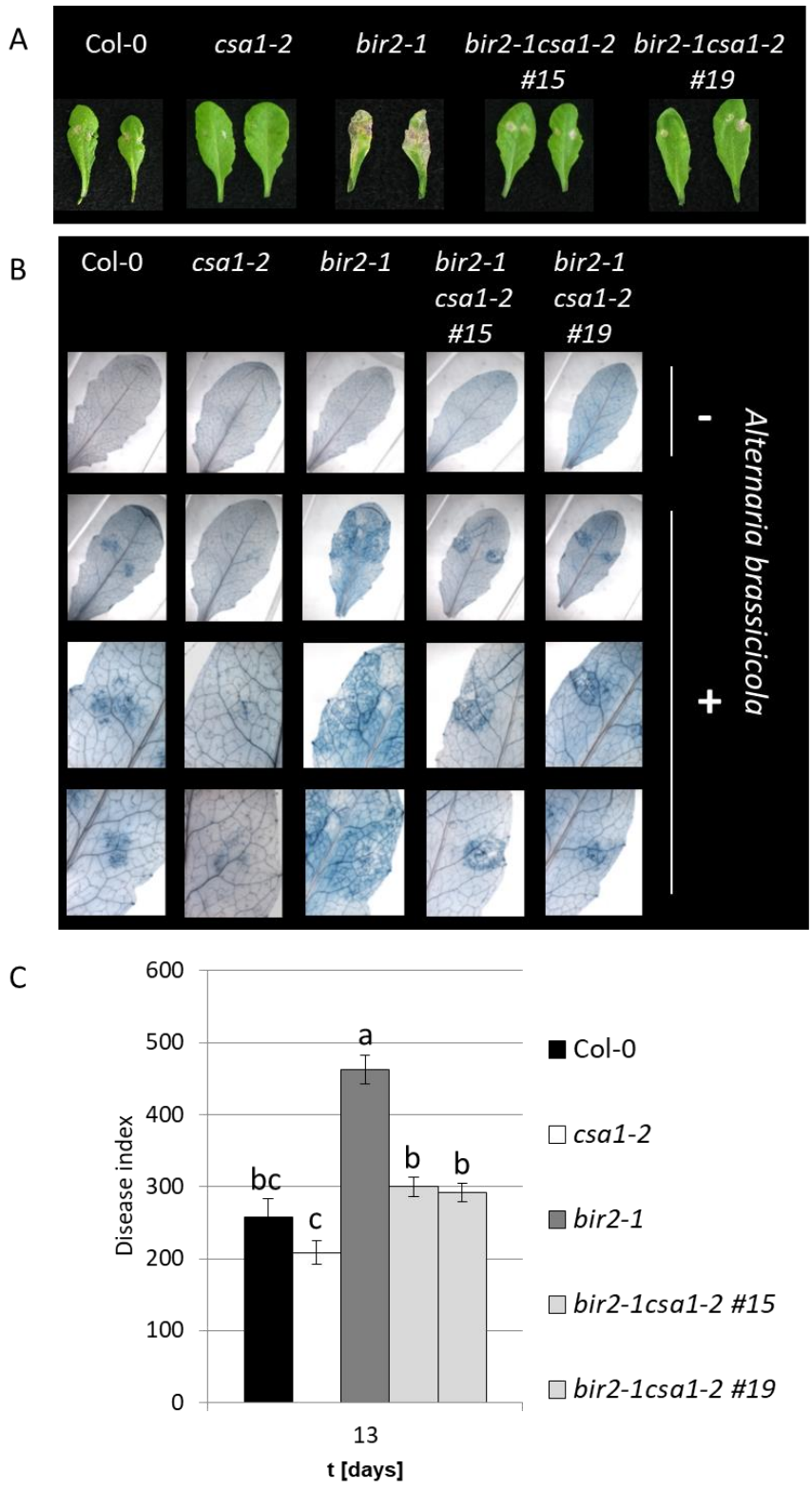

Figure 3.23: *bir2-1csa1-2* shows partial rescue of cell death formation after infection with *A. brassicicola*

Mutant phenotypes of 6 week old plants of the indicated genotypes were monitored after infection with the necrotrophic fungal pathogen *Alternaria brassicicola* A) picture of the symptom development on two representative leaves of each line 13 days after inoculation. B) Trypan blue staining after 4 days of infection with the necrotrophic pathogen *Alternaria brassicicola*. C) Disease index after 13 days is shown as mean ± SE (n=6). Error bars show the standard deviation of the mean, student t-test indicates a significant difference for bars labelled with different letters ($p<0.05$).

Double mutants of *csa1-2* and *bir2-1* were tested for *Alternaria*-induced symptom development. Mutants of *bir2-1* show more symptoms and enhanced cell death after infection accompanied by elevated SA levels (Halter et al., 2014). Interestingly, *csa1-2bir2-1* double mutants displayed a reduction of necrotic tissue 13 days after inoculation in comparison to the *bir2-1*-single mutant (Fig. 3.23A). Trypan blue staining was performed to visualize dead tissue after inoculation of the indicated Arabidopsis lines with the fungus for four days. A spreading cell death formation over almost the whole area of the leaf in *bir2-1* mutants indicates a loss of cell death control, while cell death in wild type is restricted to the region of the applied spot containing *Alternaria* spores (Fig. 3.23B). This is in accordance with the literature, as Col-0 is resistant to this fungus (Gachon and Saindrenan, 2004). The double-mutant *bir2-1csa1-2* showed a partial rescue. Here, the spot of the infected region was slightly bigger when compared to the wild type Col-0. This indicates that the runaway cell death formation observed in the single-*bir2-1*-mutants can be restricted by mutations in *CSA1*. Furthermore, the disease index was significantly reduced, compared to the single-knock-out of *bir2-1* (Fig. 3.23C). These results can be considered as partial rescue, as the double-mutant does not display the same phenotype as the *csa1-2* single mutant.

We measured also the total SA-levels of *bir2-1* mutants in comparison to the double-mutants. This experiment confirmed the enhanced SA-levels in *bir2-1* single mutants (Halter et al., 2014). However, *csa1-2bir2-1* mutants displayed the same SA content as wild type, demonstrating that *csa1-2* can reduce the enhanced *bir2-1* mediated SA levels (Fig. 3.24).

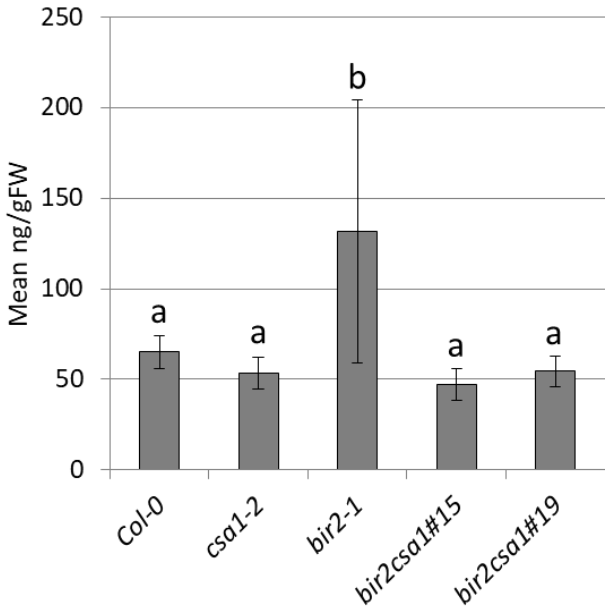

Figure 3.24: *csa1-2bir2-1* double mutants contain reduced SA levels compared to *bir2-1* single knock-out mutants

Total SA levels were detected in untreated 6 week old Arabidopsis plants of the indicated genotypes by method. Results are mean ratios of ng SA to g fresh weigh ± SE (n=6). Error bars show the standard deviation of the mean, student t-test indicates a significant difference for bars labelled with different letters (p<0.05).

3.3.3.3 Loss of CSA1 does not change the MAMP-dependent ROS burst in *bir2-1*

BIR2 is an important negative regulator of the MAMP-pathway by constitutively binding BAK1, thereby preventing the interaction with the respective ligand-binding receptors, such as FLS2 (Halter et al., 2014). To test, whether *bir2-1*-dependent ROS-burst phenotypes are also affected by the loss of *CSA1*, ROS assays were performed by using 100 nM flg22.

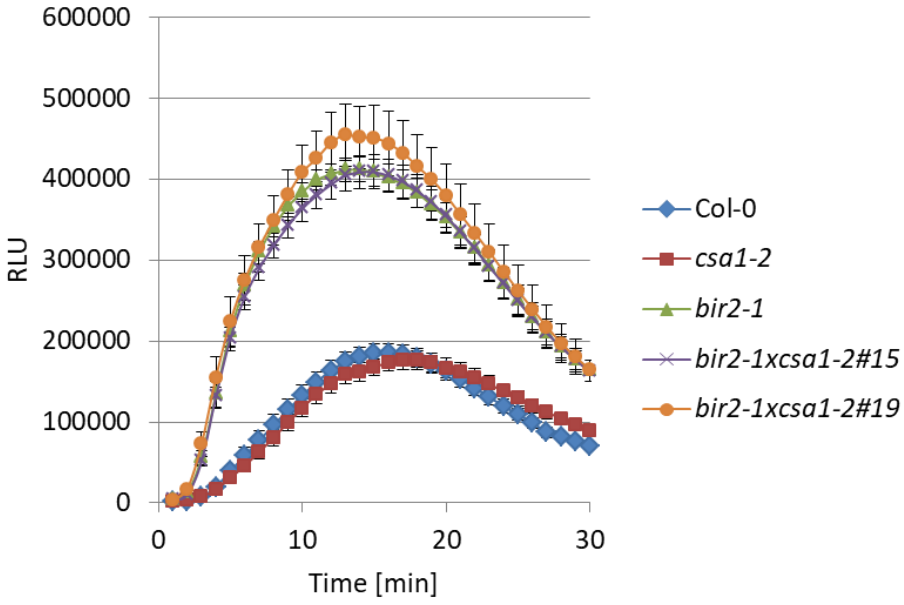

Figure 3.25: CSA1 has no influence on FLS2-induced ROS burst in the double mutant *bir2-1csa1-2*

ROS production was measured with a luminol-based assay on leaf discs of the indicated *Arabidopsis* lines over a period of 30 min after elicitation with 100 nM flg22. ROS production is represented as relative light units (RLU) and results are mean ± SE (n=9).

As shown in figure 3.25, *csa1-2* mutants showed ROS production comparable to wild type levels, whereas *bir2-1* mutants showed an increased ROS production. The loss of *CSA1* in both tested double-mutant lines did not change the ROS production compared to *bir2-1*, indicating that cell death formation and MAMP responses shown for FLS2 are independent from each other.

Summarizing the results of *bir2-1csa1-2* revealed that CSA1 is at least partially responsible for following phenotypes: (i) Infection experiments using the necrotrophic fungus *Alternaria brassicicola* led to reduced lesion sizes measured by disease index determination in the double-mutant line *bir2-1csa1-2* compared to *bir2-1* and (ii) to less cell death formation visualized by trypan blue staining. (iii) Subsequent measurements of total SA-levels of the double-mutants *bir2-1csa1-2*, showed comparable results to SA-levels of the wild type Col-0 and therefore a reduction compared to the elevated SA-levels measured in the single knock-out *bir2-1*. (iv) ROS assay experiments recapitulated the former results that a loss of *CSA1* in *csa1-2* does not influence the production of ROS after elicitation with flg22 compared to Col-0 and does not alter the ROS production in the double-mutant *bir2-1csa1-2* compared to *bir2-1* as well. CSA1 can interact with BIR2. Functional assays on *bir2-1csa1-2* revealed that CSA1 is at least partially responsible for the cell death formation initiated by the absence of BIR2.

3.3.3.4 Loss of CSA1 shows rescue of the *bak1*-dependent cell death phenotype

Mutations in *bak1-4* leading to the loss of *BAK1* show a cell death phenotype of which the mechanism is still elusive. As BIR3 interacts constitutively with BAK1, we tested whether BAK1-mediated cell death is also dependent on CSA1.

Phenotypically there is no difference in growth of both double mutant lines *bak1-4csa1-2* #1 and #23 compared to the single-knock-out line *bak1-4*. The smaller leaf size and shorter petioles are BL-dependent phenotypes and are not altered by the additional *csa1-2* mutation (Kemmerling et al., 2007b). Flowering plants have a similar phenotype compared to the single-*bak1-4* mutant (Fig. 3.26B). The reduction in size of *bak1*-mutants is due to the lack of BL signaling (Wang et al., 2001) and likewise seen in the flowering stem, as well the rosette diameter of all showed mutants, hence BL-pathway seems also not to be affected by a loss of *CSA1*.

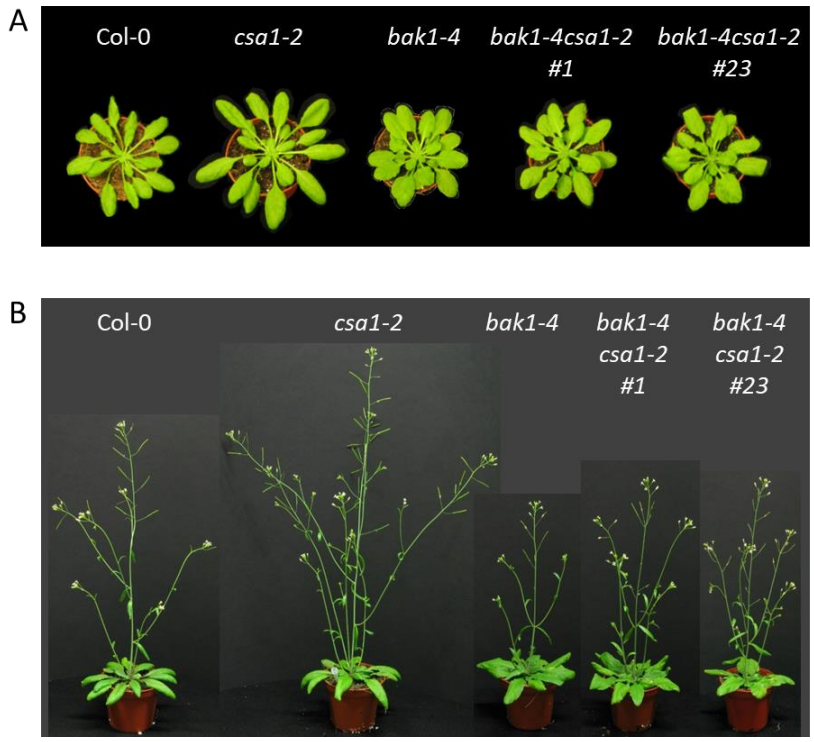

Figure 3.26: *bak1-4* single- and *bak1-4csa1-2*-double mutants share the same morphological phenotype

A) Morphology of 6 week old plants cultivated under short day conditions. B) Comparison of flowering plants. Cultivation under long day conditions for 8 weeks. Double mutants of *bak1-4csa1-2* display the same phenotype as the single knock-out of *bak1-4*, whereas *csa1-2* mutants show a slightly taller flowering stem, compared to wild type Col-0.

BAK1-mediated cell death is partially understood (see 1.1.3.1). Different downstream components such as EDS1 are already described to play a positive role in BAK1-mediated cell death, indicating an NLR-dependent pathway. Still, no NLR is reported so far. In order to test the influence of CSA1 in the BAK1-mediated cell death pathway, trypan blue stains for dead cells were conducted with and without *Alternaria* infection.

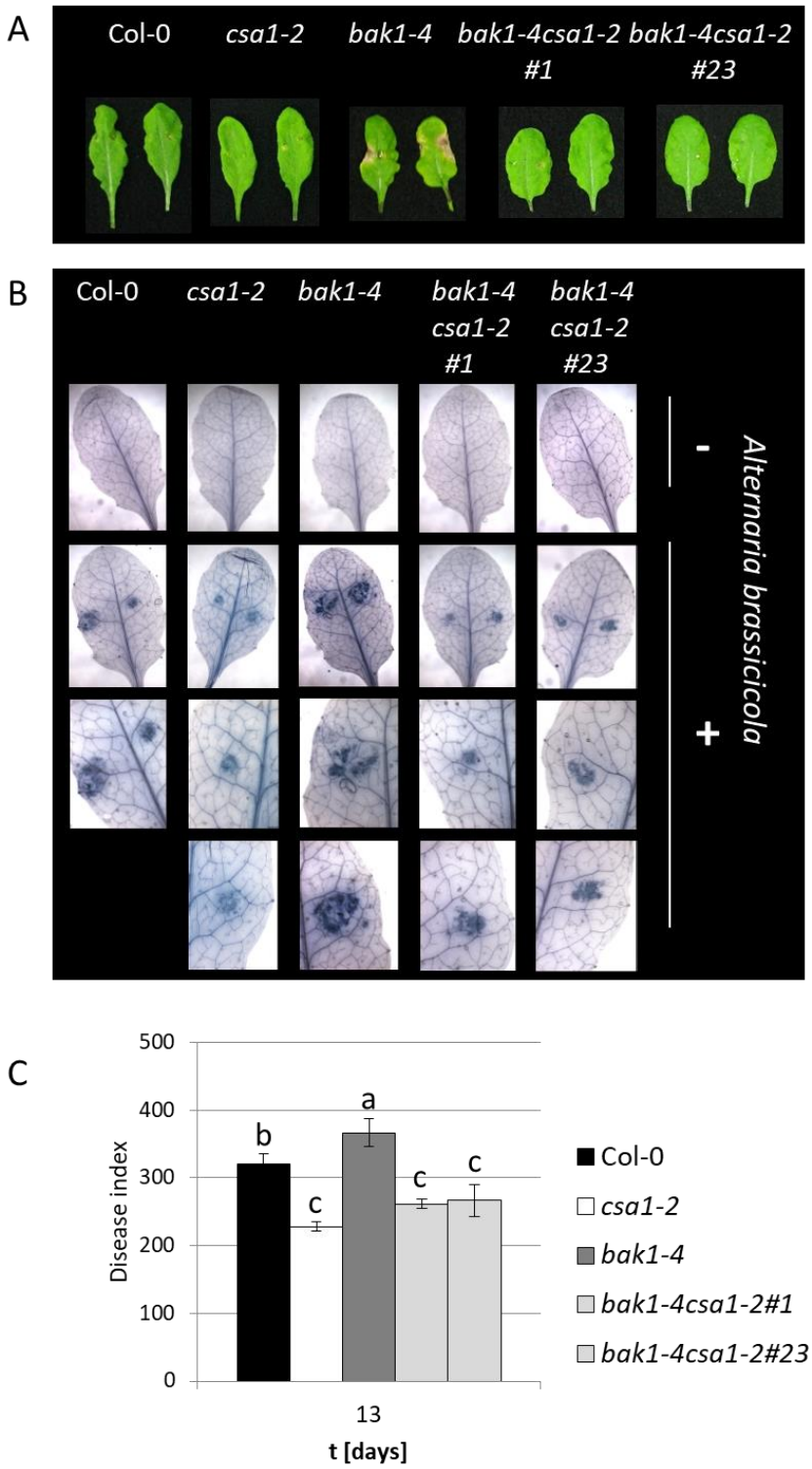

Figure 3.27: Loss of *CSA1* in the background of *bak1-4* leads to a reduction of cell death symptoms

Mutant phenotypes of 6 week old plants of the indicated genotypes were monitored after infection with the necrotrophic fungal pathogen *Alternaria brassicicola* A) Picture of the symptom development on two representative leaves of each line after 13 days of inoculation B) Trypan blue staining 4 days after infection. The dye stains only dead cells within the indicated Arabidopsis lines. Untreated leaves are indicated with a “minus” (-), treated leaves with a “plus” (+). C) Disease index after 13 days is shown as mean ± SE (n=4). Error bars show the standard deviation of the mean, student t-test indicates a significant difference for bars labelled with different letters ($p<0.05$).

Phenotypically, the double-mutant of *bak1-4csa1-2* display less cell-death-formation after infection with the necrotrophic fungus *A. brassicicola,* when compared to the single-knock-out *bak1-4* (Fig. 3.27A). Trypan blue staining was used to visualize dead tissue in the different lines. The spreading cell death, observed in *bak1-4* single mutants, was restricted to the site of infection in the *bak1-4csa1-2* double mutants, demonstrating that the loss of *CSA1* in the *bak1-4* background possesses the ability to prevent cell death formation (Fig. 3.27B). The disease index of *bak1-4csa1-2* was significantly reduced, indicating a rescue of symptom development of the fungus compared to *bak1-4* lines after treatment (Fig. 3.27C).

Total SA levels were also analyzed as before, as it is well described that cell death formation within *bak1-4*-lines correlates with elevated SA levels (Gao et al., 2017). As shown in Figure 3.28, total SA levels of one double mutant line (#1) showed comparable SA-levels to wild type and *csa1-2* single-mutants, whereas the second mutant line (#23) showed significant differences to the *bak1-4* single-mutant line.

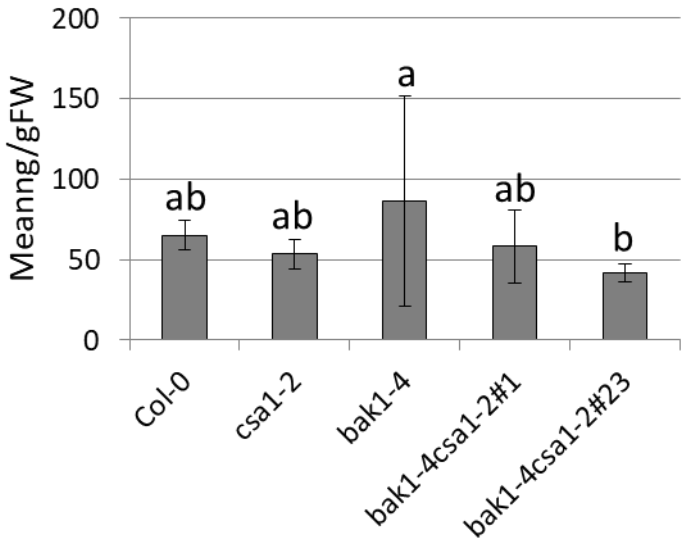

Figure 3.28: *csa1-2bak1-4* mutants display reduced SA levels compared to the *bak1-4* single knock-out

Total SA levels were detected in untreated 6 week old Arabidopsis plants of the indicated genotypes by method. Results are mean ratios of ng SA to g fresh weigh ± SE (n=6). Error bars show the standard deviation of the mean, student t-test indicates a significant difference for bars labelled with different letters ($p<0.05$).

3.3.3.5 Loss of *CSA1* shows no effect on FLS2-mediated ROS burst in *bak1-4* after MAMP treatment

BAK1 is a well described positive regulator of plant immunity, as it is the co-receptor of many pattern recognition receptors, such as FLS2, EFR and PEPR1 (Zipfel et al., 2006; Boller and Felix, 2009a; Krol et al., 2010). We asked whether the loss of *CSA1* in the background of *bak1-4* affects only cell death formation or also PTI-signaling. To test this, we triggered the FLS2-pathway by using 100nM flg22 as elicitor.

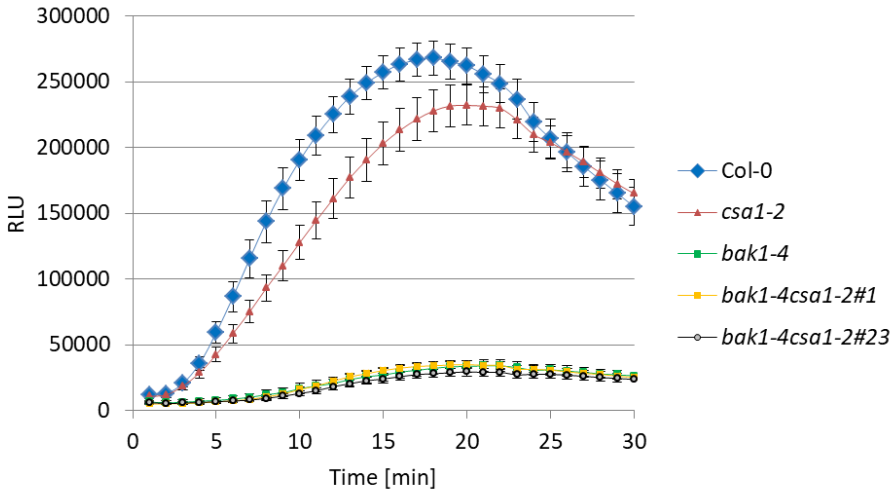

Figure 3.29: *bak1-4csa1-2* shows the same ROS burst pattern as the single knock-out of *bak1-4*

ROS production was measured with a luminol-based assay on leaf discs of the indicated Arabidopsis lines over a period of 30 min after elicitation with 100 nM flg22. ROS production is represented as relative light units (RLU) and results are mean ± SE (n=9). The loss of *CSA1* in the double mutant of *bak1-4csa1-2* shows no alteration of the ROS-production compared to the single-ko of *bak1-4*.

The ROS burst assay showed a typical peak after 10 min elicitation using flg22 in case of Col-0 as well as for *csa1-2*. The reduced ROS-production of *bak1-4*-mutants was still maintained in the double-mutants, demonstrating that CSA1 has no effect on FLS2-induced ROS burst (Fig. 3.29). This shows that cell death formation and PTI-signaling are independently regulated, at least for the FLS2-pathway.

Summarizing the results of the interplay of BAK1 and CSA1 regarding cell death, we could clearly show that the cell death formation within the *bak1-4*-mutant is dependent on CSA1. The experiments performed with the necrotrophic fungus *A. brassicicola* confirmed a rescue of the spreading necrosis visualized by trypan blue staining (Fig. 3.27), as well a rescue of symptom development measured by disease indices. We were also able to show that the SA level is significantly decreased in the double mutant (#23) compared to the single-mutant

line *bak1-4.* The ROS burst assays using flg22 as elicitor demonstrated that FLS2-signaling is not affected in the double-mutant *bak1-4csa1-2* compared to the single-knock-out *bak1-4*, indicating that PTI and cell death are also here differentially regulated.

4 Discussion

4.1 Co-IP experiments reveal novel interactors of BIR3

The BIR-family (in this work BIR2 and BIR3) displays a central role in the negative regulation of BAK1 and its co-regulated pathways (Gao et al., 2009b; Halter et al., 2014; Imkampe et al., 2017). From BIR1 to BIR3, all constitutively bind to BAK1, the multifunctional co-receptor of surface located LRR-RLKs (RLKs), positively regulating BL-, MAMP- and DAMP-signaling respectively (Li et al., 2002; Nam and Li, 2002; Chinchilla et al., 2006; Postel et al., 2010; Ross et al., 2014). Subsequent downstream-signaling exerted by the ligand-bound receptor and BAK1 is inhibited by different members of the BIR-protein family (so far described for BIR1 to BIR3) (Gao et al., 2009a; Halter et al., 2014; Imkampe et al., 2017). Only BIR3 is described to additionally bind to ligand-binding receptors apart from BAK1, such as FLS2 and BRI1 (Imkampe et al., 2017; Großeholz et al., 2020). In this work Co-IP experiments performed by transient expression in tobacco revealed the interaction of BIR3 with two additional immunity-related receptors apart from FLS2 (Imkampe et al., 2017): PEPR1 and EFR (Fig. 3.2B). This confirmed the idea of BIR3 being a multiple negative regulator of BAK1-dependent ligand-binding receptors. For BRI1 and FLS2, a direct interaction with BIR3 could be confirmed using BIFC and Yeast-two-hybrid systems, respectively (Imkampe, 2015). Here, Co-IP experiments performed in Arabidopsis confirmed the interaction of BIR3 and BRI1 *in planta* (Fig. 3.2A). The finding that BIR3 binds also to ligand-binding receptors prompted us to the following question: could BIR3 function as a general negative regulator in PRR-mediated signaling? Therefore, one aim of this work was to reveal whether BIR3 can generally interact with further LRR-RLKs using MS analyses.

4.2 The BIR3 interactome

4.2.1 MS analyses reveal further LRR-RLKs

To answer the question, whether BIR3 is a general regulator of LRR-RLKs, two independent MS analyses were performed. As a proof of concept, all members of the SERK-family appeared in both MS analyses. This is in line with previous findings showing interaction of all SERKs with BIR3 (Imkampe et al., 2017). Furthermore, the conducted MS analyses revealed 32 LRR-RLKs in total, whereas 10 LRR-RLKs, including all five SERK proteins, showed up in both, including two RLKs already described to signal with the help of BAK1 (STRESS INDUCED

FACTOR 3 (SIF3) and SOBIR1 (Liebrand et al., 2013; Stegmann et al., 2017; Guo et al., 2018; Yuan et al., 2018)), two (MDIS1-INTERACTING RECEPTOR LIKE KINASE2 / MIK2 and HYDROGEN-PEROXIDE-INDUCED CA^{2+} INCREASES / HPCA1) which seem to signal without the help of SERK proteins and one with unknown function (At5g14210). SOBIR1 was initially described to restore the cell death phenotype of *bir1-1*, a loss-of-function mutant of BIR1 (Gao et al., 2009a). Years later, SOBIR1 was shown to be a general regulator for RLPs involved in plant immunity and development in a BAK1-dependent manner (Leslie et al., 2010; Liebrand et al., 2013; Zhang et al., 2013; Gubert and Liljegren, 2014; Liebrand et al., 2014; Albert et al., 2015; Hohmann and Hothorn, 2019). SIF3, the second LRR-RLK depending on BAK1 for signaling, on the contrary represents a LRR-RLK solely described to be involved in plant immunity as it regulates basal PTI-responses upon treatment with *Pst* DC3000, such as callose deposition, stomatal closure and ROS accumulation (Yuan et al., 2018). Those responses were shown to be dependent on BAK1, but only after pathogen treatment (*Pst* DC3000), suggesting a ligand dependent complex formation with BAK1, yet the MAMP is not known so far (Yuan et al., 2018). As BIR3 is described to constitutively bind in a constitutive manner to BAK1 in order to prevent unwanted signaling, it makes sense to detect RLKs where BAK1 functions as co-receptor. It is noticeable that both are also involved in PTI, thus potentially expanding the repertoire of BIR3´s involvement in plant immunity. Whether BIR3 also negatively regulates these signaling pathways, and whether BIR3 binds these RLKs directly and/or fulfills its role in inhibiting signaling *via* the binding of BAK1, have still to be investigated. As mentioned before, BIR3 is described to constitutively bind to and negatively regulate BAK1 and BAK1-dependent pathways (Imkampe et al., 2017; Ma et al., 2017; Hohmann et al., 2018). It is striking that both, MIK2 and HPCA1, two potential BAK1-independent LRR-RLKs, showed up in both conducted MS analyses. MIK2 belongs to the sub-family XIIb of LRR-RLKs, containing 24 LRRs, whereas HPCA1 consists of 9 LRRs and is part of the subfamily VIII-1 of LRR-RLKs. Taking into account that RLKs containing 15 to 30 LRRs are considered to be potential ligand- binding receptors, HPCA1 does not fall into this category (Hohmann et al., 2017; Van der Does et al., 2017a; Wu et al., 2020b). Studies from January 2020 revealed the function of HPCA1 as being a hydrogen peroxide sensor which mediates H_2O_2-induced activation of Ca^{2+}-channels in guard cells, thus participating in stomatal closure (Wu et al., 2020b). In PTI, stomatal closure is an important step, as stomata display the prime entrance for invading pathogens (Yu et al., 2017). The mode of action of how HPCA1 gets activated is described as an auto-phosphorylation event after modification of

extracellular cysteine residues by H_2O_2 (Wu et al., 2020b). Hence, HPCA1 seems to represent an LRR-RLK which, most likely, acts independently of co-receptors for phosphorylation. Whether and to what extent HPAC1 plays a role in PTI and is influenced by BIR3 are still open questions. MIK2 was identified as receptor sensing cell-wall damage triggered by cellulose biosynthesis inhibition, required for salt tolerance (Van der Does et al., 2017a) and controlling pollen-tube guidance by building a receptor complex with MALE DISCOVERER1 (MDIS1) and MDIS1-INTERACTING RECEPTOR LIKE KINASE1 (MIK1) (Wang et al., 2016; Van der Does et al., 2017a). Together they recognize the female attractant LURE1, a defensin-like peptide (Wang et al., 2016). So far, no interaction with BAK1 could be shown in the MIK2 pathway controlling pollen-tube development, thus it is described to signal without the help of SERK proteins so far (Wang et al., 2016). One LRR-RLK (At5g14210) appeared in both analyses with a high-significance value on position no. 3 in both analyses using our criteria for ranking MS-candidates (see Appendix table A1 to A4). It belongs to the subfamily VI of receptor kinases and contains 10 LRRs in total, additionally to that, At5g14210 was found in an MS analysis from a collaborating lab, using BIR3 as bait as well (personal communication with Sacco de Vries, Wageningen) and represents therefore a highly-interesting candidate for further investigations.

The results of both conducted MS analyses revealed 32 additional LRR-RLKs as potential interacting partner of BIR3, thus supporting the hypothesis of BIR3 being a general interactor of LRR-RLKs. With SOBIR1 and SIF3, two RLKs could be detected which (i) signal with the help of BAK1 and (ii) are involved in plant immunity. It is notable that the spectrum of BIR3-regulated LRR-RLKs could at the same time be extended by two potential LRR-RLKs which do not rely on SERK proteins for signaling (MIK2 and HPCA1). This sheds new light on BIR3´s function which has been described to act in a BAK1-dependent manner so far (Imkampe et al., 2017; Hohmann et al., 2018). The spectrum of BIR3´s interacting partners could potentially be extended to LRR-RLKs that do not rely on BAK1. If and how BIR3 is involved in regulating the described RLKs is still elusive and needs further investigations.

4.2.2 MS-analyses reveal regulators of cell death

In the respective null-mutants of *bir1/2/3* and *bak1*, there is a decline in cell death occurrence observable (Fig. 4.1). While the loss of *BIR1 (bir1-1)* and the complex of *BAK1/BIR3 (bak1-4bir3-2)* leads to a severe autoimmune phenotype, the autoimmune phenotype of *bir2-1* and *bak1-4* mutants is less distinct and lost in *bir3-2* mutants (Gao et al.,

2009a; Halter et al., 2014; Imkampe et al., 2017). Challenging with the necrotrophic fungus *Alternaria brassicicola* reveals the degree of cell death within the weak autoimmune phenotypes *bir2-1* and *bak1-4*: *bir2-1* mutants show a stronger disease index than *bak1-4* mutants. It was shown that the dwarf phenotype in *bir1-1* mutants as well as in *bak1-4bir3-2* mutants are caused by constitutive activation of defense responses (Gao et al., 2009a; Imkampe et al., 2017), the same was shown for early necrosis, occurring in *bir2-1* mutant lines (Halter et al., 2014) (Fig. 4.1). The compact phenotype of *bak1-4*, instead, was related to BL-insensitivity, as BAK1 is the main co-receptor of BRI1, with the additional feature of runaway cell death formation after treatment with a necrotrophic pathogen (*A. brassicicola*) (He et al., 2007; Kemmerling et al., 2007b). Furthermore, the overexpression of *BIR1*, *BIR2* and *BIR3* contributes also to a differential increase in cell death (Imkampe, 2015; Guzmán-Benito et al., 2019). Hence, well balanced receptor levels of the BIR-family are crucial for surviving. A trait that is shared by BAK1 as well.

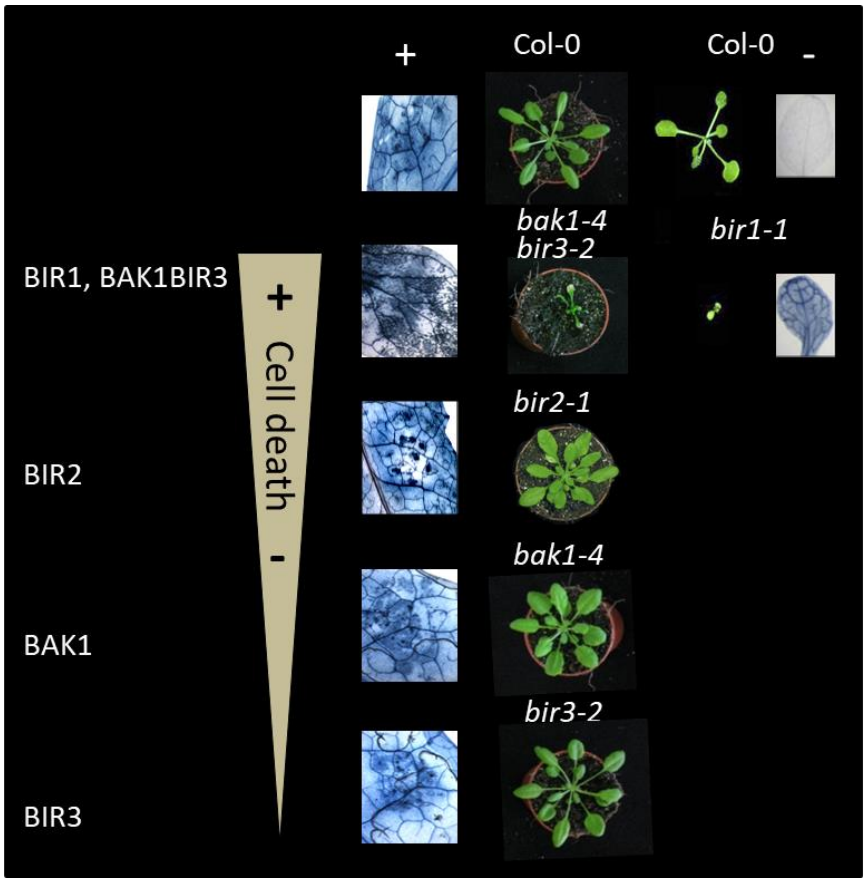

Figure 4.1: Morphological and cell death differences in mutants of the BIR-family and BAK1

Trypan blue staining (after inoculation for 13 days with *Alternaria brassicicola*, indicated with a "plus" (+)) and Morphology of 6-week-old plants cultivated under short day conditions for *bak1-4bir3-2, bir2-1, bak1-4, bir3-2* and 3 week old plants of *bir1-1* mutants grown on soil at 22°C. Trypan blue staining of *bir1-1* mutants was performed without challenging with a pathogen (indicated with a "minus" (-)) (Gao et al., 2009a). The morphological differences in the different KO-mutant lines of *bir1* to *bir3* (in complex with *bak1*) could be

related to constitutive activation of immune responses, leading to elevated cell death, visualized with trypan blue (Gao et al., 2009a; Halter et al., 2014; Imkampe et al., 2017). The loss of *BIR1* (Gao et al., 2009a) and the complex of *BAK1BIR3* leads to a severe autoimmune phenotype that is less severe in *bir2-1* mutants. The morphological phenotype of *bak1-4* mutant lines is related to BL-insensitivity, but displays also an autoimmune phenotype, when challenged with a necrotrophic pathogen (He et al., 2007). The loss of *BIR3* instead, does not show any cell death phenotype (Imkampe et al., 2017).

To study the effects of BIR3 on cell death, we performed MS analysis using BIR3 as bait, with the focus on candidates explaining the loss of cell death control. These candidates were (i) NLRs potentially acting as guards for BIR-proteins and/or BAK1 and (ii) proteins described to be involved in regulating cell death. In total, 26 cell-death-related proteins could be detected, whereas three appeared in both conducted MS analyses. These were SOBIR1, HEXOKINASE1 (HXK1) and METACASPASE4 (MC4). SOBIR1 is, next to its function of being a central regulator of RLP-signaling, described to be a positive regulator of cell death, and loss of *SOBIR1* in the background of *bir1-1*, BAK1-overepressing lines or the proteolytic cleavage insensitive mutant of BAK1, $BAK1^{D187A}$, leads to at least a partial rescue of cell death in the respective mutant line (Gao et al., 2009b; Dominguez-Ferreras et al., 2015; Zhou et al., 2019). Additionally, it could be shown that SOBIR1 interacts with BAK1 only in the absence of BIR1 leading to cell death, demonstrating that SOBIR1 promotes cell death in concert with BAK1 and revealed the role of BIR1 to prevent a SOBIR1 - BAK1 association via binding to BAK1 (Gao et al., 2009a; Liu et al., 2016). Furthermore, an overexpression of SOBIR1 leads to the activation of cell death as well (Gao et al., 2009a). Hence a control of SOBIR1 is needed to prevent unwanted interaction at least with BAK1. Imkampe (2015) tested in her thesis the relationship between the different members of the BIR-family. She could show that the overexpression of BIR3 in the background of *bir1-1* led to a partial rescue (Fig. 4.2A) (Imkampe, 2015). The same was observed, when *SOBIR1* got lost in the background of *bir1-1*. As the *sobir1-1bir1-1*-mutant line is reminiscent to the *bir1-1* 35S-BIR3-line (Fig. 4.2A / B) and due to the detection of SOBIR1 within the BIR3-interactome, one can speculate that this partial rescue caused by the overexpression of BIR3 could be due to the binding of BIR3 to SOBIR1, impeding SOBIR1-BAK1 interaction (Fig. 4.2C-a)). Another possibility would be based on the observation that *bak1* mutants partially rescue the cell death phenotype in *bir1* background as well (Liu et al., 2016; Wierzba and Tax, 2016). In this scenario one could also speculate, that the overexpression of BIR3 leads to an overprotection of BAK1, thereby mimicking a *bak1* mutant (Fig.4.2C-b)). Both possibilities would explain the partial rescue of BIR3 overexpression in *bir1-1* background. If BIR3 binds directly to SOBIR1, either independently of BAK1-binding (Fig. 4.2C-a1)) or as a ternary complex of BAK1-BIR3-SOBIR1

(Fig. 4.2.C-a2)), to bypass BAK1-SOBIR1 interaction, or if BIR3 overexpression leads to a depletion of available BAK1, mimicking a *bak1*-mutant line (Fig. 4.2C-b), needs further investigations. In both scenarios, the interaction of SOBIR1 and BAK1 would be inhibited, leading to a subsequent suppression of cell death symptoms.

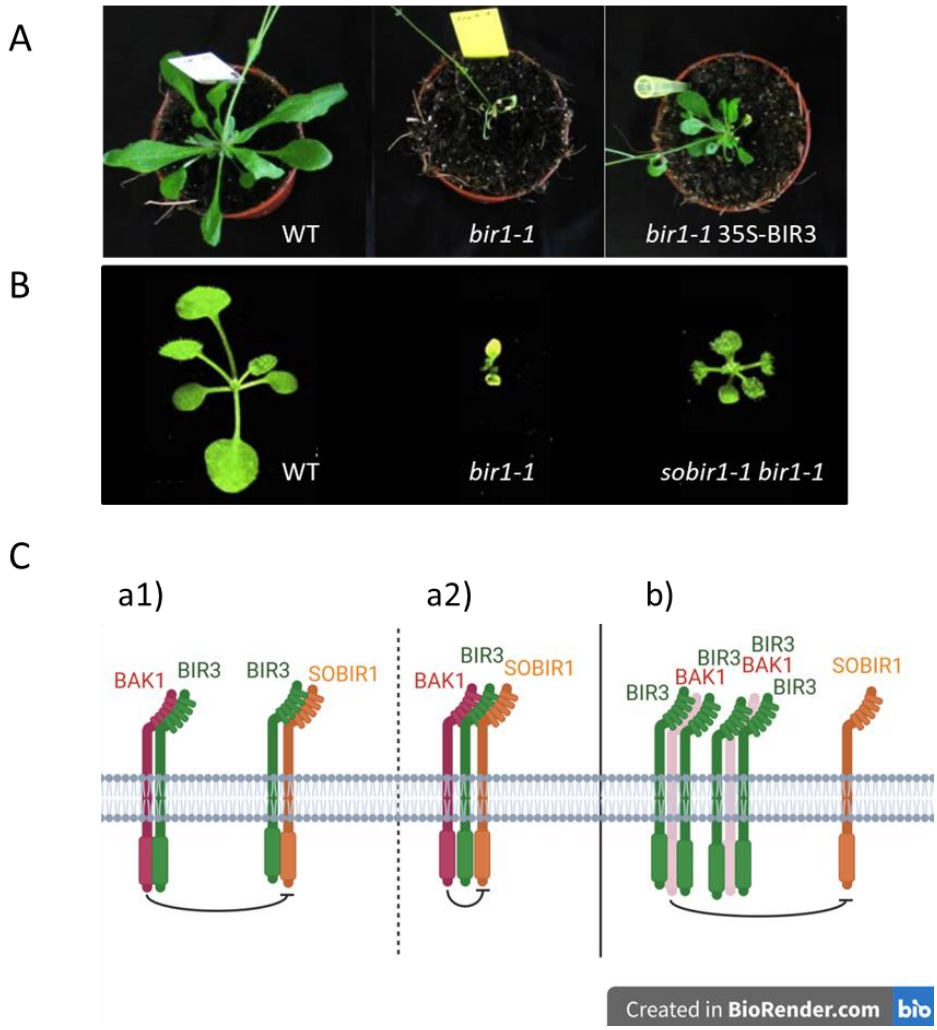

Figure 4.2: Does BIR3 mimic BIR1 by isolating BAK1 from SOBIR1?

A) The overexpression of BIR3 in the *bir1-1* mutant line leads to a partial rescue. B) The same phenotype was seen when *SOBIR1* was knocked out in the background of *bir1-1*. SOBIR1 was a candidate BIR3 interactor, detected in both MS-analyses, when BIR3 was pulled down. This connection could explain, why the overexpression of BIR3 leads to a partial rescue in the *bir1-1* background: C) by potentially preventing the association between BAK1 and SOBIR1 by BIR3, similar to the described function of BIR1 by Liu et al. (2016), either directly by binding to SOBIR1 (a1 and a2), or by b) overprotection of BAK1, mimicking *bak1*-mutants, similar to the observation by Wierzba and Tax (2016) and Liu et al. (2016). Modified (Gao et al., 2009a; Imkampe, 2015).

HXK1, the second candidate, detected twice, was described to act as a genuine glucose sensor, by catalyzing the phosphorylation of sugars (Rolland et al., 2006; Granot et al., 2014). An additional role for HXK1 is one of mediating cell death in the mutant line of D-MYO-INOSITOL 3-PHOSPHATE SYNTHASE 1 (MIPS1), due to changes in *myo*-inositol (MI) synthesis

(Bruggeman et al., 2015). The exact function of HXK1 in changing MI-contents is still under investigations. BIR3 represents a plasma-membrane (PM) localized pseudokinase which potentially could recruit HXK1 to the PM in order to exert its function. If BIR3 acts as a potential scaffold protein guiding receptor complexes toward the plasma membrane has to be shown in the future.

The third candidate, METACASPASE4 (MC4), is a cysteine protease of the type-II class of metacaspases (Watanabe and Lam, 2011). Two recent studies revealed the mechanism, how MC4 gets activated upon flg22-treatment (Hander et al., 2019; Shen et al., 2019). The work showed that PROPEP1, the precursor of the PEP1/2 and ligand for PEPR1/2, gets induced *via* MAPKs and CDPKs upon flg22-treatment, leading to the accumulation of PROPEP1 at the cytosolic face of the tonoplast. Simultaneously, flg22-treatment leads to an Ca^{2+}-influx and thus to the activation of MC4 by self-cleavage, which in turn catalyzes the cleavage of PROPEP1 to the potent PEPR1-ligand PEP1 (Hander et al., 2019; Shen et al., 2019). Indeed, in this work the interaction between BIR3 and PEPR1 could be shown, using Co-IP experiments in tobacco, but if, how and to which extent BIR3 interaction with MC4 plays a role in this pathway remains to be elucidated.

As mentioned before, the occurrence of cell death observed in loss-of-function mutants of BIR-proteins and/or BAK1 could also be explained by NLR receptors guarding the integrity of those. Two full length canonical NLRs were detected: the TIR-NBS-LRR (TNL) CONSTITUTIVE SHADE AVOIDANCE 1 (CSA1) within the first MS analysis and RECOGNITION OF PERONOSPORA PARASITICA 8 (RPP8) in the second MS analysis, a representative of the coiled-coil-NBS-LRR (CNL)-class of NLRs. Due to time restriction the effect of RPP8 was not further characterized. Additionally, two TIR-like NLRs were detected: RESISTANCE TO LEPTOSPHAERIA MACULANS3 (RLM3) and TOLL/INTERLEUKIN-1 RECEPTOR-LIKE10 (TN10). Both R-genes encode Toll interleukin-1 receptor-nucleotide binding (TIR-NB)-class proteins, lacking the LRR-domain. Those are supposed to function as adaptor proteins with the potential to bind others TNLs and / or downstream components (Peele et al., 2014). Also here, the work on both TN-class NLRs could not be started due to time restrictions.

CSA1 was the first NLR from our first MS analysis and therefore the first candidate of high interest to study. Hence, this work focuses on the regulation of cell death with regards to the TIR-NBS-LRR protein CSA1. We were strongly interested if and how this protein is involved in cell death phenotypes mediated by the loss of *BAK1*, *BIR2* and the complex *BIR3*/*BAK1* and

how this is connected to plant immunity. Therefore crossings with null-mutants of *csa1* and the mentioned BIR-proteins and BAK1 in combination with functional assays were performed.

4.3 CSA1 suppresses partially BAK1- and BIR-family mediated cell death

4.3.1 CSA1 functions as a pair with the TNL CHS3

CSA1 and CHS3 belong to the class of TIR-NBS-LRR-proteins, forming a functional NLR-pair, thus supposed to function as one unit (Monteiro and Nishimura 2018). They are arranged in a head-to-head manner in the genome, sharing an approximately 3,9 kb-region upstream of their respective start codons and are assumed to possess overlapping promoter regions (Xu et al., 2015). Hence, they might function under transcriptional co-regulation. CSA1 is a typical TNL (N-terminal TIR domain, NBS-domain, C-terminal LRR-domain, see Appendix Fig. A1), whereas CHS3 encodes an atypical TNL, bearing a single zinc-binding Lin-11, Isl-1 and Mec3-domain (LIM-domain) at the C-terminus (Yang, Shi et al. 2010). Additionally to the LIM-domain at the C-terminus, CHS3 contains a Zinc-protease domain (position aa1485 to aa1494), defined by the conserved HExxH-motif at position aa1488 to aa1492 corresponding to UniPRot and Expasy Prosite / ScanProsite results viewer (see Appendix Fig. A2). Interestingly, it has been shown that DA (LARGE IN CHINESE) 1 (DA1), a member of the same subgroup of single LIM-containing proteins as CHS3, is an active peptidase, controlling final organ and seed size, activated upon ubiquitination by two RING E3 ligases: Big Brother (BB) and DA (LARGE IN CHINESE) 2 (DA2)) (Li, Zheng et al. 2008, Dong, Dumenil et al. 2017, Vanhaeren, Nam et al. 2017). If CHS3 acts as an active protease too, or if the zinc-protease domain displays an additional ID without catalytic function, next to the LIM-domain, is still elusive and needs further investigations.

CSA1 was first described to be involved in two different pathways, as a mutation in CSA1 leads to impaired red-light signaling and plant resistance (Faigon-Soverna et al., 2006). In this publication, two mutant lines are described: (i) *csa1-1* carries an insertion of the 35S-enhancer sequence derived from Cauliflower mosaic virus (CaMV) in the second exon. This insertion leads to a truncated CSA1-protein which lacks the complete LRR-region as well as part of the NBS-domain, thus containing the full length TIR- and part of the NBS-domain, which acts as a dominant negative mutant. The second mutant line, (ii) *csa1-2*, bears an insertion in the 4th exon without enhancer sequences. This insertion leads to a knock-out

mutant with almost no mRNA detectable (Faigon-Soverna et al., 2006). It shows a weaker phenotype in comparison to *csa1-1*, explained by the authors due to redundancy with other family members, like RESISTANT TO P. SYRINGAE 4 (RPS4) or LAZARUS 5 (LAZ5) which share 64% and 63% sequence similarity with CSA1 respectively (Faigon-Soverna et al., 2006). This interpretation was supported by over-expression of RPS4 in the background of the *csa1-1* mutant line. The phenotype showed wild-type red-light signaling, likely due to a putative formation of incompatible heterodimers *via* the TIR-domains of CSA1 and RPS4. TIR-domains can function as dominant-negative forms by blocking downstream signaling (Williams et al., 2014b), explaining the function of the *csa1-1* mutant line. Using the assay, the authors could show that the overexpressed RPS4 protein in the background of *csa1-1* attenuated the *csa1-1* phenotype by intercepting the truncated CSA1-protein via its TIR domain and with this the dominant negative effect (Faigon-Soverna et al., 2006). It is noteworthy that RPS4 shares the same upstream and downstream-components as CSA1, such as HSP90, SGT1 and EDS1 (Zhang et al., 2004). In 2015, CSA1 was found in a suppressor-screen of the strong gain-of-function mutant line *chs3-2D* (Xu et al., 2015). *Chs3-2D* shows elevated defense responses as increased *PR*-gene expression, high SA-levels and enhanced resistance to *Hyaloperonospora arabidopsidis* Noco 2 (*Hp.a*. Noco2), an oomycete displaying a biotrophic lifestyle (Bi et al., 2011). Additionally, those mutant-plants are strongly affected in their morphology showing a severe dwarfism and curved leaves. Suppressor lines (*soc5* to *8*), which were mapped to the *CSA1*-gene, contained point-mutations within the NBS-domain (*soc5, 6, 8*) and the generation of a stop codon in LRR10 (*soc7*). All mutants are loss-of-function mutants and were able to fully suppress the *chs3-2D*-phenotype (Xu, Zhu et al. 2015), demonstrating for CSA1 that the NBS domain as well as the LRR-domain are likely needed for activation of the protein in terms of executing cell death (Fig.4.3).

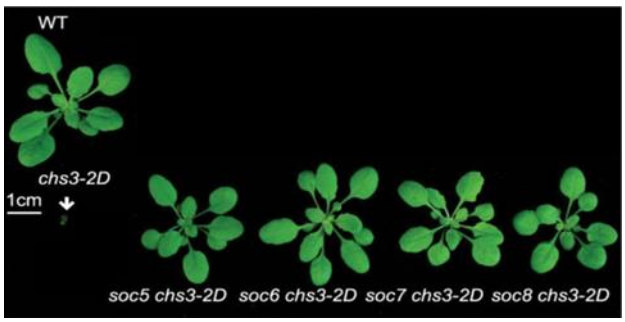

Figure 4.3: The loss of CSA1-function rescues the autoimmune-phenotype of *chs3-2D*

A suppressor screen revealed that the autoimmune phenotype occurring in the auto-active mutant *chs3-2D*, could be fully rescued by a loss of its genetically linked NLR-partner CSA1 (*soc5* to *8*) (Faigon-Soverna et al., 2006) modified.

So far, three gain-of-function-mutants of CHS3 are characterized: *chs3-1, chs3-2D* and *chs3-3D* (Yang et al., 2010; Bi et al., 2011). All of them share a mutation either within (*chs3-1:* (Yang et al., 2010) or close to the LIM-domain (*chs3-2D, chs3-3D*: (Bi et al., 2011)), resulting in a constitutively-active autoimmune-phenotype. This suggests that the C-terminus containing the LIM-domain and its surrounding regions are required either for auto-inhibition or for recruiting negative regulators of CHS3 and / or CSA1, in order to prevent activation. CHS3 is additionally described as a temperature-sensitive TNL: the gain-of-function mutant *chs3-1* showed arrested growth, chlorosis and activation of defense responses, such as elevated SA-levels and induction of *PR1* and *PR2* only when grown at 16°C or when shifted from 22°C to 4°C (Yang et al., 2010). Grown at 22°C the mutation did not cause any defense phenotype and behaved like wild-type. Subsequently conducted suppressor screens revealed mutations located in the P-loop /kinase1 and kinase2-motif of the NB-domain of CHS3 within the *chs3-1* mutation line, which abolished the autoimmune phenotype (Yang et al., 2010). Using the second gain-of-function line, *chs3-2D*, the suppressor screen unveiled two other loss-of-function mutants of CHS3 (Bi et al., 2011). Those lines have point-mutations, leading to amino-acid substitutions either in the LRR-domain (position 716) or in the LRR-linker-domain (position 1007), indicating that these regions are important for CHS3-activation. Interestingly, loss-of-function mutants (*chs3-2, -3, -4*) show no obvious phenotype, indicating that CSA1 might be auto-inhibited and/or possibly needs to be activated through CHS3 to execute its function (Yang et al., 2010). The integrated domain (ID) at the C-terminus of CHS3 seems to play a crucial role in the activation of the CHS3/CSA1 NLR-pair. In general, the ID might act as an effector sensor and central regulator at the same time in order to activate its genetically adjacent partner in order to ward off pathogens (Bialas et al., 2018). CHS3 can therefore be defined as a sensor-NLR, whereas CSA1 would be named by definition an executor-NLR (Jubic et al., 2019). Indeed, the loss of CSA1 inhibits the strong autoimmune-phenotype of the *chs3-2D*-mutant line (Xu et al., 2015), demonstrating that CSA1 is functional downstream of CHS3 and therefore necessary for signaling. Because of its function in executing cell death downstream of CHS3, the knock-out line *csa1-2* was chosen in this work to analyze if the cell-death phenomenon within the BIR-family and BAK1 could be rescued by inhibiting downstream signaling executed by CSA1 (Fig. 4.4).

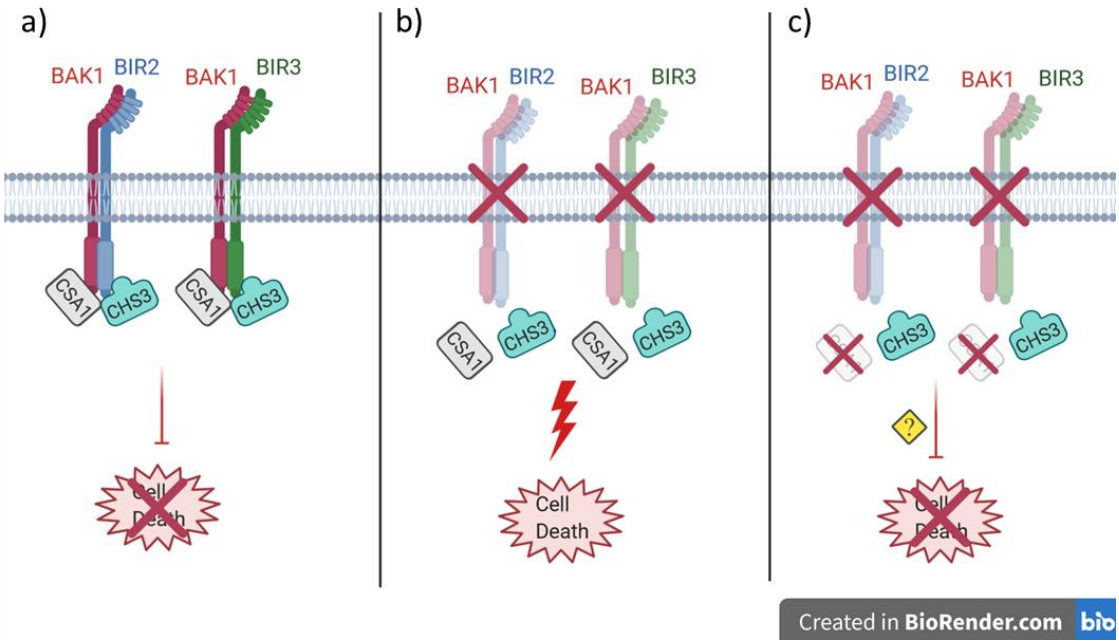

Figure 4.4: Does the NLR-pair CSA1/CHS3 get activated in the absence of BIR-proteins and BAK1?

a) Wild-type situation: the NLR-pair CHS3/CSA1 functions as guard of BIR2/3 and/or BAK1. Under uninfected conditions no cell death is mediated by CSA1/CHS3. B) Upon infection the NLR-pair CHS3/CSA1 gets activated, leading to cell death. c) Proposed hypothesis: the loss of CSA1 (executer-NLR) in the background of the autoimmune phenotypes *bir2* / *bak1bir3* / *bak1* inhibits signaling leading to cell death.

4.3.2 CSA1 and CHS3 form complexes with members of the BIR-family and BAK1

As CSA1 was found in the MS analysis of the BIR3 interactome as a putative interaction partner of BIR3, Co-IP experiments in tobacco were conducted. All tested proteins from BIR1 to BIR3 as well as BAK1 were shown to interact with CSA1. CSA1 functions as a pair with another TNL, CHILLING SENSITIVE 3 (CHS3) (Xu et al., 2015). To test, if CHS3 also binds to BAK1 and the BIR-members BIR1 to BIR3, Co-IP experiments by way of transient expression in tobacco were used. CHS3 was found to interact with all tested members. The NLR-pair RRS1/RPS4 is closely related to the pair CHS3/CSA1 and shows similarities regarding the architectural organization. Crystal structures of both TIR-domains, given by RPS4/RRS1 revealed a conserved TIR/TIR interaction interface, which is needed for a functional effector recognition complex (Williams et al., 2014). It would also be conceivable that CHS3 and CSA1 act in a comparable way by probably forming a platform via their TIR-domains which could also bind guardees such as members of the BIR-family and BAK1, instead of effectors. This would explain why both NLRs interacted in our Co-IP-experiments, what was not expected from the MS-analysis. From these experiments, we could not exclude that the observed association between both tested TNLs and the BIR-proteins and BAK1 is an indirect interaction. But what we could obtain from our results is an interacting complex of BIR-

proteins as well as for BAK1 together with the NLR-pair CHS3/CSA1. In the future interaction performed in Arabidopsis are needed to confirm the association *in planta*.

4.3.3 HIR-proteins might support the interaction *via* CHS3/CSA1, BAK1 and members of the BIR-family

Potential candidates who could mediate the complex of the NLR-pair, BAK1 and members of the BIR-family would be HYPERSENSITIVE INDUCED REACTION 1 and 2 (HIR1 and 2) which were found in our BIR3 interactome. Both contain a stomatin / prohibitin / flotillin / HflK / C domain (also known as the prohibitin domain or band 7 domain) and are already described to physically interact with the NLR RESISTANT TO P. SYRINGAE 2, RPS2 and the immune receptor FLS2 (Axtell and Staskawicz, 2003; Mackey et al., 2003; Qi et al., 2011). The band7-domain of HIR-proteins is supposed to mediate an attachment to the plasma membrane. It is believed that HIR-proteins recruit exclusive subsets of receptors and corresponding interacting proteins in order to form nanodomains (Bücherl et al., 2017). Both, HIR1 (At1g09840) and HIR2 (AT3G01290) appeared in the second MS-analysis after the BIR3-pulldown. HIR2 was additionally found in a MS-analysis using BIR2 as bait (Halter et al., 2014), thus represents a probable candidate to conduct the interaction of members of the BIR-family and BAK1 together with the NLR-pair CSA1/CHS3. This is under current investigation by Alexandra Ehinger in our working group.

4.3.4 Characterization of the single knock-out line *csa1-2*

The knock-out line *csa1-2* displays a significantly bigger rosette diameter than wild type (Fig. 3.16), which can be explained by its impaired red-light signaling leading to the shade avoidance phenotype (Faigon-Soverna et al., 2006). Challenged with *A. brassicicola*, the knock-out of *CSA1* led to a lower disease index as well as reduced symptoms visualized by trypan blue staining compared to wild type (Fig. 3.17). We further continued with testing typical PTI-responses by measuring ROS-signaling after treatment with flg22 and elf18. Both tested elicitors did not result in any differences compared to wild type (Fig. 3.18). These outcomes demonstrated that CSA1 has an influence on cell-death regulation as the knock-out leads to less cell-death symptoms than wild-type. We therefore hypothesized that CSA1 exerts its function by most likely executing cell death (Fig.4.4). Furthermore, no effect on ROS-signaling compared to wild type could be detected after elicitation with two different ligands (flg22 and elf18), hence we supposed that CSA1 exert its function primary in ETI-signaling (Fig. 5.1).

4.3.5 CSA1 has no effect on PRR-mediated immunity

In the community it is still a discussion if and how PRR- and NLR-mediated immunity diverges or does not as both show common features like production of reactive-oxygen species (ROS) (Peng et al., 2018). Recent studies focused on the dissection of both branches of immunity using different approaches to separate ETI- and PTI-signaling. The system of Ngou et al. used an estradiol-inducible mutant line for the T3SE AvrRPS4 in order to study the activation of the NLR-pair RPS4/RRS1 without provoking a PRR-induced immune response (Ngou et al., 2019). They could show that MAPK- and RBOHD-activation as typical PTI-readouts, were not induced by the activation of the NLR-pair RPS4/RRS1 alone. Additionally, no macroscopic HR could be detected. Instead, ion leakage and the activation of SA-signaling, leading to the activation of PATHOGENESIS-RELATED GENE 1 (PR1) were observed and considered as outcome of the activated ETI-signaling conferred by RPS4/RRS1 (Ngou et al., 2019). Investigations using this estradiol-inducible system extended by additional experiments revealed that PTI and ETI mutually potentiate each other, by (i) transcriptional upregulation of typical PTI-components, such as BAK1, BIK1, RbohD and MPK3 *via* the intracellular receptors RRS1/RPS4 (Ngou et al., 2020). The same was observed by Yuan et al. (2020) showing that the elevated transcript and protein level of PTI components during ETI were induced in a SA-independent manner. (ii) ROS-levels or callose deposition were only amplified when PTI and ETI were activated in parallel whereas the induction of ROS-burst could not be observed upon triggering ETI alone (Ngou et al., 2020). Furthermore, Ngou et al. (2020) demonstrated that PTI also potentiate ETI, as PAMP co-infiltration, using flg22, elf18 and pep1 combined with estradiol-induced RPS4 and RECOGNITION OF PERONOSPORA PARASITICA 4 (RPP4), two TNLs, culminated in HR, that was not seen for only PTI- or ETI-induction alone respectively. This observation led the authors speculate, that TNLs need PTI responses to cause HR, which might be different from responses conferred by CNLs, such as HOPZ-ACTIVATED RESISTANCE 1 (ZAR1) (Ngou et al., 2020). Confirming the idea that an effective ETI response only occurs in concert with PTI responses was shown by Yuan et al. (2020), which observed that the PRR-mediated phosphorylation of RbohdD is a critical step for its full activation upon ETI-signaling leading to an higher ROS-level than triggering PTI alone. Wu et al. (2020a) instead, tested both immune responses (PTI and ETI) by eliminating the helper NLR cluster of NLR REQUIRED FOR CELL DEATH (NRC4/5), necessary for the downstream signaling of the CNL late blight resistance protein Rpi-blb2, conferring resistance to *Phytophthora infestans* in tomato and *N.benthamiana*, while challenging those

mutant lines with flg22. In agreement with the observation of Ngou et al. (2019) / Ngou et al. (2020) and Yuan et al. (2020), the authors found wild-type-ROS-signaling and MAPK-activation, while the NRC4-mediated HR failed. All these observations support the idea that, despite different perception of signals, it seems that the intracellular provoked immune response referred to as ETI, functions to enhance and / or strengthens resistance, triggered most likely in parallel by surface-located PRRs, at least for the described TNLs (Ngou et al., 2020; Yuan et al., 2020). In order to classify, if and how CSA1 is involved in PRR-mediated ROS-signaling, we performed ROS-assays by using flg22 as elicitor in our crossed mutant lines *bir2-1csa1-2 and bak1-4csa1-2*. As mentioned before, neither flg22- nor elf18-treatment led to a different output than wild-type in the single knockout line *csa1-2*, demonstrating that it does not affect the induction of a ROS-burst. Testing PTI-responses in crossings lacking *CSA1* of this work (*bir2-1csa1-2 and bak1-4csa1-2,* leafs of the double mutant line *bak1-4bir3-2* were too small to conduct ROS measurements, thus absent in this trial) revealed that all tested crossings so far did not show any alteration in ROS-measurements after elicitation with flg22 compared to the respective single-knock-out lines (*bir2-1* or *bak1-4*) (Fig.3.25; Fig3.29). This shows that loss of *CSA1* does not affect typical immune responses after elicitation with flg22, such as the ROS-burst. This is consistent with the above described observations that the recognition of conserved structures *via* surface-located PRRs specifically leads to the induction of a ROS-burst, which could not be initiated by the activation of intracellular located NLR-receptors alone (Ngou et al., 2019; Wu et al., 2019a; Ngou et al., 2020; Yuan et al., 2020). Whether and to what extend PTI-signaling contributes to CSA1-signaling, as proposed by Yuan et al. (2020), has to be shown in the future.

4.3.6 The loss of CSA1 reduces SA-levels in BIR- and BAK1 depleted cells

When SA-contents were tested in loss-of-function mutants of *BIR2*, *BAK1-BIR3* or *BAK1* (alone or in concert with *BKK1*), they all showed an increase as well as an induction of SA-related genes, such as *PR1* and *PR2* (He et al., 2007; Halter et al., 2014; Imkampe, 2015; Gao et al., 2017; Imkampe et al., 2017). These observations could be a PTI-triggered immune response and/or, because all of them also display cell-death phenotypes, a sign of ongoing ETI-related immune response which is e.g. described for the NLR-pair RRS1/RPS4 (He et al., 2007; Kemmerling et al., 2007b; Heidrich et al., 2013; Halter et al., 2014; Gao et al., 2017; Imkampe et al., 2017; Lapin et al., 2019). SA-measurements in our crossed mutant-lines revealed that CSA1 signals *via* SA, as the content decreased significantly in all tested mutant

lines, lacking *CSA1*. Only in case of the triple-mutant line *bak1-4bir3-2csa1-2* the decrease was measured to a similar level as *bak1-4* mutants (Fig.3.21), both double-knock-out lines (*bir2-1csa1-2* (Fig.3.24) and *bak1-4csa1-2* (Fig. 3.28)) showed a suppression of SA-level back to wild type and *csa1-2*-single mutants which were equal.

The result for the *bir2-1csa1-2*-mutant line is in line with observations done by Imkampe (2015), who demonstrated that cell-death within *bir2-1* is SA-dependent as cell-death symptoms were significantly reduced when *bir2-1* was crossed with *nahG*, an enzyme which degrades SA to catechol. However, even the SA-content was reduced to wild-type levels, the double knock-out *bir2-1csa1-2* displays still elevated cell-death symptoms, which is also observed for the triple-mutant line *bak1-4bir3-2csa1-2*.

After 10 days of germination double mutants of *bak1-4bkk1-1* display early cell death symptoms with upregulated genes, such as *PR1/2* and *5*, key marker genes for SA-signaling, as well as *ACS6* and *7*, involved in ethylene biosynthesis. Crossed with *nahG*, a partial rescue of the cell-death phenotype was observed, indicating that the phenotype is partially SA-dependent (He et al., 2007). This could be confirmed by crossing experiments of *BAK1BKK1* using two chloroplast-localized SA-mediators, SALICYLIC ACID INDUCTION DEFICIENT 2 (*SID2)*, a catalyzer of SA-synthesis and ENHANCED DISEASE SUSCEPTIBILITY 5 (*EDS5)*, a member of the Multidrug And Toxic compound Extrusion (MATE) transporter-family and thus responsible for the translocation of SA from the chloroplast to the cytosol (Gao et al., 2017). Both genes are important for SA-accumulation and are highly expressed in the double mutant *bak1-4bkk1-1* (Gao et al., 2017). Triple-mutants (*bak1-3bkk1-1sid2-3* and *bak1-3bkk1-1eds5-2*) either lacking *SID2* or *EDS5,* showed suppressed cell death. As crossings with mediators of SA-signaling, such as *nahG*, *EDS5* and *SID2* were shown to suppress partially BAK1-mediated cell death (He et al., 2007; Gao et al., 2017). As mentioned before, SA-levels in both double mutant lines (*bak1-4csa1-2 #1* and *#23*) were also suppressed to the level of Col-0 and *csa1-2 (*in case of *#23* even less than WT/or *csa1-2*), demonstrating that CSA1 signals *via* SA in the *bak1-4* single-mutant line (Fig.3.28), which is line with Gao et al. (2017).

4.3.7 CSA1 suppresses cell-death of BAK1- and BIR-protein mediated cell death

The phenomenon that a balanced level of a protein is crucial for containing cell death is described for BAK1, as the knock-out *bak1-4* shows a runaway cell death after infection with a necrotrophic fungus (He et al., 2007; Kemmerling et al., 2007b) which is also described for BAK1-overexpressor-lines (Belkhadir et al., 2012; Dominguez-Ferreras et al., 2015). The

strongest cell death within the SERK family can be detected when *BAK1* lacks in concert with its closest homolog *BKK1.* Both SERK proteins were shown to have a dual role in positively regulating BL-signaling and negatively regulating BL-independent cell death (He et al., 2007). Furthermore, triple mutant lines of *bak1-3bkk1-1eds1-3* were partially rescued, compared to *bak1-3bkk1-1* (Gao et al., 2017). Even less suppressed lesion symptoms were observed when *bak1-3bkk1-1pad4-2*-triple mutants were tested, leading to the assumption that *BAK1BKK1*-mediated cell death is ETI-related (Gao et al., 2017). As triple-mutants lacking *NDR1* in the background of *bak1-3bkk1-1* display an identical cell death phenotype than mutant lines lacking *BAK1 and BKK1*, it was concluded that a TNL-type of NLR is more likely involved in BAK1-mediated cell death, than a CNL-type (Gao et al., 2017).

BAK1 is one of the key regulators in receptor-mediated signaling. The lack of BAK1 is not only associated with cell death, it is also associated with an impairment of adequate signaling, especially for immune responses, exerted by ligand-binding receptors. Consequently, it is likely that the depletion of BAK1 is sensed by intracellular receptors such as NLRs, activating ETI responses, after pathogen attack, in order to enhance plant resistance and/or overcome Effector-Triggered-Susceptibility (ETS). Indeed, BAK1 is a target of several effectors, such as Pto, PtoB, HopF2 and HopB1, aiming to shut down PTI-responses (Chinchilla et al., 2009; Bigeard et al., 2015; Li et al., 2016). Hence, CSA1 represents a possible TNL-class NLR controlling BAK1 in order to surveil pathogen invasions. To test this, crossings of the full knock-out line *bak1-4* and *csa1-2* were conducted. The phenotype of 6 week-old *bak1-4csa1-2*-plants was equal to *bak1-4* and could phenotypically not be distinguished (Fig. 3.26A). As treatments with the hormone BL restored the growth phenotype of *bak1*-single mutants and those lines still failed to contain cell death, the compact phenotype of *bak1-4* is BL-dependent and not cell-death-related (Kemmerling et al., 2007b). As the lack of *CSA1* in the background of *bak1-4* did not change the compact phenotype either, we assumed that CSA1 does not interfere with the BL-pathway as well. But, what about cell death containment? As cell death becomes only visible in *A. brassicicola* inoculated *bak1-4*-single mutant lines (Kemmerling et al., 2007b), we also performed *A. brassicicola* assays on *bak1-4csa1-2*-mutants to measure disease indices and monitor lesion sizes after trypan blue staining. Disease indices in the double-mutant lines *bak1-4csa1-2* were significantly reduced compared to wild type and *bak1-4* (Fig.3.27A+C). Additionally, lesions visualized by trypan blue staining remained restricted to inoculation sites to an even less degree than Col-0 (Fig. 3.27B). These results indicated that BAK1-mediated cell death is dependent on CSA1

signaling. Even more, this work revealed CSA1 of being at least the first described TNL in mediating BL-independent cell death conferred by a lack of *BAK1*. This is in line with the finding that BAK1-mediated cell death can be partially suppressed by the lack of *EDS1* and *PAD4*, two downstream components of TNL-mediated ETI-signaling (Gao et al., 2017; Lapin et al., 2019).

All BIR proteins are characterized to bind to and negatively regulate BAK1 (Gao et al., 2009a; Halter et al., 2014; Imkampe et al., 2017). In this work, we could show that CSA1 suppresses BAK1-mediated cell death, furthermore we confirmed the interaction of both by using Co-IP experiments, whereby initially CSA1 was detected in the BIR3 interactome using MS analysis. The knock-out of *BAK1* and *BIR3* (*bak1-4bir3-2)* shows nearly the same strong cell-death symptoms as the knock-out of *BIR1* in the *bir1-1* mutant line (Gao et al., 2009a; Imkampe et al., 2017). Those plants display small leaves with enhanced cell death, yellow spots, elevated SA-level and seedling lethality without producing seeds (Gao et al., 2009a; Imkampe, 2015; Gao et al., 2017; Imkampe et al., 2017). But still, there are different lines of evidence, showing that the underlying mechanism causing cell death is differentially regulated in *bir1-1* and *bir3-2bak1-4*: (i) the autoimmune phenotype of the double-mutant *bak1-4bir3-2* cannot be rescued by a cultivation at 28°C which is described for the full knock-out mutant *bir1-1* (Gao et al., 2009b; Imkampe et al., 2017). Furthermore, (ii) the double-mutant of *bak1-4bir1-1* leads to a partial rescue, whereas the double-knock out *bak1-4bir3-2* leads to a strong enhancement of cell-death symptoms compared to the single-knock-out *bak1-4* (Imkampe, 2015; Liu et al., 2016; Wierzba and Tax, 2016). (iii) It was shown that for cell-death regulation the kinase activity of BIR1 is partially needed (Gao et al., 2009a), which cannot be the case for BIR3, as it represents a kinase inactive protein (Imkampe et al., 2017). The triple-mutant *bak1-4bir3-2csa1-2* regained significantly its fitness with bigger rosette diameter (Fig. 3.19A). Additionally, *bak1-4bir3-2*-mutants lacking *CSA1* are fertile again (Fig.3.19B) and showed a reduction in cell death symptoms, considered as a partial rescue, as the phenotype of triple mutants were not reverted back to wild type. (Fig. 3.20A, B and C). Our results demonstrated that the loss of *CSA1* in the autoimmune phenotype of *bak1-4bir3-2* leads to a strong recuperation of fitness with fertile plants and a partial rescue of cell-death symptoms.

The knock-out of *BIR2* as well as overexpression leads to elevated cell death (Imkampe, 2015). It was previously explained that the relative amount of the protein is decisive for cell death containment (Imkampe, 2015). The deletion of *CSA1* in the background of *bir2-1* led to

a reduction of yellow leafs and slightly bigger rosettes in 6-week old plants, compared to wild type (Fig. 3.22A). This indicates, that CSA1 also here suppressed cell death of *bir2-1* single mutant lines. Furthermore, *bir2-1* single mutants show subordinating stems when flowering, which was not altered in the double mutants, pointing out that developmental patterns of flowering in the *bir2-1*-mutant are not affected by a loss of *CSA1* (Fig.3.22B). Monitoring lesion sizes after trypan blue staining confirmed that *bir2-1*-single mutants displayed a runaway cell death phenotype, while the double knock line *bir2-1csa1-2* showed a containment of cell death symptoms, which was less pronounced than wild type. Consequently, cell death suppression due to the lack of *CSA1* in the background of *bir2-1*, was considered as partial rescue, similar to the triple mutant line *bak1-4bir3-2csa1-2*.

The loss of *CSA1* led to a partial rescue in all tested BIR-mediated cell death phenotypes of this work (*bak1-4bir3-2csa1-2* and *bir2-1csa1-2*) so far. This makes sense, as BAK1-mediated cell death is suppressed by a lack of CSA1 and BIR3 as well as BIR2 bind constitutively to BAK1 (Halter et al., 2014; Imkampe et al., 2017). This indicates that cell death formation in all tested mutant lines might be regulated by at least two independent pathways, where one is exerted by CSA1 leading to a reduction of cell death symptoms connected with a suppression of elevated SA-level and a potential second NLR which is unknown so far. A similar scenario is proposed for the autoimmune phenotype of *bir1-1*, which shows a partial recue when crossed with (i) *PAD4* or *EDS1* respectively, representing the first pathway signaling via most likely a TNL and (ii) *SOBIR1*, representing the second proposed pathway (Gao et al., 2009a). Only the triple-mutant of *bir1/sobir1/pad4,* unifying the two proposed pathways, displayed a full rescue of the autoimmune phenotype (Gao et al., 2009a). Later studies revealed that BIR1 interacts, next to BAK1, with BONZAI1 (BON1), a calcium-dependent phospholipid-binding protein and that SNC1, a TNL, gets activated, once *BIR1* and/or *BON1* are knocked out, as either double mutants using *bir1/snc1* or *bon1/snc1* led to a partial rescue of the cell-death phenotype (Wang et al., 2011). The second proposed pathway, exerted by SOBIR1, could be partially explained, as only in the absence of *BIR1,* BAK1 and SOBIR1 form complexes culminating in cell death (Liu et al., 2016). In line with Gao et al. (2009a), also here the authors showed that the triple-mutant *bak1bir1pad4* was bigger than the double-mutant *bak1bir1*, confirming the idea of two parallel pathways exerted by BIR1. Although this is not yet supported by any biochemical evidence, a similar scenario of an additional R-gene regulating *BIR2*- and *BAK1/BIR3*-mediated cell death could explain the observed partial rescue.

4.3.8 Pseudokinases- mediators of ETI-signaling

The recent work of Wang et al. (2019) has revealed the assembly of an inflammsome-like complex in plants, which is a conglomerate of different proteins, forming a higher complex after activation: the resistosome (Fig. 4.5). The integrated NLR of the resistosome is HOPZ-ACTIVATED RESISTANCE 1 (ZAR1), a CNL, sensing in this case the uridinylation of PBS1-LIKE 2, PROTEIN KINASE 2A (PBL2) via the mode of action of the effector AvrAc from *Xantohomonas campestris*. The uridinlyated RLCK PBL2 represents the ligand for the integrated pseudokinase RESISTANCE RELATED KINASE 1 (RKS1). Only binding to RKS1, leads to a release of ADP from ZAR1, allowing the binding of ATP (“switch on”) and hence a conformational change in ZAR1. This change permits activated neighboring ZAR1 proteins to oligomerize, thereby forming the resistosome. This pentameric construct is supposed to penetrate the plasma membrane by a funnel like structure, formed by α1-helices of the N-terminal region of ZAR1 thereby inducing cell death by membrane disruption (Fig 4.5).

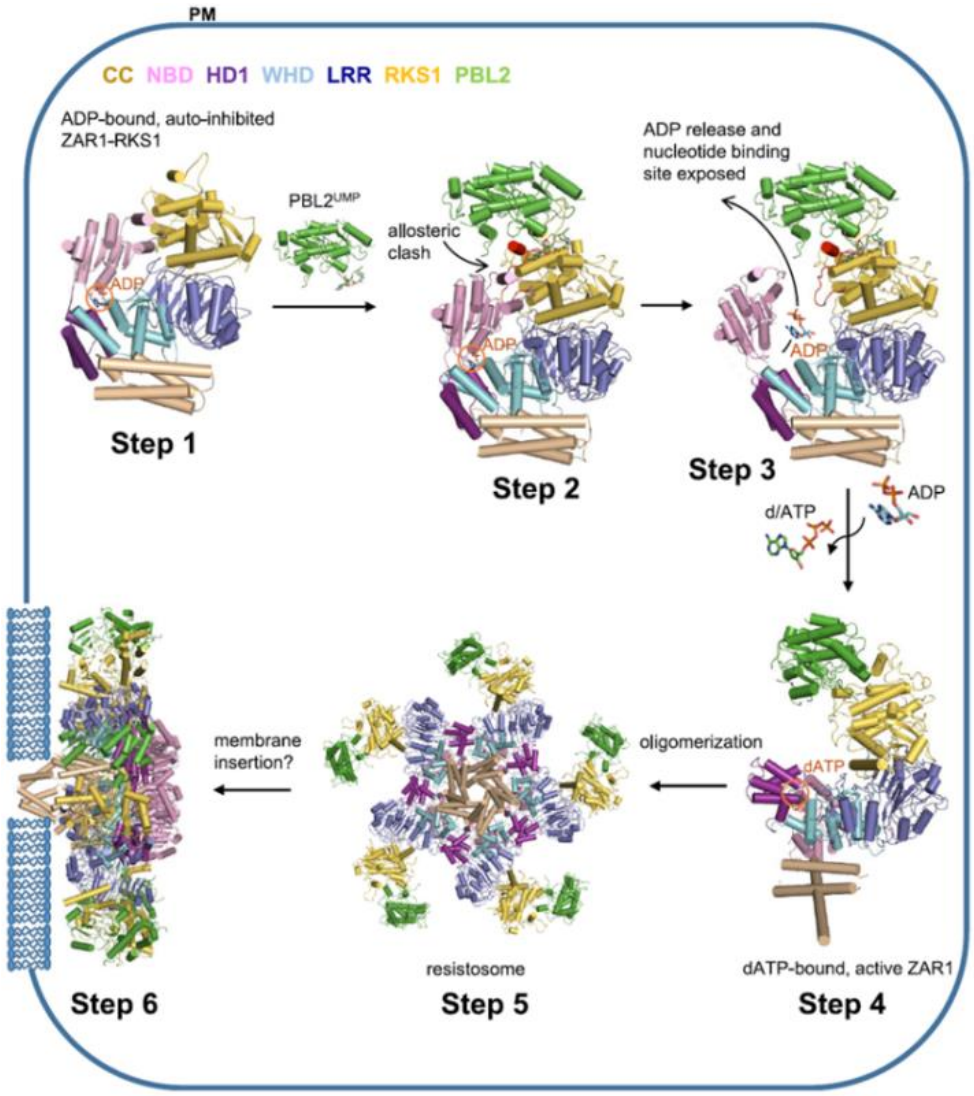

Figure 4.5: Activation of the resistosome

Step1: ZAR1 and RKS1 build an inactive preformed complex.PBL2 gets uridylated by the T3SE AvrAc from *Xantohomonas campestris*. Step2: the uridylated PBL2 represents the ligand for RKS1, causing an allosteric clash of the former inactive ZAR1-complex. Step3: the conformational change allows the release of ADP and an exchange of ATP within the NB-domain of ZAR1. Step4: The exchange of ADP to ATP activates the ZAR1-complex, which can form the pentameric complex with neighbored active ZAR1-complexes. Step5: the oligomerization forms the resistosome which is supposed to disrupt the plasma membrane with its funnel like structure built up by N-terminal α-helices (Step6) (Wang et al., 2019).

Remarkably the mechanism of activation of the resistosome (“switch on”) is conferred by a pseudokinase, RKS1, mediating the change of ADP to ATP. Another famous example for a pseudokinase which´s modification leads to an ETI-response, is HOPZ-ETI-DEFICIENT 1 (ZED1). ZED1 is amongst others a target of the T3SE HopZ1a, from *Pseudomonas syringae*. HopZ1a acetylates ZED1 at threonine 125 and 177 respectively, which is recognized by ZAR1, mediating the subsequent HR (Lewis et al., 2014). In this work it is proposed that pseudokinases could act as binding partners for ATP or as allosteric switches to regulate functional kinases. The idea of regulating functional kinases is tempting as BIR2 and BIR3

(two pseudokinases) are constitutively bound to BAK1 (an active kinase) and only in the *bak1-4bir3-2*-double mutant, we observe the strong autoimmune phenotype. The question how the pseudokinases BIR2 and BIR3 might function could be explained by negatively regulating CSA1 and/or CHS3. Probably the RLKs could be targeted by a type III secreted effector (T3SE) followed by a disruption of the complex of BIRs, BAK1 and CHS3/CSA1, subsequently leading to NLR activation and ETI-responses. However, the exact role mechanistically exerted by BIR2, BIR3 and BAK1 leading to the activation of CSA1/CHS3 is still elusive.

4.3.9 Redundancy within the NLR-family

Rescue of *bak1*, *bir2* and *bak1bir3* phenotypes by *csa1* are partial. An additional sensor needs to be postulated. One candidate could be RECOGNITION OF PERONOSPORA PARASITICA 8 (RPP8) a CNL, found in the second MS analysis of this work. RPP8 contains a special feature: the MADA-motif, which is named by the first four amino-acids of a 29-aa motif at the N-terminus of either singleton-NLRs or Solanaceaous helper-NLRs (NLR REQUIRED FOR CELL DEATH / NRCs) (Adachi et al., 2019). This motif appears in 20% of all CNLs of dicots and monocots (Adachi et al., 2019) and is described to be indispensable to confer cell death. Moreover, it shows 50% sequence identity with the N-terminal ZAR1-alpha helix, thus it is hypothesized to act in a similar way, by building a potential alpha helical structure which can possibly disrupt the integrity of the plasma membrane via a pore forming complex (see 4.3.8). This is supposed to confer cell death (Adachi et al., 2019). As RPP8 possesses a MADA-motif (Adachi et al., 2019), it implicates that RPP8 has potentially the inherent ability to confer cell death without the help of downstream components such as EDS1, NDR1 or members of the helper-NLRs (Aarts et al., 1998; Jubic et al., 2019). This would explain why SA-levels in all conducted *csa1-2*-crossings also lacking *BAK1*, *BIR2* or *BIR3BAK1* were significantly reduced but still showed cell death symptoms: While the knock-out of *CSA1* led to reduced SA-levels supporting the suppression of cell death formation, RPP8 as singleton-NLR, might still be able to confer CSA1-independent cell death. Furthermore, it is described that RPP8 is induced in response to *Hyaloperonospora arabidopsidis* and exogenous SA-levels (Mohr et al., 2010). As elevated SA-levels are a common feature of *bak1-4bir3-1-*, *bir2-1-* and *bak1-4*-mutant lines, significantly suppressed by a lack of *CSA1* in all tested double- and triple-mutants, it is conceivable that both NLRs, CSA1 and RPP8, are acting in a synergistic manner. Therefore, one can hypothesize that RPP8 might be activated due to elevated SA-levels, probably conferred by the mode of action of

CSA1. Together with the finding, that RPP8 contains a MADA-motif, hence probably functions as a singleton-NLR, could explain the residual cell death symptoms of the mutant lines *bak1-4bir3-2csa1-2* and *bir2-1csa1-2.* In this scenario, the function of CHS3/CSA1 would be more the support of basal resistance *via* elevated SA-levels, rather causing directly cell death comparable to the mode of action described for the NLR RPS4 (Lapin et al., 2019). On the other hand, after either a certain time period of SA-signaling or threshold of SA, due to probably CHS3/CSA1 activation, the second NLR, RPP8 could be activated. If RPP8 plays a role in the BAK1- BIR-mediated cell death and thus responsible for the partial rescue, has to be further investigated.

4.3.10 Redundancy within the TNL family

In the mutant line *csa1-1* a truncated version of the CSA1-protein with a full TIR- and part of the NB-domain is present, whereas *csa1-2* is a full knock out line (Faigon-Soverna et al., 2006). It could be shown that the observed phenotype of impaired light signaling as well as impaired immune response was stronger in the mutant with the truncated CSA1-protein than in the mutant where *CSA1* was absent (*csa1-2*). The authors speculated that *csa1-1* is a dominant-negative mutant, which interferes with other TNLs *via* its N-terminal TIR-domain, thus producing non-productive heterodimers. As a consequence, other TNLs can putatively be outcompeted and hindered to fulfill their function. A putative candidate to test was RPS4, as it is the next homolog of CSA1 and shares 64% sequence similarity to CSA1 across the entire protein (Faigon-Soverna et al., 2006). Indeed, the overexpression of RPS4 in the background of *csa1-1* rescued the growth phenotype back to wild type. It has been suggested that the TIR-domain of RPS4 intercepts the truncated CSA1-protein via TIR-TIR interaction and thus hindering it from executing its dominant negative effect (Faigon-Soverna et al., 2006). This finding implicates that RPS4 has the potential to functionally replace CSA1. As *csa1-2*-mutants are null alleles, lacking CSA1, it is thinkable that the partial rescue phenotypes observed in *bir2-1csa1-2* and *bak1-4bir3-2csa1-2*-mutants is caused by functional takeover of RPS4 (and / or additional TNLs). A common feature of RPS4 and CSA1 is the signaling *via* SA, implicating that both TNLs share downstream components and thus potentially be functionally replaced by each other. To test this, crossings with *rps4*-null mutants, such as *bakbir3rps4, bir2rps4* and *bak1rps4* could be conducted to answer this question. Additionally interaction assays between RPS4 and BIR1, BIR2, BIR3 and BAK1 could be performed in order to analyze if RPS4 can be found in complex with BIR proteins and/or BAK1.

4.4 Conclusion

The main objective of this work was the study of the BIR3 interactome with the focus on RLKs as BIR3 constitutively interacts with BAK1 and ligand-binding receptors of the class of LRR-RLKs to negatively regulate BAK1- and BAK1-dependent pathways (Imkampe et al., 2017). Especially cell death candidates were of high interest, potentially explaining the cell death phenotypes in mutants lacking *BAK1* and *BIR* proteins. In the list of 10 common LRR-RLKs summarized in both MS analyses we detected, apart from all five SERKs and BAK1-dependent RLKs (SOBIR1 and SIF3), the first time two LRR-RLKs which do not signal via BAK1 (HPCA1 and MIK2). Considering that BIR3 is described to regulate BAK1 and BAK1-dependent pathways so far, with this result we might extent the repertoire of BIR3 of being a general regulator of RLKs, independent whether they form complexes with SERK proteins for signaling or not.

One cell death candidate of our MS analyses was CSA1. Our studies revealed that CSA1 suppresses partially BIR-protein and BAK1-mediated cell death. The lack of CSA1 led to a reduction of SA-level, a suppression of cell death symptoms and did not interfere with flg22-induced PTI responses. Since the first description in 2007, the loss of *BAK1* is described with accompanied cell death symptoms (He et al., 2007; Kemmerling et al., 2007b). It is likely induced by intracellular NLR receptors as BAK1 is target of several effector proteins. We are the first group who found with CSA1 a TNL which potentially guards BAK1 and BIR proteins in order to activate ETI-responses in the absence of those. The partial rescue could be explained by an additional NLR(s), acting in parallel to CSA1 which guards BAK1 and BIRs, similarly proposed for BIR1 (Gao et al., 2009a). If this additional guard is conferred by the next homolog of CSA1, RPS4 or by RPP8, detected in the second MS analysis, or by a yet unknown NLR is still an open question.

5 Outlook

5.1 How is the NLR-pair CHS3 / CSA1 activated?

One big question remained in this work: how does the NLR-pair CHS3/CSA1 execute its transition from the resting state to an activated one? Usually NLRs get activated upon recognition (directly or indirectly) of effectors injected by pathogens into the cytoplasm of the host (Chiang and Coaker, 2015; Cui et al., 2015). Because NLR-activation can lead to a strong immune response, often accompanied by localized cell death at the site of infection, it has to be under tight control.

5.1.1 Structural inhibition of CSA1/CHS3?

The control of NLRs is ensured by (i) intra- and (ii) intermolecular interactions. The intramolecular inhibition can take place between the different domains of the respective NLR: while the NLR immune receptor Rx1 from potato (*Solanum tuberosum*), recognizing the *Potato virus X,* forms intramolecular interactions of its LRR-domain with the NB-ARC domain (Slootweg et al., 2013; Sukarta et al., 2016) to avoid activation, the TNL RECOGNITION OF PERONOSPORA PARASITICA 1 (RPP1) establishes a connection between the TIR- and the NB-domain in order to prevent unwanted cell death formation (Schreiber et al., 2016; Sukarta et al., 2016). Both are examples of NLRs recognizing their respective effector directly via their LRR-domains. Yet, how the binding of the effector leads subsequently to the release of the NB-domain is still unclear (Guo et al., 2019). Intermolecular interactions (often together with intramolecular ones), aiming to maintain an inactive state, are a very common features of NLR-pairs, consisting of a sensor- and an executor structure, such as e.g. RRS1 (sensor) and RPS4 (executor) from *Arabidopsis*. It was shown that the self-association of the truncated TIR+80-construct, containing the TIR-domain and terminating before the NB-motif of RPS4, is sufficient to trigger an immune response (Swiderski et al., 2009). Furthermore, the heterodimerization of the TIR-domain of RPS4 with the TIR-domain of its partner RRS1 prevents such a signaling (Williams et al., 2014a). The mode of action of how AvrRPS4, an effector from *Pseudomonas syringae pv. pisi* and PopP2 from *Ralstonia solanaceum* contributes to the activation of the RRS1-RPS4 complex has been made clearer in a recent publication. The authors revealed two different effector recognition mechanisms conferred by the NLR-pair RPS4/RRS1. (i) The first mechanism unveiled that the effector AvrRPS4 interacts with the WRKY- and TIR-domain of RRS1, promoting the interaction of the TIR^{RRS1}

domain with its C-terminal DOM56 domain in *Arabidopsis*. The effector operates thereby as molecular glue of the N- and C-terminal domains of RRS1 leading to the release of the heterodimeric interaction between the TIR-domain of RPS4 and RRS1. This allows the homodimerization of the TIR-domains of RPS4, enabling the initiation of the immune response (Guo et al., 2019). The second way of activating RPS4/RRS1 was only observed in an ecotype-specific allele of RRS1 from Wassilewskija (Ws / *Arabidopsis thaliana*). The C-terminus of the RRS1 allele comprises 83 additional amino acids, which is (i) not present in the RRS1 allele of Col-0 (only recognizing AvrRPS4) and (ii) enables the recognition of a second effector, PopP2, an acetyl transferase from *Ralstonia solanaceum* (Guo et al., 2019). Furthermore, the authors showed that mainly one threonine (1214) at the C-terminus of the Ws-RRS1 allele is phosphorylated by an unknown kinase so far and that this phosphorylation is required to keep RRS1 inactive. PopP2 acetylates two lysines within the WRKY-domain and Threonine 1214 being in close proximity to the WRKY-domain. This leads to the cancellation of the inhibitory effect conferred by the phosphorylated threonine 1214. It is believed that the interaction between the C-terminus and the TIR-domain of RRS1 is enhanced by both effectors: AvRRPS4 and PopP2, thus promoting the extrication of the TIR^{RRS1}-domain which enables subsequently the oligomerization of the TIR^{RPS4} leading to the initiation of immune signaling (Guo et al., 2019). So far this is the first time that a plant NLR is described to be regulated by phosphorylation (Guo et al., 2019). Whether the NLR-pair CHS3/CSA1 acts in a similar manner has yet to be established, but there are some aspects that may hint to possible similarities between both pairs. The first aspect is that RPS4 is the closest homolog of CSA1 and was shown to rescue the shade-avoidance phenotype of the truncated CSA1 mutant line *csa1-1*, containing the TIR-domain and parts of the NB-domain (Faigon-Soverna et al., 2006). As discussed before, the authors concluded from this result, that the TIR-domain of RPS4 might form nonproductive heterodimers, thereby negatively regulating the dominant-negative CSA1 protein as well *via* its TIR-domain, leading to wild type signaling (Faigon-Soverna et al., 2006).

5.1.2 Does the LIM domain guard BAK1 and / or BIRs?

Another aspect which speaks for an analogy between RPS4/RRS1 and CSA1/CHS3, is that CHS3 is the next homolog of RRS1 and shares the involvement of an integrated domain (ID) at the C-terminus of the protein (RRS1: WRKY-domain; CHS3: single LIM-domain) (Xu et al., 2015). Both IDs most likely evolved by duplication of an effector target, followed by fusion into the TNL (Ellis, 2016; Sarris et al., 2016; Bialas et al., 2018). These IDs are seen as

effector-sensors and can potentially be modified. This modification, in turn activates the genetically linked executor NLR, in the case of both NLR couples (i.e. RRS1/RPS4 and CHS3/CSA1, respectively). From the work on *chs3*-autoimmune phenotypes, together with the knowledge about the mode of action of RRS1/RPS4, we can hypothesize how the different domains within CHS3 could possibly contribute to certain functions: So far, three autoimmune lines of *chs3* have been described: *chs3-2D, chs3-3D* (Bi et al., 2011) and *chs3-1* (Yang et al., 2010). All mutations described in these gain-of-function mutant-lines occur within or close to the LIM-domain (*chs3-1*: G → A within the LIM-domain; *chs3-2D*: C → Y close to the LIM-domain and *chs3-3D*: M → V within linker domain between LRR and LIM-domain). This potentially indicates that the C-terminus of CHS3 is required for keeping the NLR-pair in an inactive complex, analogously to RRS1. This begs the question of whether or not activities / modifications of the LIM-domain *via* a yet unknown effector could initiate the activation of CHS3/CSA1, alike AvrRPS4 or PopP2 does by binding to the WRKY and TIR-domain in RRS1. Also here studies confirming this hypothesis are needed.

5.1.3 Do BAK1 and /or BIRs keep CSA1/CHS3 in an inactive state and does phosphorylation play a role in the activity of the complex?

Likewise or additionally to the intracellular associations promoting the inactive state, it is possible that BIR2 / BIR3 and/ or BAK1 take over the role of repressing the CHS3/CSA1-activation. Especially if one considers that the RRS1/RPS4 complex is kept in an inactive state by phosphorylation by an unknown kinase. One could hypothesize that BAK1 phosphorylates CHS3 and / or CSA1, aiming to keep the complex in the resting state. This would be in line with recent studies showing that BAK1 gets cleaved by a calcium-dependent protease into N- and C-terminal fragments (CTF), probably to prevent devastating accumulation of BAK1 at the plasma membrane (Zhou et al., 2019). Additionally to that, the authors showed that the kinase domain of the CTF, localized in the cytosol, is fully active. In our hypothesis the full active kinase domain would ensure the resting state of CHS3/CSA1 *via* phosphorylation as seen for RRS1. If and how the complex of CHS3/CSA1 is kept in the resting state is unknown so far, additionally, no direct interaction of CSA1 and CHS3 is reported, but instead it could be shown, that the loss of CSA1 in the background of the autoimmune mutant line *chs3-2D* leads to a full rescue (Xu et al., 2015), indicating that they act in a functional manner, like RRS1 and RPS4 do.

5.1.4 Do the TIR domains of CSA1 and CHS3 heterodimerize to bind BAK1 or BIR kinase domains?

Crystal structures of the TIR-domains of the heterodimeric complex of RPS4 and RRS1 demonstrated a TIR-TIR interaction interface forming a binding platform, important for effector recognition (Williams et al., 2014b). Whether the TIR-domains conferred by the heterodimer CHS3/CSA1 do interact and build a similar interface comparable to that of RPS4/RRS1 has yet to be investigated. Nevertheless, this could present a possible interaction interface for binding the kinase domains of BIRs and/or BAK1, thereby explaining the binding of both in our Co-IP experiments. From our Co-IP assays, we cannot conclude any direct interaction between the different members of the BIR-family and BAK1 and CHS3/CSA1. What we can observe instead, is that as soon as we have a null mutant of *BIR2*, *BAK1* or the complex of *BAK1* and *BIR3*, we lose cell death containment. If this is due to the loss of the repression of CHS3/CSA1, possibly conferred by phosphorylation of BAK1, leading to an activation of the immune response, has to be shown in the future.

5.1.5 What factors could explain the activation of CHS3 and CSA1?

In nature, effectors such as HopB1 display an interesting candidate to study CHS3/CSA1 activation as it possesses a protease activity capable of cleaving BAK1 in the kinase domain in order to dampen PTI (Li et al., 2016). As we hypothesized that BAK1 might keep CHS3 and CSA1 in a resting state by phosphorylation, this would be disrupted by the mode of action of HopB1. This hypothesis is under current investigation by Dagmar Kolb. On the other hand, it is conceivable that CSA1/CHS3 get activated as a consequence of the release of BAK1 and BIR2 / BIR3 due to PTI-responses, consequently leading to a disruption of the complex. In this scenario, the idea of BIR2/3 and BAK1 of being negative regulators of the CHS3/CSA1-complex would be supported. Moreover, CHS3 possesses a predicted protease domain at its C-terminus. We do not know if this protease is catalytically active, but it would be interesting to test if it is so, and if its mode of action is needed for exerting downstream signaling.

5.1.6 What are the downstream components necessary for CSA1 mediated cell death?

From different working groups it is known, that CHS3/CSA1 signaling occurs *via* downstream components such as EDS1 and SAG101 (Yang et al., 2010; Xu et al., 2015). EDS1 was therefore the next candidate to test. In this work, the generation of double- and triple-mutants using the CRISPR/Cas-line *eds1-12* with *bak1-4, bir2-1* and *bak1-4bir3-2* was initiated. Due to time restrictions all crossings were brought to homozygous lines by Liping

Yu, followed by functional assays. She could observe that EDS1 acts downstream of BAK1, BIR2 and BIR3 in complex with BAK1 and that EDS1 is involved in cell death formation as the knock-out in the respective background led to a partial rescue of cell death formation, (Liping Yu, personal communication). Furthermore, when CSA1 is knocked out, the SA-levels in both tested double mutant lines (*bak1-4csa1-2 and bir2-1csa1*-2) reverted to those of Col-0 and *csa1-2* single-mutant lines and significantly reduced levels in the triple-mutant (*bak1-4bir3-2csa1-2*). CHS3/CSA1 were also shown to signal *via* downstream components such as EDS1 and SAG101 by other groups (Yang et al., 2010; Xu et al., 2015), either by using crossings (Yang et al., 2010) or conducting suppressor screens (Xu et al., 2015), accompanied by decreased SA-levels as well. In the future, testing of further downstream components such as SAG101 and PAD4 are needed to complete our understanding of the pathway. To substantiate that CSA1 is the cause of decreased cell death symptoms and SA-levels in all crossings of this work, complementation lines were started. Therefore, genomic *CSA1*-constructs under its native promoter were used to complement the loss-of-function mutants *bak1-4bir3-2csa1-2, bir2-1csa1-2* and *bak1-4csa1*. Also this work was finished by Liping Yu followed by functional assays and revealed that all complementation lines showed the initial phenotype (Liping Yu, personal communication). This confirmed CSA1 to be responsible for the observed decrease in cell death formation of all tested mutant lines.

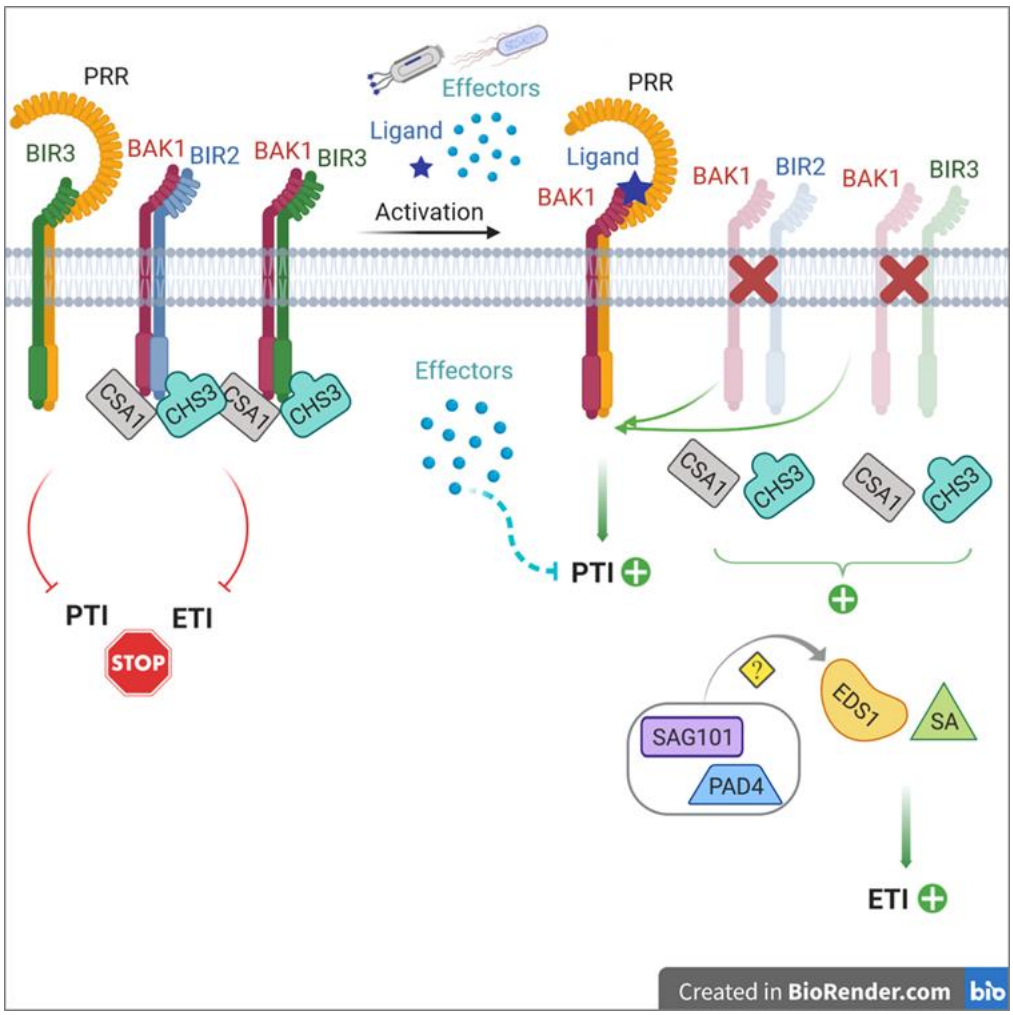

Figure 5.1: Model: signaling by CSA1 after pathogen attack

Left part: Under uninfected conditions, BAK1 gets sequestered by BIR2 and BIR3 from the respective PRR in order to prevent an immune response. Additionally, either BIR2/3 and/or BAK1 are guarded by the NLR-pair CSA1/CHS3, which is present in the resting state as well. Right part: The immune system gets activated by the attack of pathogens, containing conserved structures (MAMPs) which are recognized by surface located PRRs and/or the injection of effectors via the type-III secretion system into the cytosol in order to disturb PTI and aiming to get nutrients from the host. After ligand-binding, BAK1 gets recruited to the respective PRR in order to initiate PTI. Meanwhile, the complexes of BIR2-BAK1 and BIR3-BAK1 get released by the recruitment of BAK1 towards the PRR. If this break-up of the respective complexes initiates already the activation of the NLR pair or if the mode of action of injected effectors leads to their activation either by altering the ID of CHS3 and / or their binding partners BIR2, BIR3 and / or BAK1 are still open questions. BIRs and BAK1 would represent negative regulators of CHS3/CSA1 in this scenario. The exact mechanism is not known, but the action of the NLR-pair is certainly dependent on downstream-components causing elevated SA-levels (measured in the knock-out mutants of *bak1-4bir3-2*, *bir2-1* and *bak1-4*) and is, furthermore, dependent on EDS1, as crossings with the *eds1-12*-line led to a partial rescue of all cell death symptoms so far (Liping Yu, personal communications). Known interaction partners of EDS1, such as SAG101 or PAD4 are still under investigations, in order to clarify which further downstream components are part of this signaling module.

6 Summary

BAK1 is a multifunctional receptor kinase of surface-located-receptors involved in many processes of a plant. Both the overexpression and, the loss of BAK1 lead to cell death symptoms (He et al., 2007; Kemmerling et al., 2007b; Belkhadir et al., 2012; Dominguez-Ferreras et al., 2015). Since unbalanced BAK1-levels can easily lead to unwanted reactions, it has to be under tight control. This is ensured by members of the BAK1-interacting receptor-like kinase family, the BIR proteins. BIR1, BIR2 and BIR3 have been described to bind BAK1, thereby preventing BAK1 interaction with ligand binding PRRs. Interestingly, the maintenance of balanced protein-levels within the BIR family (BIR1 to BIR3) is as important to prevent cell death formation as described for BAK1 (Gao et al., 2009a; Halter et al., 2014; Imkampe et al., 2017). For BIR3, it has been additionally described that it directly binds to ligand-binding receptors such as BRI1 and FLS2 (Imkampe et al., 2017). In this work, I additionally showed that PEPR1 and EFR, two representatives of DAMP- and PTI-signaling respectively, interact with BIR3 too, using Co-IP experiments. The objectives of this work were (i) to search for additional LRR-RLKs and (ii) cell death-associated candidates. Using immunoprecipitation to pull-down BIR3 *via* a YFP-tag, followed by MS analysis, allowed us to identify the BIR3-interactome, thereby revealing further LRR-RLKs as well as cell-death-associated candidates. The BIR3 interactome uncovered in both MS analyses two additional RLKs, which are involved in PTI responses and signal *via* BAK1 (SOBIR1 and SIF3). Remarkably, we could also detect two other LRR-RLKs which have not been reported as signaling *via* BAK1 or any SERK protein (MIK2 and HPCA1). This suggests that BIR3 could be a general regulator of LRR-RLKs which potentially functions BAK1-independent. The first MS-analysis also revealed the TNL CSA1, which we subsequently characterized for its involvement in BAK1- and BIR-mediated cell death. We pointed out that the knock-out of *CSA1* in crossings with *bir2-1* and *bak1-4* did not interfere with flg22-mediated immune responses. Moreover, we observed a significant reduction of SA-levels connected with a partial reduction of local cell death symptoms in all mutants tested. We concluded (i) that CSA1 is a positive regulator of cell death, activated by the absence of BAK1 and BIR proteins, (ii) that the cell death induced by CSA1 is independent of PTI-triggered ROS-signaling and (iii) that the cell death conferred by CSA1 is associated with elevated SA levels. Since the BAK1- and BIR-cell-death responses are only partially rescued by *CSA1* mutation, we concluded that other components might be involved. Another BIR3-interacting NLR candidate from our BIR3

interactome analysis was RPP8 (CNL), which appears to be a promising candidate for further investigations. With this work we defined the BIR3 interactome which allowed us to shed new light on BIR3´s role as (i) a potential general regulator of LRR-RLKs, probably independent of BAK1-involvment and (ii) revealed the NLR CSA1 as a component necessary for BIR- and BAK1-mediated cell death.

7 Zusammenfassung

BAK1 ist ein multifunktionaler Korezeptor sowohl entwicklungsabhängiger Rezeptoren wie BRI1, als auch zahlreicher Immunrezeptoren. Sowohl Überexpression als auch Abwesenheit von BAK1 führen zu zelltodähnlichen Symptomen in der Pflanze (He et al., 2007; Kemmerling et al., 2007b; Belkhadir et al., 2012; Dominguez-Ferreras et al., 2015). Da BAK1 in so zahlreichen Signalwegen eine Rolle spielt und nur eine ausgeglichene Proteinmenge ungewollte Reaktionen verhindert, ist eine genaue Kontrolle des Proteins von Nöten. Dies wird durch Mitglieder der „BAK1-interacting receptor-like kinase (BIR)"- Familie gewährleistet. Interessanterweise führen sowohl Verlust als auch die Überexpression einzelner Mitglieder der BIR-Familie (BIR1, BIR2 und BIR3) ebenso zu spontanen Zelltodsymptomen, wie bei BAK1 (Gao et al., 2009a; Halter et al., 2014; Dominguez-Ferreras et al., 2015; Imkampe et al., 2017; Guzmán-Benito et al., 2019). Für BIR3 konnte zusätzlich gezeigt werden, dass es Liganden-bindende Rezeptoren, wie BRI1 und FLS2, durch direkte Interaktion negativ reguliert (Imkampe et al., 2017). In dieser Arbeit konnte das Repertoire BIR3-bindendener LRR-RLKs, mit Bezug zu Pflanzenimmunität, durch PEPR1 und EFR per Ko-Immunopräzipitations (Ko-IP)- Experimente ergänzt werden. Ein weiteres Ziel dieser Arbeit war es daher zu überprüfen, ob BIR3 zusätzliche LRR-RLKs potentiell reguliert. Ebenso galt Zelltod-bezogenen Interaktoren ein besonderes Augenmerk, da BAK1 und BIR-proteine in unnatürlich vorkommenden Proteinmengen zu Zelltod führen. Zunächst wurde BIR3 über seinen YFP-tag mittels Ko-IP angereichert, um im Anschluss per MS-Analyse das BIR3-Interaktom zu studieren. Darunter fanden sich 32 LRR-RLKs, die bisher nicht mit BIR3 in Zusammenhang gebracht wurden. Unter den Kandidaten die jeweils in beiden MS-Analysen vorkamen, befanden sich zwei RLKs, die BAK1-abhängig agieren (SOBIR1 und SIF3), aber auch zwei, die ohne Hilfe von BAK1 funktional aktiv sind (MIK2 und HPCA1). Da BIR3 bisher als negativer Regulator von BAK1 und BAK1-abhängigen Signalwegen beschrieben ist, eröffnet das Auffinden von MIK2 und HPCA1 die Möglichkeit BIR3 als allgemeinen Regulator von LRR-RLKs zu definieren, unabhängig davon ob SERK Proteine involviert sind oder nicht. Weiterhin konnte das TNL CSA1 detektiert werden, welches im Anschluss näher auf seine Wirkweise im Zusammenhang mit BAK1- und BIR-vermitteltem Zelltod untersucht wurde. Wir konnten zeigen, dass der Verlust von *CSA1* in Kreuzungen mit *bir2-1* und *bak1-4* auf die Bildung von reaktiven Sauerstoffspezies nach Behandlung mit flg22 keinerlei Einfluss hatte und zusätzlich einen signifikanten Rückgang von Salizylsäurewerten im Zusammenhang mit

einer partiellen Reduzierung Zelltod-spezifischer Symptome in allen getesteten Mutanten zu Folge hatte. Daraus wurde geschlossen, dass CSA1 den Zelltod, ausgelöst durch die Abwesenheit von BAK1 und BIR-Proteinen positiv beeinflusst und dass dieser mit erhöhten Salizylsäurewerten einhergeht. Da der BAK1- / BIR-ausgelöste Zelltod partiell durch eine Mutation in *CSA1* supprimiert wurde, nehmen wir an, dass noch weitere Komponenten beteiligt sind. RPP8 (CNL), ein weiterer Kandidat aus dem BIR3-Interaktom, scheint daher ein geeignetes Testobjekt für fortführende Untersuchungen zu sein. Mit dieser Arbeit konnten wir per MS-Analyse ein BIR3-Interaktom erstellen, welches neues Licht auf (i) BIR3 als potentiellen allgemeinen Regulator von LRR-RLKs, eventuell unabhängig von BAK1-Beteiligung wirft und (ii) mit CSA1 einen intrazellulären Rezeptor identifiziert und charakterisiert, der BIR- und BAK1-vermittelten Zelltod reguliert.

References

Aarts, N., Metz, M., Holub, E., Staskawicz, B.J., Daniels, M.J., and Parker, J.E. (1998). Different requirements for EDS1 and NDR1 by disease resistance genes define at least two R gene-mediated signaling pathways in Arabidopsis. Proceedings of the National Academy of Sciences of the United States of America **95,** 10306-10311.

Adachi, H., Contreras, M.P., Harant, A., Wu, C.-h., Derevnina, L., Sakai, T., Duggan, C., Moratto, E., Bozkurt, T.O., and Maqbool, A. (2019). An N-terminal motif in NLR immune receptors is functionally conserved across distantly related plant species. eLife **8**.

Albert, C.H., Thuiller, W., Yoccoz, N.G., Douzet, R., Aubert, S., and Lavorel, S. (2010). A multi-trait approach reveals the structure and the relative importance of intra-vs. interspecific variability in plant traits. Functional Ecology **24,** 1192-1201.

Albert, I., Bohm, H., Albert, M., Feiler, C.E., Imkampe, J., Wallmeroth, N., Brancato, C., Raaymakers, T.M., Oome, S., Zhang, H.Q., Krol, E., Grefen, C., Gust, A.A., Chai, J.J., Hedrich, R., Van den Ackerveken, G., and Nurnberger, T. (2015). An RLP23-SOBIR1-BAK1 complex mediates NLP-triggered immunity. Nature Plants **1**.

Bartels, S., Lori, M., Mbengue, M., van Verk, M., Klauser, D., Hander, T., Boni, R., Robatzek, S., and Boller, T. (2013). The family of Peps and their precursors in Arabidopsis: differential expression and localization but similar induction of pattern-triggered immune responses. J Exp Bot **64,** 5309-5321.

Belkhadir, Y., Subramaniam, R., and Dangl, J.L. (2004). Plant disease resistance protein signaling: NBS-LRR proteins and their partners. Curr Opin Plant Biol **7,** 391-399.

Belkhadir, Y., Jaillais, Y., Epple, P., Balsemão-Pires, E., Dangl, J.L., and Chory, J. (2012). Brassinosteroids modulate the efficiency of plant immune responses to microbe-associated molecular patterns. Proceedings of the National Academy of Sciences **109,** 297-302.

Bent, A.F., and Mackey, D. (2007). Elicitors, effectors, and R genes: the new paradigm and a lifetime supply of questions. Annu Rev Phytopathol **45,** 399-436.

Bentham, A., Burdett, H., Anderson, P.A., Williams, S.J., and Kobe, B. (2017). Animal NLRs provide structural insights into plant NLR function. Annals of Botany **119,** 689-702.

Bernoux, M., Ve, T., Williams, S., Warren, C., Hatters, D., Valkov, E., Zhang, X., Ellis, J.G., Kobe, B., and Dodds, P.N. (2011). Structural and functional analysis of a plant resistance protein TIR domain reveals interfaces for self-association, signaling, and autoregulation. Cell host & microbe **9,** 200-211.

Bhandari, D.D., Lapin, D., Kracher, B., von Born, P., Bautor, J., Niefind, K., and Parker, J.E. (2019). An EDS1 heterodimer signalling surface enforces timely reprogramming of immunity genes in Arabidopsis. Nature communications **10,** 772.

Bi, D.L., Johnson, K.C.M., Zhu, Z.H., Huang, Y., Chen, F., Zhang, Y.L., and Li, X. (2011). Mutations in an atypical TIR-NB-LRR-LIM resistance protein confer autoimmunity. Frontiers in Plant Science **2**.

Bialas, A., Zess, E.K., De la Concepcion, J.C., Franceschetti, M., Pennington, H.G., Yoshida, K., Upson, J.L., Chanclud, E., Wu, C.H., Langner, T., Maqbool, A., Varden, F.A., Derevnina, L., Belhaj, K., Fujisaki, K., Saitoh, H., Terauchi, R., Banfield, M.J., and Kamoun, S. (2018). Lessons in Effector and NLR Biology of Plant-Microbe Systems. Molecular Plant-Microbe Interactions **31,** 34-45.

Bigeard, J., Colcombet, J., and Hirt, H. (2015). Signaling Mechanisms in Pattern-Triggered Immunity (PTI). Molecular Plant **8,** 521-539.

Blaum, B.S., Mazzotta, S., Noldeke, E.R., Halter, T., Madlung, J., Kemmerling, B., and Stehle, T. (2014). Structure of the pseudokinase domain of BIR2, a regulator of BAK1-mediated immune signaling in Arabidopsis. J Struct Biol **186,** 112-121.

Böhm, H., Albert, I., Fan, L., Reinhard, A., and Nurnberger, T. (2014). Immune receptor complexes at the plant cell surface. Current Opinion in Plant Biology **20,** 47-54.

Boller, T., and Felix, G. (2009a). A renaissance of elicitors: perception of microbe-associated molecular patterns and danger signals by pattern-recognition receptors. Annu Rev Plant Biol **60,** 379-406.

Boller, T., and Felix, G. (2009b). A Renaissance of Elicitors: Perception of Microbe-Associated Molecular Patterns and Danger Signals by Pattern-Recognition Receptors. Annual Review of Plant Biology **60,** 379-406.

Bonardi, V., Cherkis, K., Nishimura, M.T., and Dangl, J.L. (2012). A new eye on NLR proteins: focused on clarity or diffused by complexity? Current Opinion in Immunology **24,** 41-50.

Bonardi, V., Tang, S., Stallmann, A., Roberts, M., Cherkis, K., and Dangl, J.L. (2011). Expanded functions for a family of plant intracellular immune receptors beyond specific recognition of pathogen effectors. Proceedings of the National Academy of Sciences **108,** 16463-16468.

Brandt, B., and Hothorn, M. (2016). SERK co-receptor kinases. Curr Biol **26,** R225-226.

Bruggeman, Q., Prunier, F., Mazubert, C., de Bont, L., Garmier, M., Lugan, R., Benhamed, M., Bergounioux, C., Raynaud, C., and Delarue, M. (2015). Involvement of Arabidopsis hexokinase1 in cell death mediated by myo-inositol accumulation. The Plant Cell **27,** 1801-1814.

Buchanan, B.B., Gruissem, W., and Jones, R.L. (2015). Biochemistry and molecular biology of plants. (John Wiley & Sons).

Bücherl, C.A., Jarsch, I.K., Schudoma, C., Segonzac, C., Mbengue, M., Robatzek, S., MacLean, D., Ott, T., and Zipfel, C. (2017). Plant immune and growth receptors share common signalling components but localise to distinct plasma membrane nanodomains. Elife **6**.

Castel, B., Ngou, P.M., Cevik, V., Redkar, A., Kim, D.S., Yang, Y., Ding, P., and Jones, J.D. (2019). Diverse NLR immune receptors activate defence via the RPW 8-NLR NRG 1. New Phytologist **222,** 966-980.

Century, K.S., Shapiro, A.D., Repetti, P.P., Dahlbeck, D., Holub, E., and Staskawicz, B.J. (1997). NDR1, a pathogen-induced component required for Arabidopsis disease resistance. Science **278,** 1963-1965.

Chiang, Y.-H., and Coaker, G. (2015). Effector triggered immunity: NLR immune perception and downstream defense responses. The Arabidopsis Book **2015**.

Chinchilla, D., Bauer, Z., Regenass, M., Boller, T., and Felix, G. (2006). The Arabidopsis receptor kinase FLS2 binds flg22 and determines the specificity of flagellin perception. Plant Cell **18,** 465-476.

Chinchilla, D., Shan, L., He, P., de Vries, S., and Kemmerling, B. (2009). One for all: the receptor-associated kinase BAK1. Trends Plant Sci **14,** 535-541.

Chinchilla, D., Zipfel, C., Robatzek, S., Kemmerling, B., Nürnberger, T., Jones, J.D., Felix, G., and Boller, T. (2007). A flagellin-induced complex of the receptor FLS2 and BAK1 initiates plant defence. Nature **448,** 497-500.

Coll, N., Epple, P., and Dangl, J. (2011). Programmed cell death in the plant immune system. Cell death and differentiation **18,** 1247.

Collier, S.M., Hamel, L.-P., and Moffett, P. (2011). Cell death mediated by the N-terminal domains of a unique and highly conserved class of NB-LRR protein. Molecular plant-microbe interactions **24,** 918-931.

Coppinger, P., Repetti, P.P., Day, B., Dahlbeck, D., Mehlert, A., and Staskawicz, B.J. (2004). Overexpression of the plasma membrane-localized NDR1 protein results in enhanced bacterial disease resistance in Arabidopsis thaliana. The Plant Journal **40,** 225-237.

Couto, D., and Zipfel, C. (2016). Regulation of pattern recognition receptor signalling in plants. Nature Reviews Immunology **16,** 537-552.

Cox, J., and Mann, M. (2008). MaxQuant enables high peptide identification rates, individualized p.p.b.-range mass accuracies and proteome-wide protein quantification. Nature Biotechnology **26,** 1367-1372.

Cox, J., Neuhauser, N., Michalski, A., Scheltema, R.A., Olsen, J.V., and Mann, M. (2011). Andromeda: A Peptide Search Engine Integrated into the MaxQuant Environment. Journal of Proteome Research **10,** 1794-1805.

Cui, H., Gobbato, E., Kracher, B., Qiu, J., Bautor, J., and Parker, J.E. (2017). A core function of EDS1 with PAD4 is to protect the salicylic acid defense sector in Arabidopsis immunity. New Phytologist **213,** 1802-1817.

Cui, H.T., Tsuda, K., and Parker, J.E. (2015). Effector-Triggered Immunity: From Pathogen Perception to Robust Defense. In Annual Review of Plant Biology, Vol 66, S.S. Merchant, ed, pp. 487-511.

Day, B., Dahlbeck, D., and Staskawicz, B.J. (2006). NDR1 interaction with RIN4 mediates the differential activation of multiple disease resistance pathways in Arabidopsis. The Plant Cell **18,** 2782-2791.

Deslandes, L., and Rivas, S. (2012). Catch me if you can: bacterial effectors and plant targets. Trends in Plant Science **17,** 644-655.

DeYoung, B.J., and Innes, R.W. (2006). Plant NBS-LRR proteins in pathogen sensing and host defense. Nat Immunol **7,** 1243-1249.

Dominguez-Ferreras, A., Kiss-Papp, M., Jehle, A.K., Felix, G., and Chinchilla, D. (2015). An Overdose of the Arabidopsis Coreceptor BRASSINOSTEROID INSENSITIVE1-ASSOCIATED RECEPTOR KINASE1 or Its Ectodomain Causes Autoimmunity in a SUPPRESSOR OF BIR1-1-Dependent Manner. Plant Physiology **168,** 1106-+.

Duxbury, Z., Ma, Y., Furzer, O.J., Huh, S.U., Cevik, V., Jones, J.D., and Sarris, P.F. (2016). Pathogen perception by NLRs in plants and animals: Parallel worlds. Bioessays **38,** 769-781.

Edwards, K., Johnstone, C., and Thompson, C. (1991). A SIMPLE AND RAPID METHOD FOR THE PREPARATION OF PLANT GENOMIC DNA FOR PCR ANALYSIS. Nucleic Acids Research **19,** 1349-1349.

El Kasmi, F., Chung, E.H., Anderson, R.G., Li, J., Wan, L., Eitas, T.K., Gao, Z., and Dangl, J.L. (2017). Signaling from the plasma-membrane localized plant immune receptor RPM1 requires self-association of the full-length protein. Proc Natl Acad Sci U S A **114,** E7385-E7394.

Ellis, J.G. (2016). Integrated decoys and effector traps: how to catch a plant pathogen. Bmc Biology **14**.

Elmore, J.M., and Coaker, G. (2011). The role of the plasma membrane H+-ATPase in plant-microbe interactions. Mol Plant **4,** 416-427.

Elmore, J.M., Lin, Z.J.D., and Coaker, G. (2011). Plant NB-LRR signaling: upstreams and downstreams. Current Opinion in Plant Biology **14,** 365-371.

Faigon-Soverna, A., Harmon, F.G., Storani, L., Karayekov, E., Staneloni, R.J., Gassmann, W., Mas, P., Casal, J.J., Kay, S.A., and Yanovsky, M.J. (2006). A constitutive shade-avoidance mutant implicates TIR-NBS-LRR proteins in Arabidopsis photomorphogenic development. Plant Cell **18,** 2919-2928.

Felix, G., Duran, J., Volko, S., and Boller, T. (1999). Plants recognize bacteria through the most conserved domain of flagellin. Plant J **18,** 265-276.

Feys, B.J., Wiermer, M., Bhat, R.A., Moisan, L.J., Medina-Escobar, N., Neu, C., Cabral, A., and Parker, J.E. (2005). Arabidopsis SENESCENCE-ASSOCIATED GENE101 stabilizes and signals within an ENHANCED DISEASE SUSCEPTIBILITY1 complex in plant innate immunity. The Plant Cell **17,** 2601-2613.

Freyd, G., Kim, S.K., and Horvitz, H.R. (1990). NOVEL CYSTEINE-RICH MOTIF AND HOMEODOMAIN IN THE PRODUCT OF THE CAENORHABDITIS-ELEGANS CELL LINEAGE GENE LIN-II. Nature **344,** 876-879.

Fritz-Laylin, L.K., Krishnamurthy, N., Tör, M., Sjölander, K.V., and Jones, J.D. (2005). Phylogenomic analysis of the receptor-like proteins of rice and Arabidopsis. Plant physiology **138,** 611-623.

Gachon, C., and Saindrenan, P. (2004). Real-time PCR monitoring of fungal development in Arabidopsis thaliana infected by Alternaria brassicicola and Botrytis cinerea. Plant Physiology and Biochemistry **42,** 367-371.

Gantner, J., Ordon, J., Kretschmer, C., Guerois, R., and Stuttmann, J. (2019). An EDS1-SAG101 Complex is Essential for TNL-mediated Immunity in Nicotiana benthamiana. The Plant Cell **31,** 2456-2474.

Gao, M., Wang, X., Wang, D., Xu, F., Ding, X., Zhang, Z., Bi, D., Cheng, Y.T., Chen, S., Li, X., and Zhang, Y. (2009a). Regulation of cell death and innate immunity by two receptor-like kinases in Arabidopsis. Cell Host Microbe **6,** 34-44.

Gao, M.H., Wang, X., Wang, D.M., Xu, F., Ding, X.J., Zhang, Z.B., Bi, D.L., Cheng, Y.T., Chen, S., Li, X., and Zhang, Y.L. (2009b). Regulation of Cell Death and Innate Immunity by Two Receptor-like Kinases in Arabidopsis. Cell Host & Microbe **6,** 34-44.

Gao, X., Ruan, X., Sun, Y., Wang, X., and Feng, B. (2018). BAKing up to Survive a Battle: Functional Dynamics of BAK1 in Plant Programmed Cell Death. Front Plant Sci **9,** 1913.

Gao, Y., Wu, Y., Du, J., Zhan, Y., Sun, D., Zhao, J., Zhang, S., Li, J., and He, K. (2017). Both Light-Induced SA Accumulation and ETI Mediators Contribute to the Cell Death Regulated by BAK1 and BKK1. Front Plant Sci **8,** 622.

Genot, B., Lang, J., Berriri, S., Garmier, M., Gilard, F., Pateyron, S., Haustraete, K., Van Der Straeten, D., Hirt, H., and Colcombet, J. (2017). Constitutively Active Arabidopsis MAP Kinase 3 Triggers Defense Responses Involving Salicylic Acid and SUMM2 Resistance Protein. Plant Physiology **174,** 1238-1249.

Gómez-Gómez, L., and Boller, T. (2000). FLS2: an LRR receptor–like kinase involved in the perception of the bacterial elicitor flagellin in Arabidopsis. Molecular cell **5,** 1003-1011.

Gómez-Gómez, L., and Boller, T. (2002). Flagellin perception: a paradigm for innate immunity. Trends in plant science **7,** 251-256.

Granot, D., Kelly, G., Stein, O., and David-Schwartz, R. (2014). Substantial roles of hexokinase and fructokinase in the effects of sugars on plant physiology and development. Journal of experimental botany **65,** 809-819.

Großeholz, R., Feldman-Salit, A., Wanke, F., Schulze, S., Glöckner, N., Kemmerling, B., Harter, K., and Kummer, U. (2020). Specifying the role of BAK1-interacting receptor-like kinase 3 in brassinosteroid signaling. Journal of integrative plant biology **62,** 456-469.

Grund, E., Tremousaygue, D., and Deslandes, L. (2019). Plant NLRs with Integrated Domains: Unity Makes Strength. Plant Physiology **179,** 1227-1235.

Gubert, C.M., and Liljegren, S.J. (2014). HAESA and HAESA-LIKE2 activate organ abscission downstream of NEVERSHED and EVERSHED in Arabidopsis flowers. Plant signaling & behavior **9,** e29115.

Guo, H., Ahn, H.-K., Sklenar, J., Ma, Y., Ding, P., Menke, F., and Jones, J. (2019). Phosphorylation-Regulated Activation of the Arabidopsis RRS1-R/RPS4 Immune Receptor Complex Reveals Two Distinct Effector Recognition Mechanisms. CELL-HOST-MICROBE-D-19-00719.

Guo, H.Q., Nolan, T.M., Song, G.Y., Liu, S.Z., Xie, Z.L., Chen, J.I., Schnable, P.S., Walley, J.W., and Yin, Y.H. (2018). FERONIA Receptor Kinase Contributes to Plant Immunity by Suppressing Jasmonic Acid Signaling in Arabidopsis thaliana. Current Biology **28,** 3316-+.

Gust, A.A., Pruitt, R., and Nurnberger, T. (2017). Sensing Danger: Key to Activating Plant Immunity. Trends Plant Sci **22,** 779-791.

Guzmán-Benito, I., Donaire, L., Amorim-Silva, V., Vallarino, J.G., Esteban, A., Wierzbicki, A.T., Ruiz-Ferrer, V., and Llave, C. (2019). The immune repressor BIR 1 contributes to antiviral defense and undergoes transcriptional and post-transcriptional regulation during viral infections. New Phytologist.

Halter, T., Imkampe, J., Mazzotta, S., Wierzba, M., Postel, S., Bucherl, C., Kiefer, C., Stahl, M., Chinchilla, D., Wang, X., Nurnberger, T., Zipfel, C., Clouse, S., Borst, J.W., Boeren, S., de Vries, S.C., Tax, F., and Kemmerling, B. (2014). The leucine-rich repeat receptor kinase BIR2 is a negative regulator of BAK1 in plant immunity. Curr Biol **24,** 134-143.

Hander, T., Fernández-Fernández, Á.D., Kumpf, R.P., Willems, P., Schatowitz, H., Rombaut, D., Staes, A., Nolf, J., Pottie, R., and Yao, P. (2019). Damage on plants activates Ca2+-dependent metacaspases for release of immunomodulatory peptides. Science **363,** eaar7486.

He, K., Gou, X.P., Yuan, T., Lin, H.H., Asami, T., Yoshida, S., Russell, S.D., and Li, J. (2007). BAK1 and BKK1 regulate Brassinosteroid-dependent growth and BrassinosteroidIndependent cell-death pathways. Current Biology **17,** 1109-1115.

He, Y.X., Zhou, J.G., Shan, L.B., and Meng, X.Z. (2018). Plant cell surface receptor-mediated signaling - a common theme amid diversity. Journal of Cell Science **131**.

Hegenauer, V., Furst, U., Kaiser, B., Smoker, M., Zipfel, C., Felix, G., Stahl, M., and Albert, M. (2016). Detection of the plant parasite Cuscuta reflexa by a tomato cell surface receptor. Science **353,** 478-481.

Heidrich, K., Wirthmueller, L., Tasset, C., Pouzet, C., Deslandes, L., and Parker, J.E. (2011). Arabidopsis EDS1 connects pathogen effector recognition to cell compartment–specific immune responses. Science **334,** 1401-1404.

Heidrich, K., Tsuda, K., Blanvillain-Baufumé, S., Wirthmueller, L., Bautor, J., and Parker, J.E. (2013). Arabidopsis TNL-WRKY domain receptor RRS1 contributes to temperature-conditioned RPS4 auto-immunity. Frontiers in plant science **4,** 403.

Hohmann, U., and Hothorn, M. (2019). Crystal structure of the leucine-rich repeat ectodomain of the plant immune receptor kinase SOBIR1. Acta Crystallographica Section D: Structural Biology **75**.

Hohmann, U., Lau, K., and Hothorn, M. (2017). The Structural Basis of Ligand Perception and Signal Activation by Receptor Kinases. Annu Rev Plant Biol **68,** 109-137.

Hohmann, U., Nicolet, J., Moretti, A., Hothorn, L.A., and Hothorn, M. (2018). The SERK3 elongated allele defines a role for BIR ectodomains in brassinosteroid signalling. Nature Plants **4,** 345-+.

Hohmann, U., Ramakrishna, P., Wang, K., Lorenzo-Orts, L., Nicolet, J., Henschen, A., Barberon, M., Bayer, M., and Hothorn, M. (2020). Constitutive activation of leucine-rich repeat receptor kinase signaling pathways by BAK1-interacting receptor-like kinase 3 chimera. BioRxiv.

Huffaker, A., Pearce, G., and Ryan, C.A. (2006). An endogenous peptide signal in Arabidopsis activates components of the innate immune response. Proceedings of the National Academy of Sciences **103,** 10098-10103.

Imkampe, J., Halter, T., Huang, S.H., Schulze, S., Mazzotta, S., Schmidt, N., Manstretta, R., Postel, S., Wierzba, M., Yang, Y., van Dongen, W., Stahl, M., Zipfel, C., Goshe, M.B., Clouse, S., de Vries, S.C., Tax, F., Wang, X.F., and Kemmerling, B. (2017). The Arabidopsis Leucine-Rich Repeat Receptor Kinase BIR3 Negatively Regulates BAK1 Receptor Complex Formation and Stabilizes BAK1. Plant Cell **29,** 2285-2303.

Imkampe, M.S.J. (2015). Analysis on the BAK1-interacting RLKs BIR2 and BIR3, two proteins that differentially regulate BAK1-dependent pathways (PhD thesis. University of Tübingen).

Jeworutzki, E., Roelfsema, M.R.G., Anschutz, U., Krol, E., Elzenga, J.T.M., Felix, G., Boller, T., Hedrich, R., and Becker, D. (2010). Early signaling through the Arabidopsis pattern recognition receptors FLS2 and EFR involves Ca2+-associated opening of plasma membrane anion channels. Plant Journal **62,** 367-378.

Jia, Y., McAdams, S.A., Bryan, G.T., Hershey, H.P., and Valent, B. (2000). Direct interaction of resistance gene and avirulence gene products confers rice blast resistance. The EMBO journal **19,** 4004-4014.

Jones, J.D., and Dangl, J.L. (2006a). The plant immune system. Nature **444,** 323-329.

Jones, J.D.G., and Dangl, J.L. (2006b). The plant immune system. Nature **444,** 323-329.

Jubic, L.M., Saile, S., Furzer, O.J., El Kasmi, F., and Dangl, J.L. (2019). Help wanted: helper NLRs and plant immune responses. Current Opinion in Plant Biology **50,** 82-94.

Kemmerling, B., Schwedt, A., Rodriguez, P., Mazzotta, S., Frank, M., Qamar, S.A., Mengiste, T., Betsuyaku, S., Parker, J.E., Mussig, C., Thomma, B.P., Albrecht, C., de Vries, S.C., Hirt, H., and Nurnberger, T. (2007a). The BRI1-associated kinase 1, BAK1, has a brassinolide-independent role in plant cell-death control. Curr Biol **17,** 1116-1122.

Kemmerling, B., Schwedt, A., Rodriguez, P., Mazzotta, S., Frank, M., Abu Qamar, S., Mengiste, T., Betsuyaku, S., Parker, J.E., Mussig, C., Thomma, B., Albrecht, C., de Vries, S.C., Hirt, H., and Nurnberger, T. (2007b). The BRI1-associated kinase 1, BAK1, has a Brassinoli-independent role in plant cell-death control. Current Biology **17,** 1116-1122.

Krol, E., Mentzel, T., Chinchilla, D., Boller, T., Felix, G., Kemmerling, B., Postel, S., Arents, M., Jeworutzki, E., Al-Rasheid, K.A.S., Becker, D., and Hedrich, R. (2010). Perception of the Arabidopsis Danger Signal Peptide 1 Involves the Pattern Recognition Receptor AtPEPR1 and Its Close Homologue AtPEPR2. Journal of Biological Chemistry **285,** 13471-13479.

Lapin, D., Kovacova, V., Sun, X., Dongus, J.A., Bhandari, D.D., von Born, P., Bautor, J., Guarneri, N., Stuttmann, J., and Beyer, A. (2019). A coevolved EDS1-SAG101-NRG1 module mediates cell death signaling by TIR-domain immune receptors. bioRxiv, 572826.

Lenz, H.D., Haller, E., Melzer, E., Kober, K., Wurster, K., Stahl, M., Bassham, D.C., Vierstra, R.D., Parker, J.E., Bautor, J., Molina, A., Escudero, V., Shindo, T., van der Hoorn, R.A.L., Gust,

A.A., and Nurnberger, T. (2011). Autophagy differentially controls plant basal immunity to biotrophic and necrotrophic pathogens. Plant Journal **66,** 818-830.

Leslie, M.E., Lewis, M.W., Youn, J.-Y., Daniels, M.J., and Liljegren, S.J. (2010). The EVERSHED receptor-like kinase modulates floral organ shedding in Arabidopsis. Development **137,** 467-476.

Li, J., Wen, J., Lease, K.A., Doke, J.T., Tax, F.E., and Walker, J.C. (2002). BAK1, an Arabidopsis LRR receptor-like protein kinase, interacts with BRI1 and modulates brassinosteroid signaling. Cell **110,** 213-222.

Li, L., Kim, P., Yu, L., Cai, G., Chen, S., Alfano, J.R., and Zhou, J.-M. (2016). Activation-dependent destruction of a co-receptor by a Pseudomonas syringae effector dampens plant immunity. Cell host & microbe **20,** 504-514.

Liebrand, T.W.H., van den Burg, H.A., and Joosten, M. (2014). Two for all: receptor-associated kinases SOBIR1 and BAK1. Trends in Plant Science **19,** 123-132.

Liebrand, T.W.H., van den Berg, G.C.M., Zhang, Z., Smit, P., Cordewener, J.H.G., America, A.H.P., Sklenar, J., Jones, A.M.E., Tameling, W.I.L., Robatzek, S., Thomma, B., and Joosten, M. (2013). Receptor-like kinase SOBIR1/EVR interacts with receptor-like proteins in plant immunity against fungal infection. Proceedings of the National Academy of Sciences of the United States of America **110,** 10010-10015.

Liu, Y., Huang, X., Li, M., He, P., and Zhang, Y. (2016). Loss-of-function of Arabidopsis receptor-like kinase BIR1 activates cell death and defense responses mediated by BAK1 and SOBIR1. New Phytol **212,** 637-645.

Ma, C.Y., Liu, Y.N., Bai, B., Han, Z.F., Tang, J., Zhang, H.Q., Yaghmaiean, H., Zhang, Y.L., and Chai, J.J. (2017). Structural basis for BIR1-mediated negative regulation of plant immunity. Cell Research **27,** 1521-1524.

Ma, X., Xu, G., He, P., and Shan, L. (2016). SERKing coreceptors for receptors. Trends in plant science **21,** 1017-1033.

Maekawa, T., Cheng, W., Spiridon, L.N., Töller, A., Lukasik, E., Saijo, Y., Liu, P., Shen, Q.-H., Micluta, M.A., and Somssich, I.E. (2011). Coiled-coil domain-dependent homodimerization of intracellular barley immune receptors defines a minimal functional module for triggering cell death. Cell host & microbe **9,** 187-199.

McDowell, J.M., Cuzick, A., Can, C., Beynon, J., Dangl, J.L., and Holub, E.B. (2000). Downy mildew (Peronospora parasitica) resistance genes in Arabidopsis vary in functional requirements for NDR1, EDS1, NPR1 and salicylic acid accumulation. The Plant Journal **22,** 523-529.

Meyers, B.C. (2003). Genome-Wide Analysis of NBS-LRR-Encoding Genes in Arabidopsis. The Plant Cell Online **15,** 809-834.

Mohr, T.J., Mammarella, N.D., Hoff, T., Woffenden, B.J., Jelesko, J.G., and McDowell, J.M. (2010). The Arabidopsis downy mildew resistance gene RPP8 is induced by pathogens and salicylic acid and is regulated by W box cis elements. Molecular plant-microbe interactions **23,** 1303-1315.

Monteiro, F., and Nishimura, M.T. (2018). Structural, Functional, and Genomic Diversity of Plant NLR Proteins: An Evolved Resource for Rational Engineering of Plant Immunity. In Annual Review of Phytopathology, Vol 56, J.E. Leach and S.E. Lindow, eds, pp. 243-267.

Nam, K.H., and Li, J. (2002). BRI1/BAK1, a receptor kinase pair mediating brassinosteroid signaling. Cell **110,** 203-212.

Ngou, B.P.M., Ahn, H.-K., Ding, P., and Jones, J.D. (2020). Mutual potentiation of plant immunity by cell-surface and intracellular receptors. bioRxiv.

Ngou, B.P.M., Ahn, H.-K., Ding, P., Redkar, A., Brown, H., Ma, Y., Youles, M., Tomlinson, L., and Jones, J.D. (2019). Estradiol-inducible AvrRps4 expression reveals distinct properties of TIR-NLR-mediated effector-triggered immunity. bioRxiv**,** 701359.

Nühse, T.S., Peck, S.C., Hirt, H., and Boller, T. (2000). Microbial elicitors induce activation and dual phosphorylation of the Arabidopsis thaliana MAPK 6. Journal of Biological Chemistry **275,** 7521-7526.

Nürnberger, T., Brunner, F., Kemmerling, B., and Piater, L. (2004). Innate immunity in plants and animals: striking similarities and obvious differences. Immunological Reviews **198,** 249-266.

Parker, J.E., Holub, E.B., Frost, L.N., Falk, A., Gunn, N.D., and Daniels, M.J. (1996). Characterization of eds1, a mutation in Arabidopsis suppressing resistance to Peronospora parasitica specified by several different RPP genes. The Plant Cell **8,** 2033-2046.

Peele, H.M., Guan, N., Fogelqvist, J., and Dixelius, C. (2014). Loss and retention of resistance genes in five species of the Brassicaceae family. Bmc Plant Biology **14**.

Peng, Y., van Wersch, R., and Zhang, Y. (2018). Convergent and divergent signaling in PAMP-triggered immunity and effector-triggered immunity. Molecular plant-microbe interactions **31,** 403-409.

Perraki, A., DeFalco, T.A., Derbyshire, P., Avila, J., Sere, D., Sklenar, J., Qi, X., Stransfeld, L., Schwessinger, B., Kadota, Y., Macho, A.P., Jiang, S., Couto, D., Torii, K.U., Menke, F.L.H., and Zipfel, C. (2018). Phosphocode-dependent functional dichotomy of a common co-receptor in plant signalling. Nature **561,** 248-252.

Pieterse, C.M., Leon-Reyes, A., Van der Ent, S., and Van Wees, S.C. (2009). Networking by small-molecule hormones in plant immunity. Nat Chem Biol **5,** 308-316.

Postel, S., Kufner, I., Beuter, C., Mazzotta, S., Schwedt, A., Borlotti, A., Halter, T., Kemmerling, B., and Nurnberger, T. (2010). The multifunctional leucine-rich repeat receptor kinase BAK1 is implicated in Arabidopsis development and immunity. European Journal of Cell Biology **89,** 169-174.

Qi, T., Seong, K., Thomazella, D.P., Kim, J.R., Pham, J., Seo, E., Cho, M.-J., Schultink, A., and Staskawicz, B.J. (2018). NRG1 functions downstream of EDS1 to regulate TIR-NLR-mediated plant immunity in Nicotiana benthamiana. Proceedings of the National Academy of Sciences **115,** E10979-E10987.

Robinson, R. (2015). Prion folding sends a death signal in fungus. PLoS biology **13**.

Rolland, F., Baena-Gonzalez, E., and Sheen, J. (2006). Sugar sensing and signaling in plants: conserved and novel mechanisms. Annu. Rev. Plant Biol. **57,** 675-709.

Ross, A., Yamada, K., Hiruma, K., Yamashita-Yamada, M., Lu, X., Takano, Y., Tsuda, K., and Saijo, Y. (2014). The Arabidopsis PEPR pathway couples local and systemic plant immunity. EMBO J **33,** 62-75.

Roux, M., Schwessinger, B., Albrecht, C., Chinchilla, D., Jones, A., Holton, N., Malinovsky, F.G., Tor, M., de Vries, S., and Zipfel, C. (2011). The Arabidopsis Leucine-Rich Repeat Receptor-Like Kinases BAK1/SERK3 and BKK1/SERK4 Are Required for Innate Immunity to Hemibiotrophic and Biotrophic Pathogens. Plant Cell **23,** 2440-2455.

Sarris, P.F., Cevik, V., Dagdas, G., Jones, J.D.G., and Krasileva, K.V. (2016). Comparative analysis of plant immune receptor architectures uncovers host proteins likely targeted by pathogens. Bmc Biology **14**.

Schmidt, M.S.N.J. (2017). Identification and Functional Analysis of in vitro/in vivo Phosphorylation Sites of the Arabidopsis BAK1 Interacting Receptor Kinase BIR2 (Universität Tübingen).

Schreiber, K.J., Bentham, A., Williams, S.J., Kobe, B., and Staskawicz, B.J. (2016). Multiple domain associations within the Arabidopsis immune receptor RPP1 regulate the activation of programmed cell death. PLoS pathogens **12**.

Schulze, B., Mentzel, T., Jehle, A.K., Mueller, K., Beeler, S., Boller, T., Felix, G., and Chinchilla, D. (2010). Rapid heteromerization and phosphorylation of ligand-activated plant transmembrane receptors and their associated kinase BAK1. Journal of Biological Chemistry **285,** 9444-9451.

Schwessinger, B., Roux, M., Kadota, Y., Ntoukakis, V., Sklenar, J., Jones, A., and Zipfel, C. (2011). Phosphorylation-Dependent Differential Regulation of Plant Growth, Cell Death, and Innate Immunity by the Regulatory Receptor-Like Kinase BAK1. Plos Genetics **7**.

Seuring, C., Greenwald, J., Wasmer, C., Wepf, R., Saupe, S.J., Meier, B.H., and Riek, R. (2012). The mechanism of toxicity in HET-S/HET-s prion incompatibility. PLoS biology **10**.

Shao, F., Merritt, P.M., Bao, Z., Innes, R.W., and Dixon, J.E. (2002). A Yersinia effector and a Pseudomonas avirulence protein define a family of cysteine proteases functioning in bacterial pathogenesis. Cell **109,** 575-588.

Shao, F., Golstein, C., Ade, J., Stoutemyer, M., Dixon, J.E., and Innes, R.W. (2003). Cleavage of Arabidopsis PBS1 by a bacterial type III effector. Science **301,** 1230-1233.

Shen, W., Liu, J., and Li, J.-F. (2019). Type-II Metacaspases Mediate the Processing of Plant Elicitor Peptides in Arabidopsis. Molecular plant **12,** 1524-1533.

Siligardi, G., Zhang, M., and Prodromou, C. (2018a). The stoichiometric interaction of the Hsp90-Sgt1-Rar1 complex by CD and SRCD spectroscopy. Frontiers in molecular biosciences **4,** 95.

Siligardi, G., Zhang, M.H., and Prodromou, C. (2018b). The Stoichiometric Interaction of the Hsp90-Sgt1-Rar1 Complex by CD and SRCD Spectroscopy. Frontiers in Molecular Biosciences **4**.

Slootweg, E.J., Spiridon, L.N., Roosien, J., Butterbach, P., Pomp, R., Westerhof, L., Wilbers, R., Bakker, E., Bakker, J., and Petrescu, A.-J. (2013). Structural determinants at the interface of the ARC2 and leucine-rich repeat domains control the activation of the plant immune receptors Rx1 and Gpa2. Plant physiology **162,** 1510-1528.

Smakowska-Luzan, E., Mott, G.A., Parys, K., Stegmann, M., Howton, T.C., Layeghifard, M., Neuhold, J., Lehner, A., Kong, J.X., Grunwald, K., Weinberger, N., Satbhai, S.B., Mayer, D., Busch, W., Madalinski, M., Stolt-Bergner, P., Provart, N.J., Mukhtar, M.S., Zipfel, C., Desveaux, D., Guttman, D.S., and Belkhadir, Y. (2018). An extracellular network of Arabidopsis leucine-rich repeat receptor kinases. Nature **553,** 342-+.

Spoel, S.H., and Dong, X. (2012). How do plants achieve immunity? Defence without specialized immune cells. Nature Reviews Immunology **12,** 89-100.

Stegmann, M., Monaghan, J., Smakowska-Luzan, E., Rovenich, H., Lehner, A., Holton, N., Belkhadir, Y., and Zipfel, C. (2017). The receptor kinase FER is a RALF-regulated scaffold controlling plant immune signaling. Science **355,** 287-+.

Sukarta, O.C., Slootweg, E.J., and Goverse, A. (2016). Structure-informed insights for NLR functioning in plant immunity. In Seminars in cell & developmental biology (Elsevier), pp. 134-149.

Swiderski, M.R., Birker, D., and Jones, J.D. (2009). The TIR domain of TIR-NB-LRR resistance proteins is a signaling domain involved in cell death induction. Molecular plant-microbe interactions **22,** 157-165.

Tameling, W.I., Elzinga, S.D., Darmin, P.S., Vossen, J.H., Takken, F.L., Haring, M.A., and Cornelissen, B.J. (2002). The tomato R gene products I-2 and MI-1 are functional ATP binding proteins with ATPase activity. The Plant Cell **14,** 2929-2939.

Tameling, W.I., Vossen, J.H., Albrecht, M., Lengauer, T., Berden, J.A., Haring, M.A., Cornelissen, B.J., and Takken, F.L. (2006). Mutations in the NB-ARC domain of I-2 that impair ATP hydrolysis cause autoactivation. Plant physiology **140,** 1233-1245.

Thomma, B., Nelissen, I., Eggermont, K., and Broekaert, W.F. (1999). Deficiency in phytoalexin production causes enhanced susceptibility of Arabidopsis thaliana to the fungus Alternaria brassicicola. Plant Journal **19,** 163-171.

Tsuda, K., Mine, A., Bethke, G., Igarashi, D., Botanga, C.J., Tsuda, Y., Glazebrook, J., Sato, M., and Katagiri, F. (2013). Dual Regulation of Gene Expression Mediated by Extended MAPK Activation and Salicylic Acid Contributes to Robust Innate Immunity in Arabidopsis thaliana. Plos Genetics **9**.

Van Der Biezen, E.A., and Jones, J.D. (1998). Plant disease-resistance proteins and the gene-for-gene concept. Trends in biochemical sciences **23,** 454-456.

Van der Does, D., Boutrot, F., Engelsdorf, T., Rhodes, J., McKenna, J.F., Vernhettes, S., Koevoets, I., Tintor, N., Veerabagu, M., and Miedes, E. (2017a). The Arabidopsis leucine-rich repeat receptor kinase MIK2/LRR-KISS connects cell wall integrity sensing, root growth and response to abiotic and biotic stresses. PLoS genetics **13,** e1006832.

Van der Does, D., Boutrot, F., Engelsdorf, T., Rhodes, J., McKenna, J.F., Vernhettes, S., Koevoets, I., Tintor, N., Veerabagu, M., Miedes, E., Segonzac, C., Roux, M., Breda, A.S., Hardtke, C.S., Molina, A., Rep, M., Testerink, C., Mouille, G., Hofte, H., Hamann, T., and Zipfel, C. (2017b). The Arabidopsis leucine-rich repeat receptor kinase MIK2/LRR-KISS connects cell wall integrity sensing, root growth and response to abiotic and biotic stresses. Plos Genetics **13**.

Van Doorn, W., Beers, E., Dangl, J., Franklin-Tong, V., Gallois, P., Hara-Nishimura, I., Jones, A., Kawai-Yamada, M., Lam, E., and Mundy, J. (2011). Morphological classification of plant cell deaths. Cell Death & Differentiation **18,** 1241-1246.

Van Ghelder, C., Parent, G.J., Rigault, P., Prunier, J., Giguère, I., Caron, S., Sena, J.S., Deslauriers, A., Bousquet, J., and Esmenjaud, D. (2019). The large repertoire of conifer NLR resistance genes includes drought responsive and highly diversified RNLs. Scientific reports **9,** 1-13.

Voinnet. (2015). An enhanced transient expression system in plants based on suppression of gene silencing by the p19 protein of tomato bushy stunt virus (vol 33, pg 949, 2003). Plant Journal **83,** 752-752.

Voss, M., Toelzer, C., Bhandari, D.D., Parker, J.E., and Niefind, K. (2019). Arabidopsis immunity regulator EDS1 in a PAD4/SAG101-unbound form is a monomer with an inherently inactive conformation. Journal of structural biology **208,** 107390.

Wagner, S., Stuttmann, J., Rietz, S., Guerois, R., Brunstein, E., Bautor, J., Niefind, K., and Parker, J.E. (2013). Structural basis for signaling by exclusive EDS1 heteromeric complexes with SAG101 or PAD4 in plant innate immunity. Cell host & microbe **14,** 619-630.

Wan, L., Essuman, K., Anderson, R.G., Sasaki, Y., Monteiro, F., Chung, E.-H., Nishimura, E.O., DiAntonio, A., Milbrandt, J., and Dangl, J.L. (2019a). TIR domains of plant immune receptors are NAD+-cleaving enzymes that promote cell death. Science **365,** 799-803.

Wan, W.-L., Fröhlich, K., Pruitt, R.N., Nürnberger, T., and Zhang, L. (2019b). Plant cell surface immune receptor complex signaling. Current opinion in plant biology **50,** 18-28.

Wang, J.Z., Hu, M.J., Wang, J., Qi, J.F., Han, Z.F., Wang, G.X., Qi, Y.J., Wang, H.W., Zhou, J.M., and Chai, J.J. (2019). Reconstitution and structure of a plant NLR resistosome conferring immunity. Science **364,** 44-+.

Wang, T., Liang, L., Xue, Y., Jia, P.-F., Chen, W., Zhang, M.-X., Wang, Y.-C., Li, H.-J., and Yang, W.-C. (2016). A receptor heteromer mediates the male perception of female attractants in plants. Nature **531,** 241-244.

Wang, Z., Meng, P., Zhang, X.Y., Ren, D.T., and Yang, S.H. (2011). BON1 interacts with the protein kinases BIR1 and BAK1 in modulation of temperature-dependent plant growth and cell death in Arabidopsis. Plant Journal **67,** 1081-1093.

Wang, Z.Y., Seto, H., Fujioka, S., Yoshida, S., and Chory, J. (2001). BRI1 is a critical component of a plasma-membrane receptor for plant steroids (vol 410, pg 380, 2001). Nature **411,** 219-219.

Watanabe, N., and Lam, E. (2011). Arabidopsis metacaspase 2d is a positive mediator of cell death induced during biotic and abiotic stresses. The Plant Journal **66,** 969-982.

Wiermer, M., Feys, B.J., and Parker, J.E. (2005). Plant immunity: the EDS1 regulatory node. Current Opinion in Plant Biology **8,** 383-389.

Wierzba, M.P., and Tax, F.E. (2016). An allelic series of bak1 mutations differentially alter bir1 cell death, immune response, growth, and root development phenotypes in Arabidopsis thaliana. Genetics **202,** 689-702.

Williams, S.J., Sohn, K.H., Wan, L., Bernoux, M., Sarris, P.F., Segonzac, C., Ve, T., Ma, Y., Saucet, S.B., and Ericsson, D.J. (2014a). Structural basis for assembly and function of a heterodimeric plant immune receptor. Science **344,** 299-303.

Williams, S.J., Sohn, K.H., Wan, L., Bernoux, M., Sarris, P.F., Segonzac, C., Ve, T., Ma, Y., Saucet, S.B., Ericsson, D.J., Casey, L.W., Lonhienne, T., Winzor, D.J., Zhang, X.X., Coerdt, A., Parker, J.E., Dodds, P.N., Kobe, B., and Jones, J.D.G. (2014b). Structural Basis for Assembly and Function of a Heterodimeric Plant Immune Receptor. Science **344,** 299-303.

Wu, C.-H., Adachi, H., De la Concepcion, J.C., Castells-Graells, R., Nekrasov, V., and Kamoun, S. (2019a). A CRISPR/Cas9 mediated 53 kb deletion of the NRC4 gene cluster of tomato does not affect bacterial flagellin-triggered immunity. BioRxiv**,** 697425.

Wu, C.-H., Adachi, H., De la Concepcion, J.C., Castells-Graells, R., Nekrasov, V., and Kamoun, S. (2020a). NRC4 gene cluster is not essential for bacterial flagellin-triggered immunity. Plant Physiology **182,** 455.

Wu, F., Chi, Y., Jiang, Z., Xu, Y., Xie, L., Huang, F., Wan, D., Ni, J., Yuan, F., and Wu, X. (2020b). Hydrogen peroxide sensor HPCA1 is an LRR receptor kinase in Arabidopsis. Nature **578,** 577-581.

Wu, J.B., Reca, I.B., Spinelli, F., Lironi, D., De Lorenzo, G., Poltronieri, P., Cervone, F., Joosten, M., Ferrari, S., and Brutus, A. (2019b). An EFR-Cf-9 chimera confers enhanced resistance to

bacterial pathogens by SOBIR1-and BAK1-dependent recognition of elf18. Molecular Plant Pathology **20,** 751-764.

Xu, F., Zhu, C.P., Cevik, V., Johnson, K., Liu, Y.N., Sohn, K., Jones, J.D., Holub, E.B., and Li, X. (2015). Autoimmunity conferred by chs3-2D relies on CSA1, its adjacent TNL-encoding neighbour. Scientific Reports **5**.

Yamaguchi, Y., Pearce, G., and Ryan, C.A. (2006). The cell surface leucine-rich repeat receptor for AtPep1, an endogenous peptide elicitor in Arabidopsis, is functional in transgenic tobacco cells. Proceedings of the National Academy of Sciences **103,** 10104-10109.

Yamaguchi, Y., Huffaker, A., Bryan, A.C., Tax, F.E., and Ryan, C.A. (2010). PEPR2 is a second receptor for the Pep1 and Pep2 peptides and contributes to defense responses in Arabidopsis. The Plant Cell **22,** 508-522.

Yang, H., Shi, Y., Liu, J., Guo, L., Zhang, X., and Yang, S. (2010). A mutant CHS3 protein with TIR-NB-LRR-LIM domains modulates growth, cell death and freezing tolerance in a temperature-dependent manner in Arabidopsis. Plant Journal **63,** 283-296.

Yu, J.Y., Tehrim, S., Zhang, F.Q., Tong, C.B., Huang, J.Y., Cheng, X.H., Dong, C.H., Zhou, Y.Q., Qin, R., Hua, W., and Liu, S.Y. (2014). Genome-wide comparative analysis of NBS-encoding genes between Brassica species and Arabidopsis thaliana. Bmc Genomics **15**.

Yu, X., Feng, B., He, P., and Shan, L. (2017). From Chaos to Harmony: Responses and Signaling upon Microbial Pattern Recognition. Annu Rev Phytopathol **55,** 109-137.

Yu, X., Xu, G., Li, B., de Souza Vespoli, L., Liu, H., Moeder, W., Chen, S., de Oliveira, M.V., de Souza, S.A., and Shao, W. (2019). The receptor kinases BAK1/SERK4 regulate Ca2+ channel-mediated cellular homeostasis for cell death containment. Current Biology **29,** 3778-3790. e3778.

Yuan, M., Jiang, Z., Bi, G., Nomura, K., Liu, M., He, S.Y., Zhou, J.-M., and Xin, X.-F. (2020). Pattern-recognition receptors are required for NLR-mediated plant immunity. bioRxiv.

Yuan, N., Yuan, S., Li, Z., Zhou, M., Wu, P., Hu, Q., Mendu, V., Wang, L., and Luo, H. (2018). STRESS INDUCED FACTOR 2, a Leucine-Rich Repeat Kinase Regulates Basal Plant Pathogen Defense. Plant Physiol **176,** 3062-3080.

Zhang, M., Kadota, Y., Prodromou, C., Shirasu, K., and Pearl, L.H. (2010). Structural basis for assembly of Hsp90-Sgt1-CHORD protein complexes: implications for chaperoning of NLR innate immunity receptors. Molecular cell **39,** 269-281.

Zhang, W., Fraiture, M., Kolb, D., Löffelhardt, B., Desaki, Y., Boutrot, F.F., Tör, M., Zipfel, C., Gust, A.A., and Brunner, F. (2013). Arabidopsis receptor-like protein30 and receptor-like kinase suppressor of BIR1-1/EVERSHED mediate innate immunity to necrotrophic fungi. The Plant Cell **25,** 4227-4241.

Zhang, Y., Dorey, S., Swiderski, M., and Jones, J.D. (2004). Expression of RPS4 in tobacco induces an AvrRps4-independent HR that requires EDS1, SGT1 and HSP90. The Plant Journal **40,** 213-224.

Zhou, J.G., Wang, P., Claus, L.A.N., Savatin, D.V., Xu, G.Y., Wu, S.J., Meng, X.Z., Russinova, E., He, P., and Shan, L.B. (2019). Proteolytic Processing of SERK3/BAK1 Regulates Plant Immunity, Development, and Cell Death. Plant Physiology **180,** 543-558.

Zipfel, C., Kunze, G., Chinchilla, D., Caniard, A., Jones, J.D.G., Boller, T., and Felix, G. (2006). Perception of the bacterial PAMP EF-Tu by the receptor EFR restricts Agrobacterium-mediated transformation. Cell **125,** 749-760.

Appendix

table A 1: total list of all kinases found in MSI

MSI				
AGI-code	Protein kinase	ratio of intensities BIR3/ eGFP	unique in BIR3YFP-lane?	Q-value
AT2G13790, AT2G13800	SERK4, SERK5	1,2E+10	yes	0
AT4G33430	BAK1/SERK3	4,3E+09	yes	0
At5G14210	LRR-RLK	4,2E+09	yes	0
AT3G19320	LRR-family protein	4,2E+08	yes	0
AT1G34210	SERK2	3,1E+08	yes	0
AT4G23180	CRK10	2,7E+08	yes	0
AT1G22720	Protein kinase superfamily protein	2,7E+08	yes	0
At1g27190	BIR3	1,9E+08	yes	0
At3g14840	LIK1	1,4E+08	yes	0
AT3G22060	Receptor-like protein kinase-related family protein	9,1E+07	yes	0
AT3G51550	FERONIA	7,2E+07	yes	0
At4g31390	ABC1-LIKE KINASE 1	5,6E+07	yes	0
AT2G31880	SOBIR1	5,1E+07	yes	0
At5g49760	HPCA1	4,7E+07	yes	0
AT3G52990	Pyruvate kinase	4,0E+07	yes	0
AT1G80460	NHO1 glycerol kinase	3,9E+07	yes	0
AT4G16130	ISA1	2,2E+07	yes	0
At1g79600	ABC1-LIKE KINASE 3, ABC1K3	1,6E+07	yes	0
AT1G71830	SERK1	1,4E+07	yes	0
At5g41260	BSK8	1,3E+07	yes	2,1E-03
AT3G17770	Dihydroxyacetone kinase	1,3E+07	yes	0
AT4G32300	SD2-5 G-type lectin S-RLK	7,1E+06	yes	8,3E-03
AT5G63410	LRR-RLK	5,6E+06	yes	0
AT3G57530	CPK32	5,1E+06	yes	3,5E-03
At1g27190	BIR3	1,7E+03	no	0
AT1G79550	PGK	1,8E+01	no	0
At5g38990	Malectin/receptor-like protein kinase family protein	9	no	0
AT2G37710	LECRK-IV.1	9	no	0
AT1G51805	IOSL1	5	no	0
At4g08850	LRR-RLK	4	no	0
AT3G24550	PERK1	4	no	0
AT1G78860	curculin-like (mannose-binding) lectin family protein	3	no	3,7E-04
AT5G63680	Pyruvate kinase family protein;	9	no	0
AT1G52290	PERK15	2	no	0
AT4G29130	HXK1	2	no	0

table A 2: total list of all kinases found in MSII

MSII				
AGI-code	Protein kinase	ratio of intensities BIR3/ eGFP	unique in BIR3YFP-lane?	Q-value
AT4G33430	SERK3, BAK1	5,1E+10	yes	0
AT2G13790, AT2G13800	SERK4, SERK5	1,6E+10	yes	0
At5G14210	LRR-RLK	8,1E+09	yes	0
AT1G51805	SIF3	8,3E+08	yes	0
AT1G34210	SERK2	7,7E+08	yes	0
AT1G53430	NILR2	6,2E+08	yes	0
At1g27190	BIR3	5,9E+08	yes	0
AT4G23180	CRK10, RLK4	5,6E+08	yes	0
AT2G37710	L-type lectin-domain containing RK	5,2E+08	yes	0
At4g08850	MIK2	4,8E+08	yes	0
At3g14840	LIK1	2,9E+08	yes	0
AT1G52290	PERK15	2,6E+08	yes	0
AT5G38990	Malectin/receptor-like protein kinase family protein	2,5E+08	yes	0
AT3G51550	FERONIA	1,9E+08	yes	0
At1g53440	LRR-RLK	1,8E+08	yes	0
AT4G11480	CRK32	1,7E+08	yes	0
AT2G31880	SOBIR	1,7E+08	yes	0
AT4G04570	CRK40	1,4E+08	yes	0
AT3G54090	FLN1	1,4E+08	yes	0
AT3G63260	ATMRK1	1,3E+08	yes	0
AT1G21270	WAK2	1,2E+08	yes	0
AT1G69200	FLN2 fructokinase-like protein	1,2E+08	yes	0
AT2G26730	LRR-RLK	9,6E+07	yes	0
AT5G10290	LRR-RLK	9,4E+07	yes	0
At2g23200	Protein kinase superfamily protein	8,8E+07	yes	0
AT3G28450	BIR2	8,7E+07	yes	0
AT1G60940	SNF1-RELATED KINASE 2B	8,3E+07	yes	0
AT1G71830	SERK1	8,1E+07	yes	0
AT3G24550	PERK1	7,9E+07	yes	0
AT5G54590	CRLK1	7,9E+07	yes	0
At5g16590	LRR1	6,9E+07	yes	0
At3g17770	Dihydroxyacetone kinase	6,3E+07	yes	0
At4g35230	BSK1	6,2E+07	yes	0
AT1G15530	LECRK-S.1	5,7E+07	yes	0
AT2G17290	CPK6	5,6E+07	yes	0
AT4G29810	MK1, MKK2,	4,8E+07	yes	0
AT2G28940	Protein kinase superfamily protein	4,5E+07	yes	1,9E-03
AT4G16130	ISA1	3,9E+07	yes	0
AT5G08590	ASK2;SERINE/THREONINE KINASE 2	3,7E+07	yes	4,5E-03
AT4G01370	MAPK4, MPK4	3,7E+07	yes	1,1E-03
AT3G23750	BARK1	3,6E+07	yes	0
AT1G63500	BSK7	3,3E+07	yes	0
At5g10020	SIRK1	3,1E+07	yes	0
AT5G49760	HPCA1	3,0E+07	yes	0
AT1G11330	S-locus lectin protein kinase family protein	2,9E+07	yes	0
AT3G21220	MEK5, MKK5	2,9E+07	yes	2,3E-03
AT3G46290	HERK1	2,9E+07	yes	0
AT2G18730	DGK3	2,9E+07	yes	0
AT5G63400	ADK1	2,7E+07	yes	0
AT4G23250	CRK17	2,7E+07	yes	5,3E-03
AT2G35390	Ribose-phosphate pyrophosphokinase	2,6E+07	yes	1,4E-03
AT1G10522	PRIN2 Serine/Threonine-kinase	2,5E+07	yes	6,6E-03
AT5G51560	LRR-RLK	2,5E+07	yes	1,0E-03
At1g56140	LRR-RLK	2,4E+07	yes	0
AT3G21630	CERK1	2,4E+07	yes	1,0E-03
AT3G50000	CKA2 casein kinase II	2,2E+07	yes	0
AT5G14060	CARAB-AK-LYS, lysine-sensitive aspartate kinase	2,1E+07	yes	0
AT1G70530	CRK3	1,8E+07	yes	1,1E-03
At2g17340	pantothenate kinase	1,7E+07	yes	0
AT4G23300	CRK22	1,6E+07	yes	1,9E-03
AT3G17840	RLK902	1,4E+07	yes	1,4E-03
AT3G06580	GALK Mevalonate/galactokinase family protein	1,3E+07	yes	0
AT1G11350	CBRLK1	1,2E+07	yes	1,1E-03
AT3G08680	LRR-RLK	1,1E+07	yes	0
At5g56350	Pyruvate kinase	9,0E+06	yes	0
AT1G48480	RKL1	6,9E+06	yes	9,7E-04
AT3G50500	SNF1-RELATED PROTEIN KINASE 2-2	6,8E+06	yes	2,3E-03
AT4G27300	G-type lectin S-receptor-like ser/thr-kinase SD1-1	6,4E+06	yes	1,1E-03
At2g02780	LRR-RLK	5,2E+06	yes	6,2E-03
AT4G11010	NDPK3	7,0E+01	no	0
AT1G79550	PGK	2,6E+01	no	0
AT1G10760	SEX1 Pyruvate phosphate dikinase	2,1E+01	no	0
AT3G52990	Pyruvate kinase	1,8E+01	no	0
AT3G02880	LRR-RLK	1,5E+01	no	0
AT4G09320	NDPK1	1,5E+01	no	0
AT5G14640	SK13 shaggy-like kinase 13	1,3E+01	no	1,1E-03
AT5G01920	STATE TRANSITION 8, STN8	1,3E+01	no	0
AT4G35780	STY17	1,2E+01	no	7,0E-03
AT1G33590	LRR-RLK	1,1E+01	no	0
AT1G68830	STN7 protein kinase	1,1E+01	no	0
AT4G23650	CDPK6	9	no	0
AT5G35170	Adenylate kinase family protein	9	no	0
AT1G07110	6-phosphofructo-2-kinase/fructose-2,6-bisphosphatase	9	no	0
AT3G22960	Plastidial pyruvate kinase 1	8	no	0
AT1G06700	Protein kinase superfamily protein	7	no	0
AT3G10920	MSD1	6	no	0
AT5G52920	PKP-BETA1 plastidic pyruvate kinase beta subunit 1	6	no	0
AT3G20820	LRR-RLK	5	no	0
AT1G56190	Phosphoglycerate kinase family protein	5	no	0
AT3G12780	PGK1	5	no	0
AT3G09820	ADK1, ATADK1	4	no	0
AT1G80380	GLYK	4	no	0
AT1G32060	PRK	2	no	0

table A 3: total list of all LRR-RLKs found in MSI

MS I				
AGI-code	LRR-RLK	ratio of intensities BIR3/ eGFP	unique in BIR3YFP-lane?	Q-value
AT2G13790, AT2G13800	SERK4, SERK5	1,2E+10	yes	0
AT4G33430	BAK1/SERK3	4,3E+09	yes	0
At5G14210	LRR-RLK	4,2E+09	yes	0
AT3G19320	LRR-RLK	4,2E+08	yes	0
AT1G34210	SERK2	3,1E+08	yes	0
At1g27190	BIR3	1,9E+08	yes	0
AT2G31880	SOBIR1	5,1E+07	yes	0
At5g49760	HPCA1	4,7E+07	yes	0
AT1G71830	SERK1	1,4E+07	yes	0
AT5G63410	LRR-RLK	5,6E+06	yes	0
At1g27190	BIR3	1,7E+03	no	0
AT1G51805	SIF3	5	no	0
At4g08850	MIK2	4	no	0

table A 4: total list of all LRR-RLKs found in MSII

MS II				
AGI-code	LRR-RLK	ratio of intensities BIR3/ eGFP	unique in BIR3YFP-lane?	Q-value
AT4G33430	SERK3, BAK1	5,1E+10	yes	0
AT2G13790, AT2G13800	SERK4, SERK5	1,6E+10	yes	0
At5G14210	LRR-RLK	8,1E+09	yes	0
AT1G51805	SIF3	8,3E+08	yes	0
AT1G34210	SERK2	7,7E+08	yes	0
AT1G53430	NILR2	6,2E+08	yes	0
At1g27190	BIR3	5,9E+08	yes	0
At4g08850	MIK2	4,8E+08	yes	0
At3g14840	LIK1	2,9E+08	yes	0
At1g53440	LRR-RLK	1,8E+08	yes	0
AT1G33600	LRR-RLK	1,7E+08	yes	0
AT2G31880	SOBIR	1,7E+08	yes	0
AT2G26730	LRR-RLK	9,6E+07	yes	0
AT5G10290	LRR-RLK	9,4E+07	yes	0
AT3G28450	BIR2	8,7E+07	yes	0
AT1G71830	SERK1	8,1E+07	yes	0
At5g16590	LRR1	6,9E+07	yes	0
AT3G23750	BARK1	3,6E+07	yes	0
At5g10020	SIRK1	3,1E+07	yes	0
AT5G49760	HPCA1	3,0E+07	yes	0
AT5G51560	LRR-RLK	2,5E+07	yes	1,0E-03
At1g56140	LRR-RLK	2,4E+07	yes	0
AT3G17840	RLK902	1,4E+07	yes	1,4E-03
AT3G08680	LRR-RLK	1,1E+07	yes	0
AT1G48480	RKL1	6,9E+06	yes	9,7E-04
At2g02780	LRR-RLK	5,2E+06	yes	6,2E-03
AT3G02880	LRR-RLK	1,5E+01	no	0
AT1G33590	LRR-RLK	1,1E+01	no	0
AT3G20820	LRR-RLK	5	no	0

table A 5: total list of all cell death candidates of MSI

MSI				
AGI-code	CD-candidate	ratio of intensities BIR3/GFP	unique in BIR3YFP-lane?	Q-value
AT5G17880	CSA1	7,1E+08	yes	9,9E-03
AT2G34040	API5	2,5E+08	yes	0
AT2G31880	SOBIR1	5,1E+07	yes	0
AT2G19860	HXK2	2,4E+07	yes	4,1E-03
AT4G37640	ACA2	1,6E+07	yes	7,4E-04
AT1G79340	MC4	1,2E+07	yes	0
AT3G57530	CPK32	5,1E+06	yes	3,5E-03
AT2G37710	LECRK-IV.1	9	no	0
AT5G13490	AAC2	2	no	0
AT2G41100	ATCAL4, TCH3	2	no	0
AT1G65960	GAD2	2	no	0
AT4g18760	SNC2, RLP51	2	no	0
AT4G29130	HXK1	2	no	0
AT2G46520	cellular apoptosis susceptibility protein	2	no	0

table A 6: total list of all cell death candidates of MSII

MSII				
AGI-code	CD-candidate	ratio of intensities BIR3/GFP	unique in BIR3YFP-lane?	Q-value
AT1G69840	HIR2	5,4E+08	yes	0
AT5G62390	BAG7	5,2E+08	yes	0
AT5G43470	RPP8	3,2E+08	yes	0
AT3G18130	RACK 1C	3,0E+08	yes	0
AT1G55210	Disease resistance-responsive family protein	2,8E+08	yes	0
AT4G29130	HXK1	2,7E+08	yes	0
AT1G72930	TN10, TOLL/INTERLEUKIN-1 RECEPTOR-LIKE	1,9E+08	yes	0
AT2G31880	SOBIR1	1,7E+08	yes	0
AT1G79340	ATMC4, ATMCP2D	1,5E+08	yes	0
AT5G50250	CHLOROPLAST RNA-BINDING PROTEIN 31B, CP31B	1,1E+08	yes	0
AT5G61900	BON1	6,0E+07	yes	1,0E-03
AT5G62740	HIR1, HIR4	4,1E+07	yes	0
AT4G34180	CYCLASE1	3,6E+07	yes	0
AT4G16990	RLM3	3,2E+07	yes	9,9E-04
AT2G04410	RIN4	8,5E+05	yes	3,6E-03
AT3G01290	HIR2,HIR3	5,9E+01	no	0
AT1G20620	ATCAT3, CATALASE 3	3	no	0
AT4G35090	CAT2, CATALASE 2	2	no	0

Figure A 1: Sequence of CSA1 with predicted protein domains

Sequence of CSA1 with predicted domains based on Uniprot and Expasy prosite / ScanProsite Results Viewer and consensus sequences. Domains are marked with following color code: TIR domain (TIR / yellow), NB-ARC-domain (grey) including the P-loop (dark grey) and LRR-domain (LRR / turquoise).

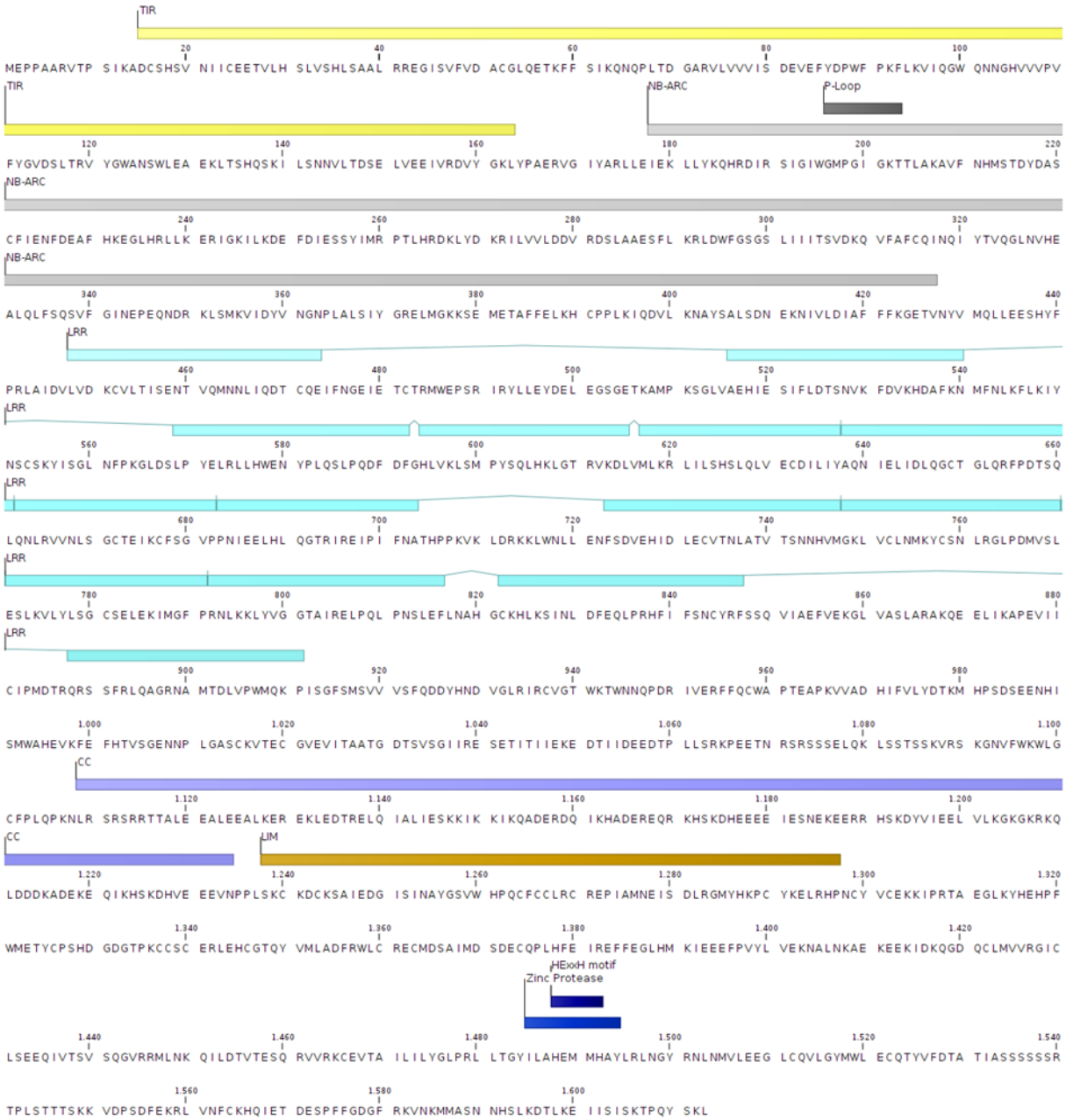

Figure A 2: Sequence of CHS3 with predicted protein domains

Sequence of CHS3 with predicted domains based on Uniprot and Expasy prosite / ScanProsite Results Viewer and consensus sequences. Domains are marked with following color code: TIR domain (TIR / yellow), NB-ARC-domain (grey) including the P-loop (dark grey), LRR-domain (LRR / turquoise), coiled-coil domain (CC / purple), LIM-domain (LIM / brown) and a zinc protease domain including the HExxH motif (blue), required for protease function.

List of abbreviation

°C	Degree Celsius
µ	Micro (10-6)
%	Percent sign
35S	Promoter of cauliflower mosaic virus
A	Alanine
aa	Amino acid
A. brassicicola	Alternaria brassicicola
ADP	Adenosine diphosphate
Alternaria	Alternaria brassicicola
Arabidopsis	Arabidopsis thaliana
A. thaliana	Arabidopsis thaliana
ATP	Adenosine triphosphate
AtPep1	Arabidopsis thaliana peptide 1
A. tumefaciens	Agrobacterium tumefaciens
avr	Avirulence
avrPto	Avirulence protein of Pseudomonas syringae pv. tomato
avrRpm1	Avirulence protein 1 from P. syringae pv. maculicola
avrRps4	Avirulence protein of Pseudomonas syringae
avrRpt2	Avirulence protein 2 from P. syringae pv. tomato
BAK1	BRI1-associated kinase
BIK1	Botrytis-induced kinase 1
BIR	BAK1-interacting RLK
BIR	Baculovirus inhibitor-of-apoptosis repeat
BKK1	BAK1-like 1
BL	Brassinolide
BON1	Bonzai 1
bp	Base pair
BR	Brassinosteroid

BRI1	Brassinosteroid-insensitive 1
Ca2+	Calcium ion
CBB	Coomassie brilliant blue
CC	Coiled-coil
cDNA	Complementary DNA
CDPK	Calcium dependent protein kinase
CERK1	Chitin elicitor receptor kinase 1
CHS3	Chilling sensitive 3 (TNL)
Cl-	Chloride ion
CNL	CC-NB-LRR
CSA1	Constitutive shade avoidance 1 (TNL)
Co-IP	Co-immunoprecipitation
Col-0	Columbia-0
CuRe1	Cuscuta receptor 1
DAMP	Danger-associated molecular pattern
DMSO	Dimethyl sulfoxide
DNA	Desoxyribonucleic acid
dNTPs	Deoxyribonucleotide triphosphate
dpi	Days post inoculation
ECD	Extracellular domain
E. coli	Escherichia coli
EDS1	Enhanced disease susceptibility 1
EFR	EF-TU receptor
e.g.	for example
ERCTA	Erecta (er)
ESI	Electrospray ionization
ET	Ethylene
ETI	Effector-triggered immunity
EtOH	Ethanol

ETS	Effector-triggered susceptibility
FLS	Flagellin-sensing
fwd	Forward
g	Gram
GFP	Green fluorescent protein
h	Hour
H+	Hydrogen ion
HopAO1	Effector of Pseudomonas syringae
Hpa	Hyaloperonospora arabidopsidis
HPLC	High-performance liquid chromatography
HR	Hypersensitive response
HRP	Horseradish peroxidase
IP	Immunoprecipitation
JA	Jasmonic acid
K+	Potassium ion
kb	Kilo base pair
kDa	Kilo Dalton
KD	Kinase domain
KO	Knock-out
L	Liter
LB	Lysogeny broth
LC-MS/MS	Liquid chromatography-mass spectrometry/mass spectrometry
LPS	Lipopolysaccharide
LRR	Leucine-rich repeat
LYK	LysM-containing receptor-like kinase
LYM	Lysine-motif
LysM	Lysine motif
M	Molar
m	Milli (10-3)

Mg2+	Magnesium ion
MAMP	Microbe-associated molecular pattern
MAPK	Mitogen-activated protein kinase
MEKK	MAPK / ERK (extracellular signal-regulated kinase) kinase kinase
min	Minute
MKK	Mitogen activated protein (MAP) kinase kinase
MPK	MAP kinase
MS	Mass spectrometry
MQ	Milli Q water (ultrapure water)
m/z	Mass to charge
n	Nano (10-9)
n	Sample size
NADPH	Nicotinamide adenine dinucleotide phosphate
N. benthamiana	Nicotiana benthamiana
NB-LRR	Nucleotide-binding leucine-rich repeat
NDR1	Non-race specific disease resistance 1
NLP	Ethylene-inducing peptide 1 (Nep1)-like protein
NO	nitric oxide
OX	Overexpression
OG	Oligogalacturonide
P-site	Phosphorylation site
PAD	Phytoalexin deficient
PAMP	Pathogen-associated molecular pattern
PBL	AvrPphB Susceptible1 (PBS1)-like proteins
PBS1	AvrPphB susceptible 1
PCD	Programmed cell death
PCR	Polymerase chain reaction
PEP	Posterior error probability
PEPR	Pep1 receptor

PG	Polygalacturonase
PGN	Peptidoglycan
PopP2	Pseudomonas outer protein P2 (effector of Ralstonia solanacearum
PR	Pathogenesis related
PRR	Pattern recognition receptor
PTI	PAMP or pattern triggered immunity
Pto	AvrPto/AvrPtoB interacting kinase
Pto	Pseudomonas syringae pv. tomato
RBOHD	Respiratory burst oxidase homolog D
Rev	Reverse
R-gene	Resistance gene
RIN4	RPM1-interacting protein 4
RLCK	Receptor-like cytoplasmic kinase
RLK	Receptor-like kinase
RLP	Receptor-like protein
RLU	Relative light units
ROS	Reactive-oxygen species
rpm	Round per minute
RPM1	Resistance to Pseudomonas syringae pv. maculicola protein 1
RPP1	Recognition of Peronospora parasitica 1
R-protein	Resistance protein
RRS1	Resistance to Ralstonia solanacearum 1
RT	Room temperature
s	Second
SA	Salicylic acid
SAG10	Senescence associated gene 101
SAR	Systemic acquired resistance
Sec	Second
SERK	Somatic embryogenesis receptor kinase

SNC1	Suppressor of NPR1-1 constitutive 1
SOBIR1	Suppressor of bir1
SOC	Super optimal broth (SOB) with catabolite repression
Sod	Superoxide dismutase
STAND	Signal transduction ATPases with numerous domains
T3SS	Type III secretion system
T3SE	Type III secretion effector
TF	Transcription factor
TIR	Toll/interleukin-1 (IL-1) receptor
TLR	Toll-like receptor
Tm	Melting temperature
TM	Transmembrane
TMV	Tobacco mosaic virus
TNL	TIR-NB-LRR
V	Volt
v/v	Volume per volume
w/v	Weight per volume
WAK1	Wall-associated kinase 1
WB	Western blot
WRKY	Tryptophan, arginine, lysine, tyrosine containing transcription factor
Ws-0	Wassilewskija-0
wt	Wild type
XA21	Xanthomonas resistance 21
Y2H	Yeast-two-hybrid
YFP	Yellow fluorescent protein

List of tables

List of figures

Danksagung

Je remercie de tout mon cœur mes grands-parents qui m'ont soutenu depuis le début de mes études, Merci Mamy, Merci Papy!!!!!

Zudem bedanke ich mich bei Prof. Dr. Thorsten Nürnberger für die Unterstützung meiner Arbeit, die Bewertung dieser und die Übernahme des Zweitgutachtens.

Ich bedanke mich bei Prof. Dr. Jürg Felix für die herausfordernden Fragen und das kritische Auseinandersetzen von Ergebnissen als Betreuer meines Graduiertenprogramms.

Bei PD Dr. Andrea Gust und Prof. Dr. Klaus Harter möchte ich mich ebenso herzlich für die Prüfung meiner mündlichen Qualifikation bedanken.

Zudem möchte ich ein Dank an die Gärtnerei mit Johanna, Sofia und Annina aussprechen, die immer unterstützend an meiner Seite waren.

Auch möchte ich mich bei Liane Schön für Ihre Hilfe und Unterstützung bei allen Verwaltungsaufgaben und -fragen bedanken.

Ich möchte mich bei allen derzeitigen und vor allem ehemaligen Mitgliedern der Pflanzenbiochemie, besonders N2 mit Niko, Raffa, Jens und Julia, für die tägliche Hilfe im Labor und Offenheit bedanken. Ihr habt meine Promotionsphase durch viel Humor besser gemacht. Danke!

Meinen Eltern und Geschwistern danke ich für ihr fortwährendes Vertrauen in meine Person als Mensch und Wissenschafterlin.

Schließlich gilt mein ganz besonderer Dank meiner Familie, meinem Mann Martin für die seelisch-moralische Unterstützung während dieser Zeit und meinen Kindern Frederic und Jacob für ihre Geduld!